CARBON DIOXIDE HYDROGENATION TO METHANOL AT LOW PRESSURE AND TEMPERATURE

THÈSE N^{O} 1726 (1997)

PRÉSENTÉE AU DÉPARTEMENT DE CHIMIE

ÉCOLE POLYTECHNIQUE FÉDÉRALE DE LAUSANNE

POUR L'OBTENTION DU GRADE DE DOCTEUR ÈS SCIENCES

PAR

Alain BILL
Ingénieur chimiste diplômé EPF
originaire de Muenchenbuchsee (BE)

acceptée sur proposition du jury:

Prof. M. Grätzel, directeur de thèse
Dr B. Eliasson, corapporteur
Prof. A. Renken, corapporteur
Prof. A. Wokaun, corapporteur

Lausanne, EPFL
1998

Acknowledgments

I would like to express my sincere gratitude to Professor Dr. M. Graetzel (EPFL), for the trust and the freedom he gave me in my work.

I am also very grateful to Dr. B. Eliasson (ABB Corporate Research Center Ltd, Baden-Dättwil) and to Prof. Dr. A. Wokaun (Paul Scherrer Institute, Villigen) for their participation in stimulating discussions and the time they spent helping me. Without their support, this work would not have been possible.

I could not have conducted my experiments without the kind consistent and helpful assistance of E. Killer (ABB), particularly when testing the methanol synthesis catalysts. Special thanks are due to W. Egli (ABB) for his computing assistance with kinetic data modeling.

I would also like to thank Dr. J. Weigel (PSI) for her friendly advise and for helping me with the DRIFTS measurements, and to Dr. J. Kritzenberger (PSI) and E. Ortelli (PSI) for their assistance with the modulation experiments.

I will always be grateful to Dr. U. Kogelschatz (ABB) for introducing me to the subject "silent discharge", for answering my many questions and for stimulating my interest. Special thanks to F. Moisy and Dr. L.-M. Zhou (visiting scientists) for providing various measurements.

Particular thanks go to E. Uenala (PSI), F. Geiger (PSI), Dr. J. Wambach (PSI) and Dr. R. Köppel (ETHZ) for their comments.

I am also grateful to Prof. Dr. A. Renken (EPFL) for being co-referee, a job which includes considerable work and little acknowledgment.

Finally, I would like to thank my parents for their understanding and support, and in particular my wife, Madeleine, for her continual support, love and confidence.

Abstract

The measurements obtained were used to investigates the methanol synthesis reaction from pure carbon dioxide and hydrogen over binary (CuO/ZrO_2) and ternary supported catalysts ($CuO/ZnO/Al_2O_3$).

A comparison of different catalysts is presented. The influence of the most important reaction parameters, i.e. temperature, pressure, space velocity and feed gas composition is examined at moderate temperatures (≤ 300 °C) and pressures (≤ 20 bar).

The influence of the partial pressures of hydrogen, carbon dioxide, carbon monoxide, water and methanol are studied in detail with the most efficient catalyst. According to the results, water has a decisive effect on the catalyst activity and performance. The measured results were used to derive a possible Langmuir-Hinshelwood kinetic model of the methanol synthesis reaction.

The catalyst surface is analyzed by in situ diffuse reflectance Fourier transform infrared spectroscopy. The identification and evolution of intermediates on $CuO/ZnO/Al_2O_3$ catalysts confirm that the reaction proceeds by prior formation of the carbonate on the copper, followed by hydrogenation of the carbonate to the formate and thereafter to methoxy and methanol. For CuO/ZrO_2 catalysts results demonstrate that the methanol formation occurs via π - bound formaldehyde and methoxy.
Responses of sine shape variation applied to the reactants are also examined.

The conversion of CO_2 with hydrogen to methanol is investigated in dielectric-barrier discharges with and without catalysts at low temperatures (≤ 100 °C) and pressures (≤ 10 bar). The combination of discharges and catalysts lower the activation energy of the reaction resulting in a decrease in the catalyst optimum temperature. The presence of the catalyst in the discharge increases the methanol yield and selectivity by more than a factor of 10.

Electrochemical reduction of carbon dioxide is briefly investigated by using TiO_2/Ni complex and TiO_2/Ru complex thin film electrodes. A considerable decrease in overvoltage is achieved together with respectable current densities.

Résumé

Ce travail présente une étude de la réaction de synthèse du méthanol à partir de carbone dioxyde et d'hydrogène sur des catalyseurs constitués du cuivre associé à l'oxyde de zirconium (CuO/ZrO_2) et du cuivre associé aux oxydes de zinc et d'aluminium ($CuO/ZnO/Al_2O_3$).

Dans la première partie de ce travail, nous nous proposons d'étudier successivement les propriétés des catalyseurs.

L'influences de la température, de la pression, du temps de séjour et de la composition du gaz de réaction sur leur performance est examinée à des températures (≤ 300 °C) et des pressions (≤ 20 bar) modérées.
L'influence des pressions partielles d'hydrogen, de dioxyde de carbone, de monoxyde de carbone, d'eau et de méthanol sur la cinétique de réaction est étudiée à l'aide du catalyseur le plus performant. Il a été observé que l'eau a un effet primordial sur l'activité et la performance du catalyseur. Une relation cinétique a été établie pour la réaction de synthèse du méthanol à températures et pressions modérées.
La surface du catalyseur a été analysée à l'aide de la spectroscopie infrarouge de réflectance diffuse. L'identification et l'évolution des espèces adsorbées sur la surface du catalyseur ternaire ($CuO/ZnO/Al_2O_3$) a confirmé la formation en premier lieu de carbonates sur le cuivre, suivie par leur hydrogénation en formiates, puis en methoxy et en méthanol. Pour le catalyseur binaire (CuO/ZrO_2), les résultats montrent que la formation de méthanol se produit par l'intermédiaire de formaldehyde (liaison - π) et de methoxy.
Les réponses du système à des modulations sinusoïdales des réactants ont également été examinées.

Dans une deuxième partie, l'hydrogénation du CO_2 en méthanol à été abordée dans un réacteur à décharge silencieuse, en présence ou non de catalyseur, à des températures (≤ 100 °C) et pressions (≤ 10 bar) basses. La combinaison de la décharge électrique et du catalyseur a permis d'abaisser l'énergie d'activation et par conséquent d'abaisser la température de travail du catalyseur. La présence de catalyseur a également permis d'augmenter d'un facteur 10 le rendement et la sélectivité en méthanol.

Dans une dernière partie, la réduction par voie électrochimique du dioxyde de carbone est brièvement abordée à l'aide de complexes de nickel et de ruthénium déposés sur une électrode à couche mince de TiO_2. Une diminution considérable du potentiel de réduction est obtenue en même temps que des densités de courant respectables.

Table of contents

Abstract **III**

Résumé **IV**

Table of contents **V**

Notations **IX**

1. Introduction and review of the literature **1**
  1.1. The carbon dioxide problem 1
    1.1.1. Carbon dioxide and the greenhouse effect 1
    1.1.2. Carbon dioxide mitigation options 2
  1.2. Methanol synthesis 4
    1.2.1. History of methanol synthesis 4
    1.2.2. Methanol synthesis over supported metal catalysts 5
      a) The role of carbon dioxide 7
      b) The active sites for methanol synthesis 8
      c) Mechanism 8
  1.3. Stoichiometry and thermodynamics 9
    1.3.1. Equations and thermodynamic data 9
    1.3.2. Selectivity 11

2. Materials and methods **13**
  2.1. Scope 13
  2.2. Catalysts 13
    2.2.1. Catalysts characterization 13
    2.2.2. Catalysts activation 14
  2.3. Experimental set-up and catalytic tests 16
    2.3.1. The tubular reactor 16
    2.3.2. The DRIFTS reactor 17
    2.3.3. The modulation reactor 19

3. Testing of methanol synthesis catalysts **23**
  3.1. Scope 23
  3.2. Introduction 23
  3.3. Apparatus 24
  3.4. Catalysts activation 24

3.5. Results and discussion 24
3.5.1. Temperature variation 24
a) Products distribution 24
b) Apparent activation energy 28
3.5.2. Pressure variation 30
3.5.3. Space velocity variation 32
3.5.4. H_2/CO_2 ratio variation 34
3.5.5. CO_2/CO ratio variation 35

4. Gas phase kinetics **39**
4.1. Scope 39
4.2. Introduction 39
4.3. Apparatus 40
4.4. Results and discussion 41
4.4.1. Carbon dioxide partial pressure variation 41
4.4.2. Hydrogen partial pressure variation 44
4.4.3. Carbon monoxide partial pressure variation 46
4.4.4. Water partial pressure variation 47
4.4.5. Methanol partial pressure variation 49
4.4.6. Kinetic model at moderate pressure and temperature 51
a) Model development 51
b) Model evaluation 52

5. Identification of the surface species and reaction scheme **57**
5.1. Scope 57
5.2. Introduction 57
a) Identification of the surface species 57
b) Periodic experiments 60
5.3. Apparatus 60
a) The DRIFTS reactor 60
b) The modulation reactor 61
5.4. Results and discussion 62
5.4.1. Identification of the surface species 62
5.4.2. Periodic experiments 67
a) Carbon dioxide modulation 67
b) Hydrogen modulation 71
5.4.3. Reaction scheme 74

6. An alternative approach (A): Carbon dioxide hydrogenation to methanol in dielectric-barrier discharges 77
6.1. Scope 77
6.2. Introduction 77
6.3. The dielectric-barrier discharge 78
6.4. Materials and methods 79
6.5. Results and discussion 81
  6.5.1. Temperature variation 81
    a) Carbon dioxide dissociation 81
    b) Carbon dioxide hydrogenation 82
  6.5.2. Pressure variation 83
  6.5.3. Electrical power variation 84
  6.5.4. H_2/CO_2 ratio variation 86
  6.5.5. Residence time variation 87
  6.5.6. Measurement with catalyst 87
  6.5.7. Measurement with air 88
6.6. Conclusions 88

7. An alternative approach (B) Carbon dioxide electroreduction 89
7.1. Scope 89
7.2. Introduction 89
7.3. Materials and methods 91
    a) Complexes synthesis 91
    b) Electrode preparation 92
    c) Electrochemical measurements 92
7.4. Results and discussion 92
  7.4.1. Cyclic voltametry with the TiO_2/Ni-complex 92
  7.4.2. Cyclic and differential pulsed voltametry with the TiO_2/Ru-complex 93
    a) Differential pulsed voltametry of a Ru-complex solution on a GCE 93
    b) Cyclic voltametry of the TiO_2/Ru complex thin film electrode 94
    c) Products identification 96
7.5. Conclusions 95

8. Bibliography **99**
8.1. Literature statistics 99
8.2. References 100

Appendix **109**
A.1. Chemical equilibrium constants 109
A.2. Catalysis parameters 112
A.3. Reactors in detail and their parameters 115
  A.3.1. The tubular reactor 115
  A.3.2. The DRIFTS reactor 116
  A.3.3. The modulation reactor 117
A.4. Calibration of the GC 119
A.5. Simulation of the periodic experiments 121
  A.5.1. Case of parallel reactions 121
  A.5.2. Case of consecutive reactions 122
  A.5.3. Case of consecutive and parallel reactions 123

Current Résumé **125**

Notations

Abbreviations

Symbol	Definition	Units
Å	ångstrom	
ads	adsorbed specie	
at.	atomic	
BET	Brunauer - Emmet - Teller	
BJH	Barret - Joyner - Halenda	
BPC	Back Pressure Controller	
cat i	catalyst i (subscript)	
DBD	Dielectric Barrier Discharge	
deg	degree	
DRIFTS	Diffuse Reflectance Infrared Fourier Transform Spectroscopy	
eq	equation	
eV	electronvolt	
E_a	apparent activation energy	[$J.mol^{-1}$]
FID	Flame Ionization Detector	
Fig.	figure	
FMC	Flow Meter Controller	
FTIR	Fourier Transform Infrared Spectroscopy	
g	in gas phase (subscript)	
GC	Gas Chromatograph	
GCE	Glassy Carbon Electrode	
ΔG^0	standard reaction Gibbs energy	[$J.mol^{-1}$]
H	height	[m]
HV	High-Voltage	
ΔH^0	standard reaction enthalpy	[$J.mol^{-1}$]
i	specie i (subscript)	
ID	internal diameter	
IR	infrared	
kJ	kilojoule	
K_i	adsorption coefficient for specie i	
k_α	rate constant for reaction α	
$K_\alpha(T)$	equilibrium constant related to equation α as a function of the temperature	

l	length	[m]
l_{bed}	catalytic bed length	[m]
liq	in liquid phase (subscript)	
log	logarithm	
M	molar concentration	$[mol.l^{-1}]$
MCT	Mercury - Cadmium - Telluride	
MS	Mass Spectrometry	
mol	mole	
N	standard conditions (0°C, 1013.25 mbar)	
n_i	moles of specie i	[mol]
$\dot{n}_i$	molar flow of specie i	$[mol.h^{-1}]$
$\bar{n}_i$	mean value of the exponent of specie i in the power law rate expression	
opt.	optimum	
P	pressure	[bar or Pa]
ppm	parts per million	
ppmv	parts per million by volume	
p_i	partial pressure of specie i	[bar or Pa]
Q_i	volumetric flow rate of specie i	$[Nml.min^{-1}$ or $Nl.h^{-1}]$
Q_{total}	total volumetric flow rate	$[Nml.min^{-1}$ or $Nl.h^{-1}]$
r	mole ratio	[-]
R	stoichiometric number	[-]
react	from the reaction (subscript)	
ref.	reference	
RSS	Residual Sum of Squares	
RWGS	Reverse Water-Gas Shift reaction	
R_i	overall reaction rate of specie i	$[g_i.kg_{cat}^{-1}.s^{-1}]$
$\bar{R}_i$	mean overall reaction rate of specie i	$[g_i.kg_{cat}^{-1}.s^{-1}]$
$R_{i,c}$	overall calculated rate of specie i	$[g_i.kg_{cat}^{-1}.s^{-1}]$
r^2	correlation coefficient	
R_M^2	multiple correlation coefficient	
sat.	saturated	
SCE	Saturated Calomel Electrode	
SHE	Standard Hydrogen Electrode	
STDEV	Standard Deviation	
Synth.	synthetic	
S_{BET}	catalyst surface area determined according the Brunauer-Emmet-Teller isotherm	$[m^2.g_{cat}^{-1}]$
S_i	selectivity of species i	[-]
S_v	gas hourly space velocity	$[h^{-1}]$
\$	US dollar	
t	ton (metric)	

T	temperature	[°C or K]
TCD	Thermal Conductivity Detector	
vol.	volume	
vs.	versus	
V_{cat}	catalyst volume	[cm^3 or Nml]
w.	weight	
x_i	mole fraction of species i	[-]
X_i	conversion of specie i	[-]
y_i	mole fraction of specie i (in the gas phase)	[-]
Y_i	yield of species i	[-]
3D	three dimensions	
α	proportional	
δ	vibration: angle bending (scissors)	
ν	vibration: stretching of one bond	
ν_{as}	vibration: antisymetric stretching of two bonds	
ν_s	vibration: symetric stretching of two bonds	
ϕ_i	phase shift of specie i	[deg]
$\varnothing_i$	diameter of specie i	[m]
Θ_i	surface coverage fraction of specie i	[-]
τ	contact or transit time	[s]
ω	frequency	[Hz]

Name and formula of chemical compounds

Al_2O_3	alumina
Cu_2O	copper (I) oxide
CuO	copper (II) oxide
TiO_2	titanium oxide
ZnO	zinc oxide
ZrO_2	zirconium oxide

Ar	argon
C	carbon (graphite)
CH_4	methane
$HCO -$	formyl
$CH_2O -$	hydroxy methylene
$CH_3O -$	methoxy
CH_3OH	methanol
CO	carbon monoxide
CO_2	carbon dioxide
$HCOO -$	formate
$HCOOH$	formic acid
$CO_3 -$	carbonate
$HCO_3 -$	hydrogeno carbonate
CH_3OCH_3	dimethyl ether
C_3H_7NO	N, N-dimethylformamide (DMF)
$C_{16}H_{36}ClNO_4$	tetrabutylammonium-perchlorate (TBAP)
C_nH_{2n+2}	higher alcanes
$C_nH_{2n+2}OH$	higher alcohols
CFC, HCFCs	halocarbon refrigerants

H_2	hydrogen
$- OH$	hydroxyl
H_2O	water
He	helium
N_2	nitrogen
N_2O	nitrous oxide
O	oxygen atom
O_3	ozone

Institutes names

ABB	Asea Brown Boveri Corporate Research Ltd.
ETHZ	Eidgenössichen Technischen Hochschule Zürich Swiss Federal Institute of Technology-Zürich
EPFL	École Polytechnique Fédérale de Lausanne Swiss Federal institute of Technology-Lausanne
NIST	National Institute of Standards and Technology
PSI	Paul Scherrer Institute

Conversion factors

1 Gtc = 1 Gigaton carbon

1 ton (metric) = 10^3 kg

1 Å = 10^{-10} m

1 bar = 10^5 Pa

SI prefixes

Symbol	**Prefix**	**Factor**
G	giga	10^9
M	mega	10^6
k	kilo	10^3
m	milli	10^{-3}
μ	micro	10^{-6}
n	nano	10^{-9}

1. Introduction and review of the literature

1.1. The carbon dioxide problem

1.1.1. Carbon dioxide and the greenhouse effect

There is no doubt that human activities are changing the atmospheric concentrations and distributions of greenhouse gases (Fig. 1). The ever-increasing consumption (by combustion) of fossil fuels since the industrial revolution some 250 years ago - together with specific industrial activities such as cement production, and the deforestation of the Earth's tropical rain forest - has caused a very marked increase in the global concentration of the major greenhouse gas: carbon dioxide.

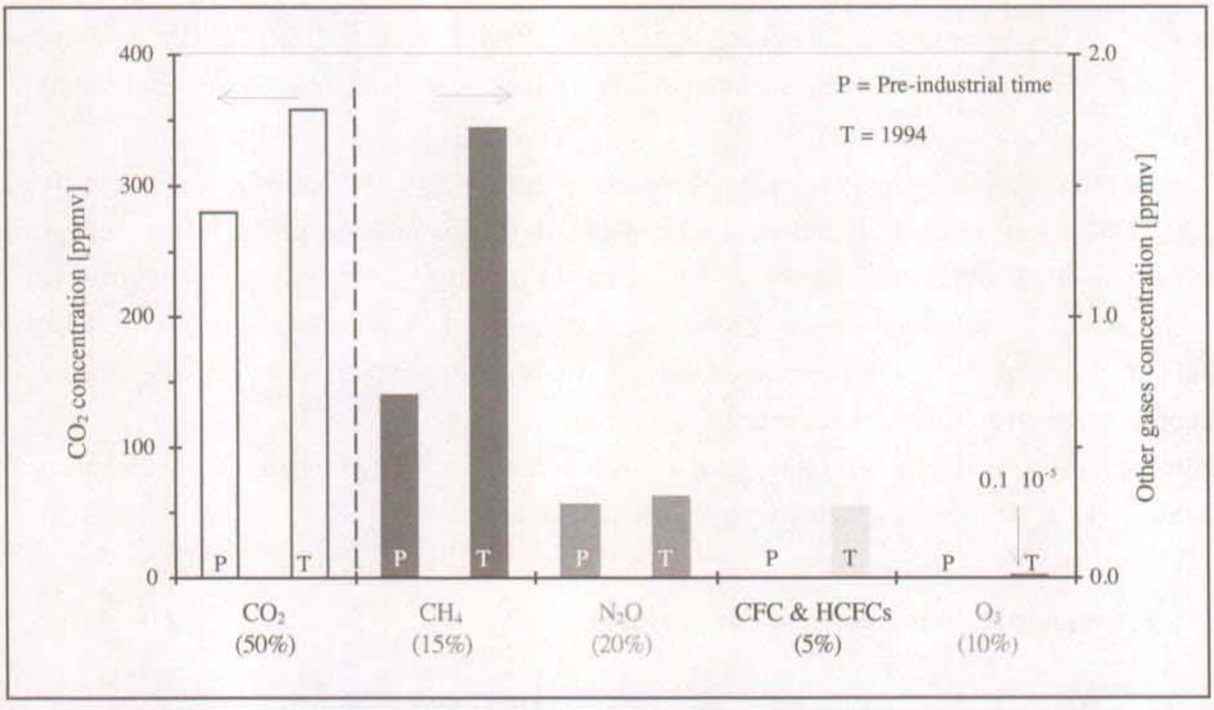

Fig. 1: A sample of greenhouse gases affected by human activities (from ref. (Kirk 1991)) (The percentage indicates the warming contribution by the gas)

Its concentration has increased from about 280 ppmv in pre-industrial times to 358 ppmv in 1994 (Kirk 1991) (Fig. 2). This represents a net increase of 27.8 %. CO_2 equilibrium concentration is governed by photosynthesis and respiration of the earth's biosphere and physical and chemical interaction with the oceans. All these processes operate on different time-scales (ranging from year to centuries), CO_2 being subsequently transferred to various reservoirs, some of which immediately return CO_2 to the atmosphere (uptake into vegetation and surface layer of the ocean) and some of which have a less immediate, but no less important effect (transfer to soils and to the deep ocean).

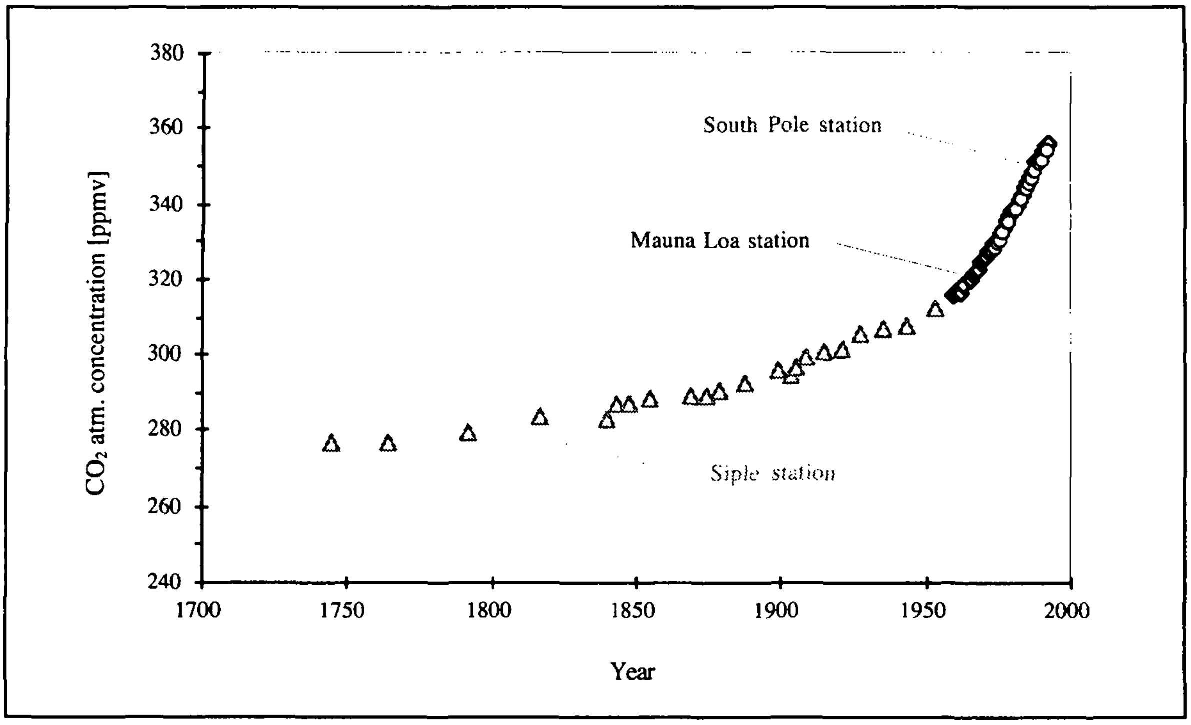

Fig. 2: CO_2 concentrations over the past 300 years from ice records (Siple station, Antarctica) and, since 1958, from measurement site Mauna Loa (Hawaii) and South Pole (Antarctica) stations)

The natural CO_2 exchange between the earth's surface and the atmosphere is approximately 200.0 GtC.year^{-1} in each direction. This amount is considerably larger than the anthropogenic emissions of 8.0 GtC.year^{-1}. About 6.0 GtC.year^{-1} of the latter come from the combustion of fossil fuels and 2.0 GtC.year^{-1} from deforestation of tropical rain forests. Nature removes about 4.5 GtC.year^{-1} of the anthropogenic emissions from the atmosphere. Thus the CO_2 loading of the atmosphere increases by 3.5 GtC.year^{-1}.

Although carbon dioxide is a rather inert molecule that does not participate in the chemistry of the atmosphere, it is the principal anthropogenic greenhouse gas.

1.1.2. Carbon dioxide mitigation options

The technological options that may contribute to reducing carbon dioxide emissions can be categorized as follow:

- Minimize emissions

This is already being done by introducing very efficient equipment. One can produce energy with higher efficiency, increase efficiencies of conversion and end use, conserve energy, and recycle products.

- Zero emissions

One can choose energy sources that are CO_2 free such as hydro, wind, nuclear, geothermal or solar. One could also burn biomass and practice reforestation and thus gain power with no net emissions of CO_2.

- CO_2 control and CO_2 chemistry

This approach concerns recovering CO_2 from sources that contain it in much higher concentrations than the atmosphere. Absorption, adsorption and membrane processes are evaluated for these purposes. The technology is available, for example, in the coal power plant at Shady Point in Oklahoma where 200 t of carbon dioxide are removed daily from the flue gases of a 300 MW power plant (Eliasson 1994).

The question then arises: what can one do with the recovered CO_2?

One option is to dispose it in natural fields (elimination in aquifers, confination in depleted gas or oil wells, injection for enhanced oil recovery, disposal in ocean). This is now done in Norway (Sleipner gas field) where 2'740 $t.day^{-1}$ of CO_2 are removed from natural gas. This CO_2 is then compressed and injected into a water-filled sandstone reservoir (deep aquifer) (Smith 1996).

Another option is to use it directly (without conversion) as a solvent, additive for beverage, propellant in place of CFC, ... In Shady Point, all the recovered carbon dioxide is liquefied and sold to the food industry (Eliasson 1994).

And the last option, which deserves our attention, is to use it as a source in the synthesis of chemicals (synthesis of fuels, intermediates and/or fine chemicals) like the catalytic CO_2 hydrogenation to methanol.

Carbon dioxide can be converted to methanol by combining it with hydrogen and using the right kind of catalyst. Of course, the hydrogen must be available on a large scale and its production must be achieved without any emission of CO_2 to the atmosphere. This implies that the hydrogen must be produced by using renewable energies like solar, hydro or biomass fuel. Methanol, in addition to being a fuel on its own, can be looked at as a storage and transport medium for hydrogen. Methanol has also the advantage that it is liquid under normal conditions. It can be stored and transported as easily as gasoline, and can be used in conventional combustion engines without requiring any major adjustments. Methanol has twice the energy density of liquid hydrogen, and half the energy density of gasoline. Methanol synthesis can thus be looked upon as a way of converting hydrogen into an energy carrier that can be more conveniently stored and transported.

1.2. Methanol synthesis

1.2.1. History of methanol synthesis

Methanol is believed to have been discovered by R. Doyle in 1661 through the rectification of crude vinegar over milk of lime. He named the new compound *adiaphorus spiritus lignorum.* There was no written history or record of its use for any purpose, either domestic or industrial, before the 19th century.

The chemical or molecular identity of methanol was first established independently by J.B.A. Dumas and J. von Liebig in 1834. The term "methyl" was introduced into chemistry in 1835 on the basis of their work.

Since then, efforts have been made by various investigators to synthesize methanol, and a successful attempt was the synthesis by dry distillation of wood, obtained by M. Berthelot in 1857. Referring to its synthesis origin and route, methanol has since been called "wood spirit" by some people. Obviously this nickname is fading away due to its totally different synthesis route.

As early as 1913, A. Mittasch and co-workers at BASF successfully produced organic compounds containing oxygen, including methanol, from carbon monoxide and hydrogen in the presence of iron oxide catalysts during developmental work on the synthesis of ammonia. The decisive step in the large-scale industrial production of methanol was made by M. Pier and coworkers in the early 1920s with the development of a sulfur-resistant zinc oxide-chromium oxide catalyst. By the end of 1923 the process had been converted from the development to the production stage at the BASF Leuna Work. Processes based on the above work were performed at high pressure (250 - 350 bar) and 320 - 450 °C. These processes defined methanol production for more than 40 years.

In the 1960s, however, ICI introduced a highly selective copper-zinc oxide catalyst, putting an end to the high pressure methanol synthesis technology. These catalysts operated at fairly mild reaction conditions (50 - 100 bar and 200 - 300 °C). Use of these more active catalysts was made possible because more efficient synthesis gas purification processes had became available, mainly removing the catalyst poisons (metal carbonyls and sulfur).

Today's industrial production of methanol is exclusively based on this technology. As an example, in 1995, $25.1 \cdot 10^6$ t of methanol were produced worldwide. The worldwide methanol production and its market price since 1986 are illustrated in figure 3 (Fiedler*et al.* 1990, Methanex 1995).

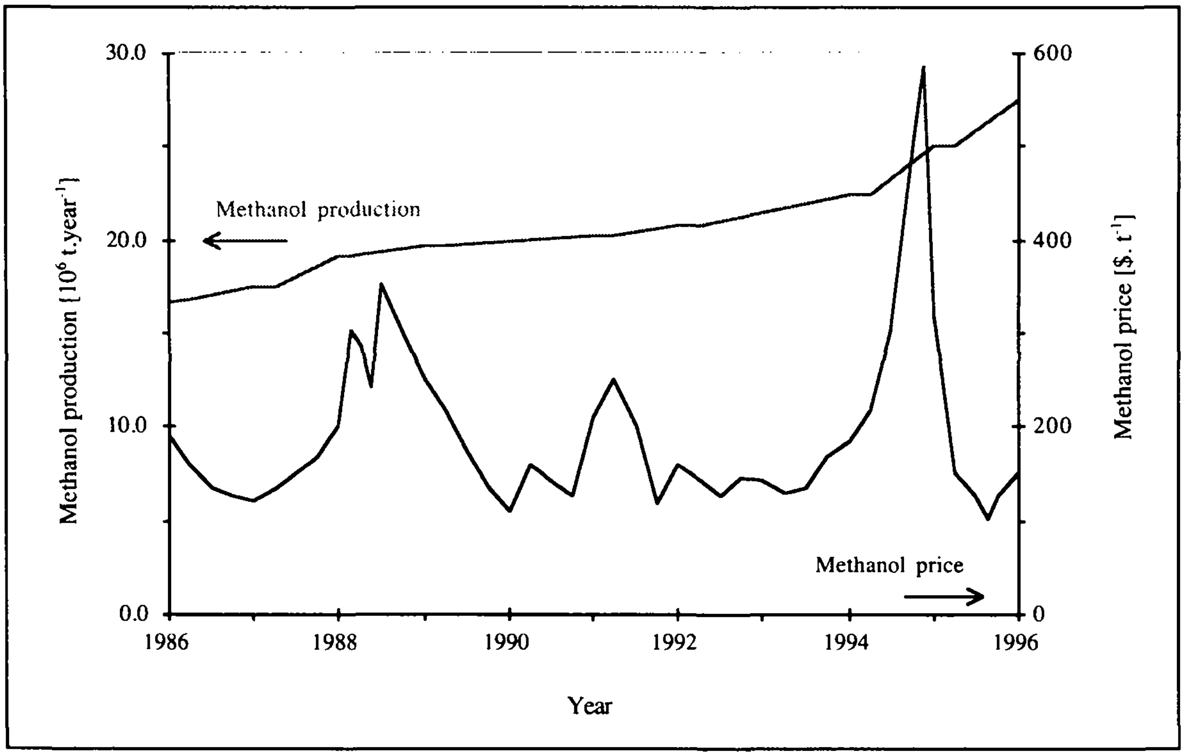

Fig. 3: Worldwide methanol production and the methanol price (Spot market)

1.2.2. Methanol synthesis over supported metal catalysts

As mentioned previously, the methanol synthesis was first performed over a zinc oxide-chromium oxide catalyst. This catalyst, which was used at 250 - 350 bar and 320 - 450 °C, was highly stable to the sulfur and chlorine compounds present in the synthesis gas (Hawkins *et al.* 1988, Marschner *et al.* 1983, Mittasch *et al.* 1923, Natta 1955). In 1966, a copper-based catalyst was introduced for the methanol synthesis for sulfur-free synthesis gas containing a high proportion of carbon dioxide (Davies *et al.* 1967). This copper oxide-zinc oxide catalyst, thermally stabilized by aluminia, was extremely active and highly selective. Furthermore, the synthesis could be carried out at 220 - 250 °C and 50 bar, thereby avoiding premature aging of the catalyst due to sintering of copper.

All currently used low pressure catalysts contain copper oxide and zinc oxide with one or more stabilizing additives. A summary of typical copper-based catalysts is given in table 1.

Table 1: Summary of typical catalysts composition for low pressure methanol synthesis

Manufacturer	Components				Ref.
	Cu [% at.]	**Zn** [% at.]	**Al** [% at.]	**C (graphite)** [% at.]	
BASF	65 - 75	20 - 30	5 - 10	-	(Bröcker 1978)
Süd Chemie	65 - 75	18 - 23	5 - 10	-	(Schneider *et al.* 1987)
ICI	61	30	9	-	(Gallagher *et al.* 1965)
Du Pont	50	19	31	31	(Höppener *et al.* 1986)
Haldor Topsøe	50 - 60	21 - 25	15 - 28	6 - 8	(Topsøe 1987)

Even though technological processes (low pressure) have been commercially available for the past 30 years, various aspects of the mechanism by which methanol is produced are not yet clearly understood. In the literature, there is still much controversy over the nature of the active components of the catalysts and the reaction steps that take place on them. The reasons for these conflicting studies are:

- The elementary composition of the catalysts is often not exactly the same.

- The preparation methods are not always identical (coprecipitation, impregnation, ...). Significant differences in the methanol activity, as well as in the products distribution, were found for catalysts of the same nominal composition but made in different ways (Koeppel 1991).

- The reaction conditions are different. The nature of the catalysts (structure, atoms distribution, ...) might vary with the working conditions. Moreover many investigations are done under conditions far removed from industrial practice (low partial pressures, high purity of the gases, ...).

However, as already reported in 1984 by Chinchen (Chinchen *et al.* 1984) the major questions to be answered are still:

a) What is the major synthesis reaction, i.e. CO hydrogenation, CO_2 hydrogenation, or both?

b) What are the active sites for methanol synthesis on a $CuO/ZnO/Al_2O_3$ catalyst?

c) What are the surface mechanisms of chemical reaction and which reaction step is rate-determining?

Of course, this list is not exhaustive. There are other questions with a scientific interest, i.e., what is the role of water in the synthesis? What are the causes for catalysts deactivation? etc.

Although considerable work is still required to overcome remaining ambiguities, a basic overview can be drawn from our existing knowledge.

a) The role of carbon dioxide

As all industrial plants operate with $CO/CO_2/H_2$ mixtures as shown in table 2 (Cybulski 1994), it is not obvious which carbon oxide is the C-source for methanol. Moreover both gases are easily inter-convertible through the forward/reverse water-gas shift reaction (eq 5).

Table 2: Summary of typical syngases composition (from ref. (Cybulski 1994))

	Syngas types		
Component	**CO-rich gas** [% mol]	**Balanced gas** [% mol]	**H_2-rich gas** [% mol]
Hydrogen	35.0	55.0	71.0
Carbon monoxide	51.0	19.0	18.0
Carbon dioxide	13.0	5.0	7.0
Methane	0.1	0.1	0.1
Nitrogen/inerts	0.9	20.9	3.9
$\frac{H_2}{CO}$ ratio[1]	0.69	2.89	3.94
$\frac{H_2 - CO_2}{CO + CO_2}$ ratio[1]	0.34	2.08	2.56

In most studies it was assumed or/and concluded that adsorption of carbon monoxide was the starting point. Klier et al. have published a series of articles (Klier 1982, Klier *et al.* 1982) based on the theory that methanol was produced predominantly by the hydrogenation of CO. Their studies were done on a CuO/ZnO catalyst (Cu/Zn = 30/70 % at.) at a pressure of 75 bar and temperatures between 225 and 250 °C. They also stated that while CO_2 hydrogenation could also take place, the rate was much slower than the CO hydrogenation.

However, the work already done in 1975 by Kagan et al. (Kagan *et al.* 1975) favored the view that it is the CO_2 component of the gas mixture which is the precursor to methanol. Additional arguments supporting this claim have also been published by Rozovskii (Rozovskii 1980). This has been confirmed by Chinchen et al. (Chinchen *et al.* 1984, Chinchen *et al.* 1987) using labeled CO_2.

---

[1] H_2, CO_2, and CO represent the respective concentrations [mol].

b) The active sites for methanol synthesis

An area of controversy in heterogeneous catalytic methanol synthesis concerns the nature of the active sites for methanol synthesis. What is the role played by the individual catalyst components (Cu, ZnO, Al_2O_3)? What is the state of the copper in a working catalyst? And what role is played by the support itself (the non-copper components)?

Most commercial catalysts for methanol synthesis contain copper. This fact led to the hypothesis that the active sites are located on the copper component. Then which is the copper state: Cu^0 or Cu^{+1}? Klier (Klier 1982) claimed that it is Cu^{+1} ions, stabilized on the surface of ZnO, which form the active centers. It must be pointed out that traces of impurities or presence of alkali metals stabilize Cu^{+1} ions on the surface of the catalyst (Sheffer *et al.* 1989a, Sheffer *et al.* 1989b). However, Chinchen et al. (Chinchen *et al.* 1986a) assumed that the active centers were formed by metallic copper atoms located on the surface of the catalyst. Recent accurate in situ measurements (Clausen *et al.* 1991a, Clausen *et al.* 1991b) over a number of $CuO/ZnO/Al_2O_3$ catalysts of different compositions and copper particle sizes showed that the critical steps in the reaction mechanism occur on the surface of copper crystallites. Although it is now clear that metallic copper is the active component for the methanol synthesis, a synergy effect exists between the copper phase and the support (Burch *et al.* 1990, Le Peltier *et al.* 1996). The support should also be considered as an integral part of the "active sites" and not only as an inhibitor of copper crystal sintering (by acting as a dispersant and separator of the copper crystals) and giving physical strength to the catalyst. The activity of the support (oxides) facilitates the dissociative adsorption of H_2 and stabilizes the surface oxygen which remains in close contact with metallic copper. It was found that active catalysts have 30 - 60 % of their copper surface area covered with oxygen after methanol synthesis (Bowker *et al.* 1988, Denise *et al.* 1982).

c) Mechanism

The formation of methanol can be described by an adsorption-desorption mechanism. According to various investigations on $CuO/ZnO/Al_2O_3$ (Bailie *et al.* 1995, Bowker *et al.* 1988, Bowker *et al.* 1981, Fujita *et al.* 1995, Nakamura *et al.* 1995) the methanol synthesis occurs through hydrogenation of CO_2 into formates (unidendate or bidendate) (Bowker *et al.* 1988, Liu *et al.* 1984, Millar *et al.* 1992b, Robinson 1989), which are then reduced (two possible pathways) to methoxy (Kiennemann *et al.* 1990) and further hydrogenated to methanol. The hydrogenation of the formates into methanol is the rate determining step. When working with pure CO_2 or a mixture of $H_2/CO/CO_2$, the remaining O(ads) is removed by CO or H_2 , depending on reaction conditions, to give CO_2 or H_2O (eq 1 and 2).

$$O_{(ads)} + H_2 \leftrightarrow H_2O \tag{1}$$

$$O_{(ads)} + CO \leftrightarrow CO_2 \tag{2}$$

The concurrent forward/reverse water-gas shift reaction probably occurs via O(ads) rather than formate intermediates (Chinchen *et al.* 1987).

Figure 4 schematically resumes the reaction between surface species and molecular pathways.

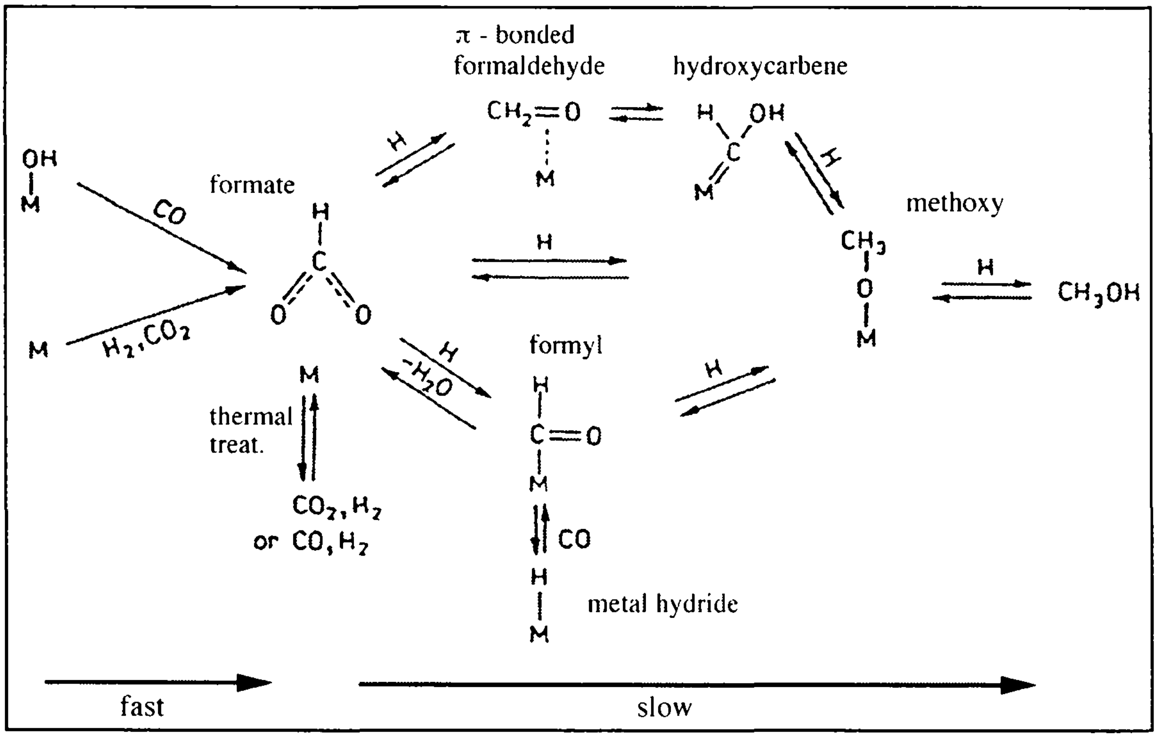
π - bonded
formaldehyde
hydroxycarbene
$CH_2=O$
M
H
OH
C
M
H
OH
M
formate
CO
M
H_2,CO_2
H
C
O
O
M
H
H
methoxy
CH_3
O
M
H
CH_3OH
H
$-H_2O$
formyl
H
C=O
M
H
thermal
treat.
CO_2,H_2
or CO,H_2
CO
H
M
metal hydride
fast
slow

Fig. 4: Methanol synthesis reaction mechanism from CO, CO_2, or syngas over $CuO/ZnO/Al_2O_3$ catalysts. (The picture is reproduced from ref. (Skrzypek et al. 1994))

1.3. Stoichiometry and thermodynamics

1.3.1. Equations and thermodynamic data

Methanol synthesis has nearly always been expressed in terms of the hydrogenation of CO:

$$CO + 2H_2 \leftrightarrow CH_3OH_{(g)} \qquad (3)$$

But as mentioned previously, methanol synthesis over Cu-based catalysts proceeds exclusively via CO_2 hydrogenation:

$$CO_2 + 3H_2 \leftrightarrow CH_3OH_{(g)} + H_2O_{(g)} \qquad (4)$$

As shown in table 3 (Chase *et al.* 1985), the reactions between CO and H_2, as well as between CO_2 and H_2 are both exothermic. They are also thermodynamically unfavorable, showing positive Gibbs free-energy changes at higher temperatures.

Table 3: Summary of thermodynamic values (from ref. (Chase et al. 1985))

	Standard thermodynamic values		
Equation	**Temperature** [°C]	**$(\Delta H^0)_T$** [kJ.mol^{-1}]	**$(\Delta G^0)_T$** [kJ.mol^{-1}]
3	25.0	-90.6	-25.3
	225.0	-97.9	+21.2
4	25.0	-49.5	+3.4
	225.0	-58.1	+41.5
5	25.0	+41.2	+28.6
	225.0	+39.8	+20.4

Simultaneously with methanol synthesis, the reverse water-gas shift reaction (RWGS) takes place depending on the reaction conditions:

$$CO_2 + H_2 \leftrightarrow CO + H_2O_{(g)} \qquad (5)$$

As shown in table 3, this reaction is only slightly dependent upon the temperature.
These three reactions can be assumed to occur in the methanol synthesis. A schematic view is summarized in figure 5.

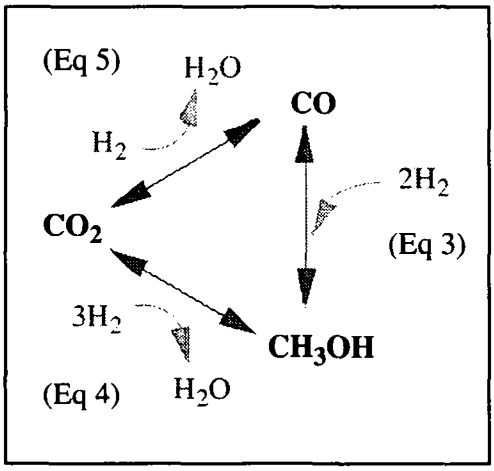

Fig. 5: Schematic view of all reactions

Only two of these are stoichiometrically independent and define the equilibrium composition of the gas mixture. Several authors propose expressions for the chemical equilibrium constants as a function of the temperature (Bisset 1977, Cherednichenko 1953, Graaf *et al.* 1986, Skrzypek *et al.* 1995, Wade *et al.* 1981) and some of the relationships are listed in appendix A.1..

Thermodynamically speaking, the highest conversions, and thus the highest methanol yield, are obtained at low temperatures and high pressures.

1.3.2. Selectivity

Many other side reactions to the formation of methanol can take place, such as the formation of higher alcohols:

$$nCO + 2nH_2 \leftrightarrow C_nH_{2n+1}OH + (n-1)H_2O \qquad (6)$$

hydrocarbon and waxes formation:

$$CO + 3H_2 \leftrightarrow CH_4 + H_2O_{(g)} \qquad (\Delta H^0)_{225} = -214.6\ [kJ.mol^{-1}] \qquad (7)$$
$$(\Delta G^0)_{225} = -96.4\ [kJ.mol^{-1}]$$

$$CO_2 + 4H_2 \leftrightarrow CH_4 + 2H_2O_{(g)} \qquad (\Delta H^0)_{225} = -174.8\ [kJ.mol^{-1}] \qquad (8)$$
$$(\Delta G^0)_{225} = -282.8\ [kJ.mol^{-1}]$$

expressed in a more general way, the Fischer-Tropsch reactions:

$$nCO + (2n+1)H_2 \leftrightarrow C_nH_{2n+2} + nH_2O \qquad (9)$$

eventually the Boudart reaction:

$$2CO \leftrightarrow CO_2 + C \qquad (\Delta H^0)_{225} = -173.6\ [kJ.mol^{-1}] \qquad (10)$$
$$(\Delta G^0)_{225} = -84.1\ [kJ.mol^{-1}]$$

as well as the formation of ethers (especially dimethyl ether), esters and ketones.

Reactions subsequent to the methanol synthesis can also take place like the dimethyl ether formation:

$$2CH_3OH \leftrightarrow CH_3OCH_3 + H_2O_{(g)} \qquad (\Delta H^0)_{225} = 0.9\ [kJ.mol^{-1}] \qquad (11)$$
$$(\Delta G^0)_{225} = -84.0\ [kJ.mol^{-1}]$$

The formation of most byproducts is thermodynamically favored over methanol synthesis (larger negative change of free energy). Because methanol constitutes the main product, however, these reactions are controlled kinetically rather than thermodynamically.

This all shows all the importance of using the most suitable catalyst which enables the reaction to take place within a reasonable time and which is selective in favoring the desired reaction with minimum by-products.

2. Materials and methods

2.1. Scope

Two topics are presented in this chapter. The first deals with the catalysts, which are specified, and the second describes the different experimental configurations used in this work.

2.2. Catalysts

Three highly active and highly selective catalysts for methanol synthesis from hydrogen and carbon oxides were investigated. Two of them were from industrial origin (catalysts B & C) and one of them was from an academic origin (catalyst A).

2.2.1. Catalysts characterization

All three catalysts were copper-based catalysts. They are all designed for low pressure and low temperature use. The catalysts were ground and put through a sieve to obtain particle sizes of 50 - 150 μm or 250 - 500 μm, depending on which reactor was used. Density was typically 1.2 g.ml^{-1}. Figure 6 illustrates the catalyst in both ground and pellets form.

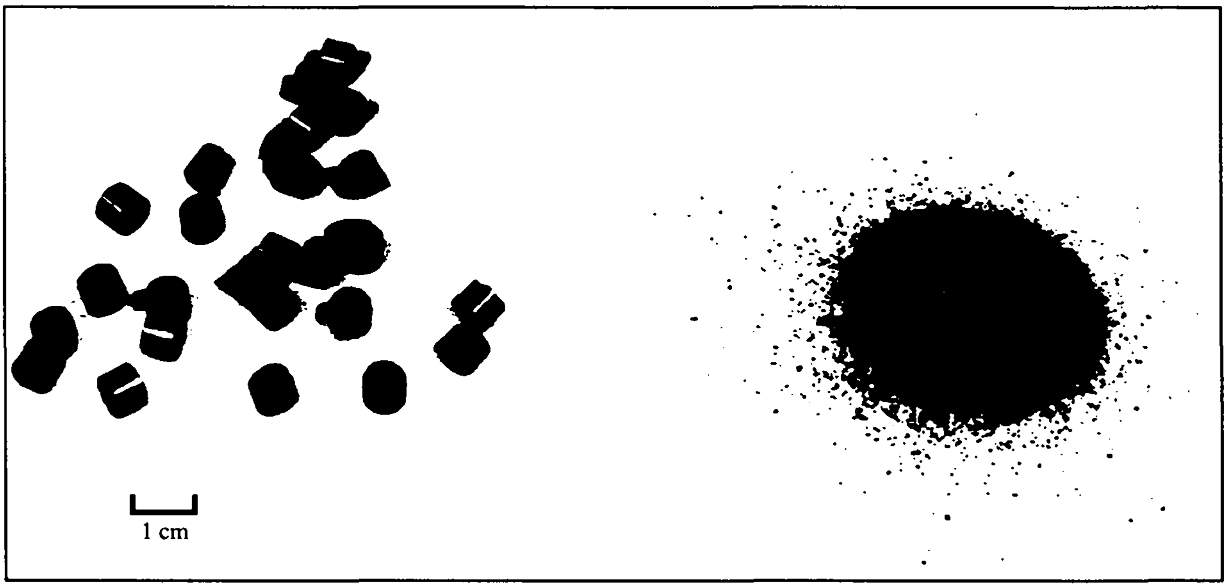

Fig. 6: Catalyst view (left: as pellets, right: ground and sieved)

The BET surface areas (S_{BET}), as well as desorption average pore diameters (d_P) were determined by nitrogen physisorption at -196 °C (ASAP 2000, Micromeritics Instruments, Georgia, USA). The pore size distributions were calculated from the desorption branches of the isotherm following the BJH-method and using the Halsey equation (De Boer 1958, De Boer *et al.* 1965a, De Boer *et al.* 1965b).

Typical values for the surface properties are shown in table 4.

Table 4: Summary of the surface properties

	Surface properties		
Catalyst (composition)	**S_{BET} (before use)** $[m^2.g_{cat}^{-1}]$	**S_{BET} (after use (~ 250 h))** $[m^2.g_{cat}^{-1}]$	**Presence of micropores** [Ø < 20 Å]
A (CuO/ZrO_2)	101.72	85.05	yes
B ($CuO/ZnO/Al_2O_3$)	104.14	78.75	yes
C ($CuO/ZnO/Al_2O_3$)	73.58	58.56	yes

After approximately 250 hours under working conditions the loss in surface area was around 20 %.

2.2.2. Catalysts activation

A catalyst must be activated before it can be used. For the tested catalysts, the copper oxide must be reduced to catalytic copper. The reduction is highly exothermic and the temperature shouldn't rise to high values to avoid damaging the catalyst. Therefore the procedure is usually undertaken over a rather long time span, using diluted H_2. Reduction was carried out using a gas mixture (Sauerstoffwerk, Lenzburg, CH) consisting of H_2 (1.5 % vol.), CO (0.5 % vol.), CO_2 (4.0 % vol.) and N_2 (balance). The total flow rate was 450 Nml.min^{-1} and the pressure 3 bar. Temperature steps and time intervals are summarized in table 5.

Table 5: Temperature protocol for the catalyst pretreatment

Step	Time interval [min]	Temperature [°C]
1	120	up to 180
2	60	fixed at 180
3	30	up to 220
4	60	fixed at 220

Catalyst and oven temperature, as well as the partial pressure of water during the pretreatment are shown in figure 7.

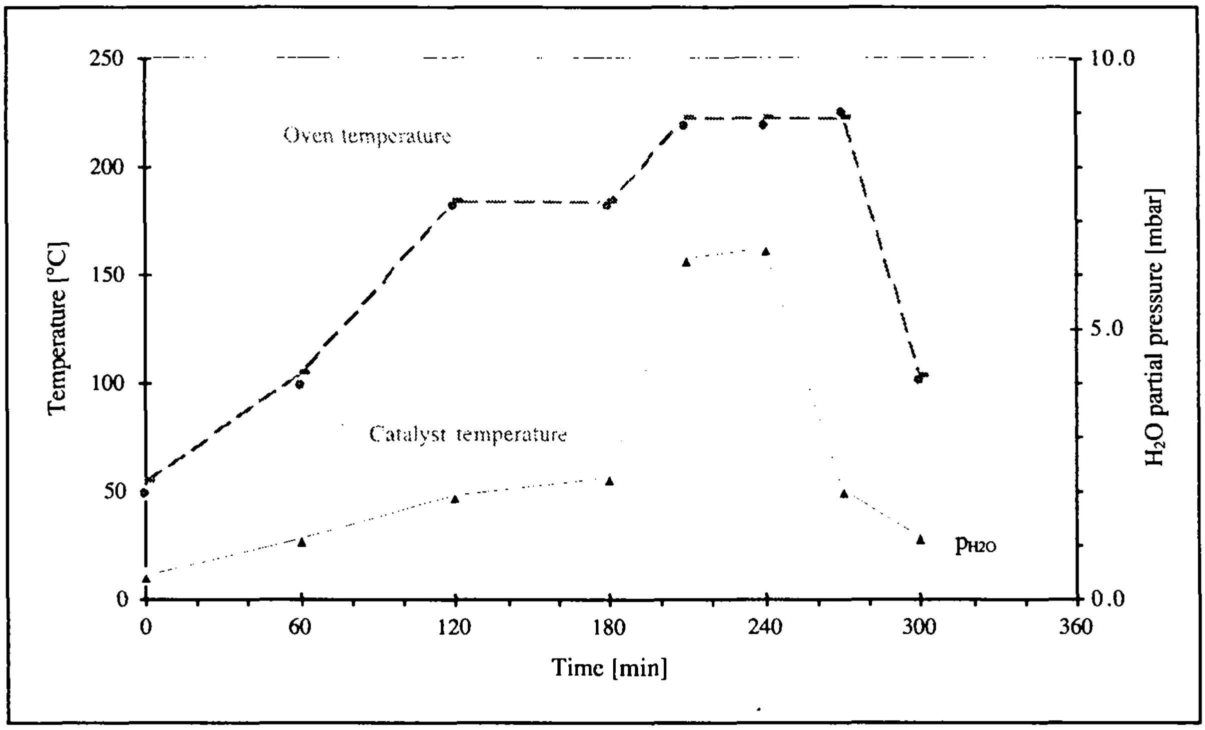

Fig. 7: Catalyst temperature and water partial pressure profile during the pretreatment of the catalyst B ($P = 3$ bar, $Q_{total} = 450$ $Nml.min^{-1}$, $S_v = 3375$ h^{-1}, $\tau = 1$ s)

During the first temperature step (up to 180 °C), the water partial pressure increases slowly. It is mostly due to the removal of the water present in the system and the beginning of the catalyst reduction. The net increase of the partial pressure of water, between 180 and 220 °C (step 3), is more related to the copper reduction. The copper oxides undergo the following reactions:

$$H_2 + 2CuO \leftrightarrow H_2O + Cu_2O \quad (12)$$

$$H_2 + Cu_2O \leftrightarrow H_2O + 2Cu \quad (13)$$

The temperature at which the copper oxide is reduced is dependent on the catalytic system (Le Peltier 1989, Robinson 1989). For example, free CuO atoms reduce at 220 °C (or 1.4 V). A CuO/ZnO system (40/60 % w.) is already reduced at 190 °C.

At the end of the reduction, the temperature was decreased down to 100 °C before adjusting the parameters for the measurements.

2.3. Experimental set-up and catalytic tests

The three different set-ups used are described in detail (with a schematic view), as well as the typical catalytic tests performed.

Set-ups were first characterized performing a blank run (without a catalyst). For the selected experimental conditions no products other than H_2 and CO_2 were detected.

Moreover, reference points were introduced in each measurement serie to valid the catalyst stability.

2.3.1. The tubular reactor

The reactor was of the conventional plug-flow fixed bed type (see appendix A.3.1.). It consisted of a stainless steel tube (l = 150 mm, ID = 15 mm) located inside the oven of a gas chromatograph (Serie 9500, Finnigan Corporation, Sunnyvale, USA). Oven heating was feedback-regulated (within ± 0.5 °C) from a thermocouple positioned close to the exterior wall of the reactor. Two additional thermocouples were used for precise temperature measurement in the center of the catalyst bed and inside the pre-heated reactor inlet space. Gas reactants were supplied from pre-calibrated electronic flow-meter controllers (FMC series F, Bronkhorst Hi-Tec, Ruurlo, The Netherlands), and pressure was controlled by an electronic back-pressure regulator (Research Control Valve, Badger Meter, Oklahoma, USA). The purity of the gases (Sauerstoffwerk, Lenzburg, CH) used for the synthesis was 99.9 % for CO_2, 99,99 % for CO, 99.995 % for H_2 and 99.99 % for He (diluant) (He 99.996 % was used for the GC). Liquid reactants (analytical grade) were supplied by a precision pump (series M, RCT, Heidelberg, Germany). The reactor and plumbing were found to be leak-tight up to 35 bar. The exit stream from the reactor was analyzed by gas chromatography (HRGC 5300, Carlo Erba Instruments, Rodano, Italy), equipped with a Porapak QS packed column and TCD and FID detection capability. Analysis was made by periodic injection (~ 20 minutes) via a 6-way gas sampling loop. The entire line from the back-pressure regulator up to, and including the sampling loop, was kept to 135 °C to avoid product condensation. Calibrations for all reactants and likely products were made with the aid of pre-mixed gases of known composition (Sauerstoffwerk, Lenzburg, CH) (see appendix A.4.).

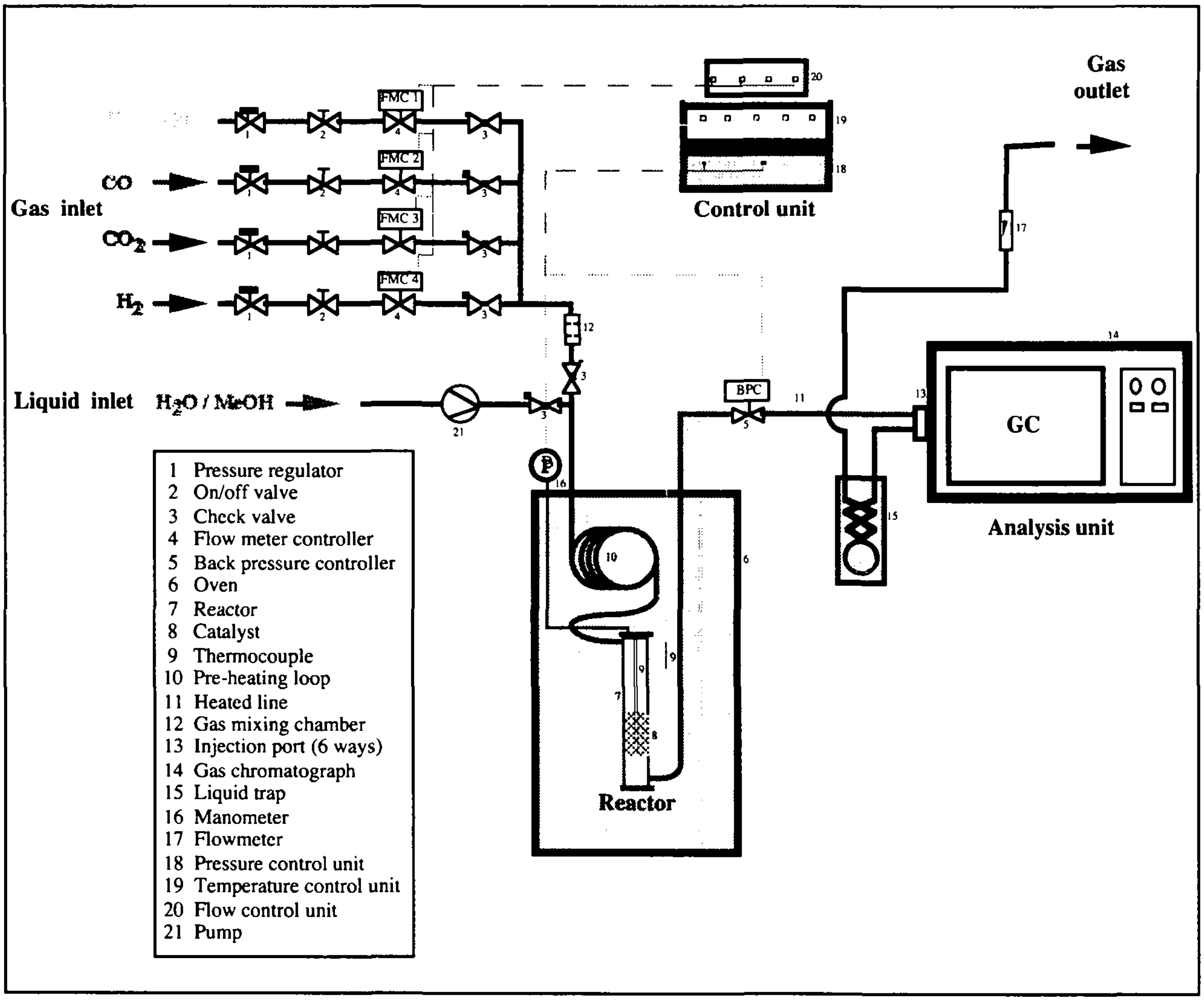
Gas outlet
Control unit
Gas inlet
CO
CO2
H2
Liquid inlet H2O / MeOH
FMC 1
FMC 2
FMC 3
FMC 4
BPC
GC
Analysis unit
Reactor
1 Pressure regulator
2 On/off valve
3 Check valve
4 Flow meter controller
5 Back pressure controller
6 Oven
7 Reactor
8 Catalyst
9 Thermocouple
10 Pre-heating loop
11 Heated line
12 Gas mixing chamber
13 Injection port (6 ways)
14 Gas chromatograph
15 Liquid trap
16 Manometer
17 Flowmeter
18 Pressure control unit
19 Temperature control unit
20 Flow control unit
21 Pump

Fig. 8: Schematic view of the tubular reactor setup

Catalysts were ground, sieved, and the fraction with diameters from 250 - 500 μm was loaded (~ 8 g for the catalysts testing - ~ 0.5 g for the kinetics measurements) to fill the isothermal zone of the reactor. To eliminate the influence of the reactor walls on the flow pattern, the catalyst particle diameter was at least 10 times smaller than the reactor diameter. To minimize axial gradients, the ratio of the catalytic bed length to the particle diameter was in a range between 5 - 50 (Baiker *et al.* 1989, Dautzenberg 1988, Horàk *et al.* 1978, Thomas *et al.* 1967). Sample activation was done according to point 2.2.2.. Representative steady-state sampling was verified by allowing pre-equilibration for at least 30 minutes after step changes in the reactant pressures, temperatures, etc. No irreversible deactivation was observed on-stream, which was checked by finally returning to the original experimental conditions.

The precise running conditions are given in the corresponding chapters (chapter 3 and 4) where the different results are discussed.

2.3.2. The DRIFTS reactor

The DRIFTS reactor has been described in detail elsewhere (Weigel 1996). In essence the reactor was the high temperature/high pressure cell. The cell and the diffuse reflectance unit were located in a FTIR spectrometer (Brucker, IFS 55 S Equinox, Rheinstetten, Germany) equipped with a MCT photo detector. Cell temperature was feedback-regulated from a thermocouple placed directly in the sample holder. Gas reactants were supplied from pre-calibrated electronic flow-meter controllers (Brooks Instruments, Veenendaal, The Netherlands) and conducted upwards through the sample catalyst. The desired pressure was adjusted by a needle valve placed after the cell. Purity of the gases (Carbagas, Rümlang, CH) was greater than 99.99 %. The activation procedure (see below), as well as the measurements were carried out in situ, within the cell and the optical unit already adjusted in the spectrometer. A spectrum of the freshly reduced catalyst was then recorded as a background (1024 scans). Subsequent to the introduction of reactants defining the time origin, the surface species were detected by recording DRIFT spectra (800 cm^{-1} ≤ wavenumber ≤ 4000 cm^{-1}) as a function of the reaction time at a resolution of 4 cm^{-1}. Depending on the experiment, 64 to 256 scans were accumulated for each spectrum. Gaseous products were removed by the continuous stream of reactants passing over the catalyst. In this way the strong overlap of the signals of gaseous species with the ones of the adsorbates was reduced.

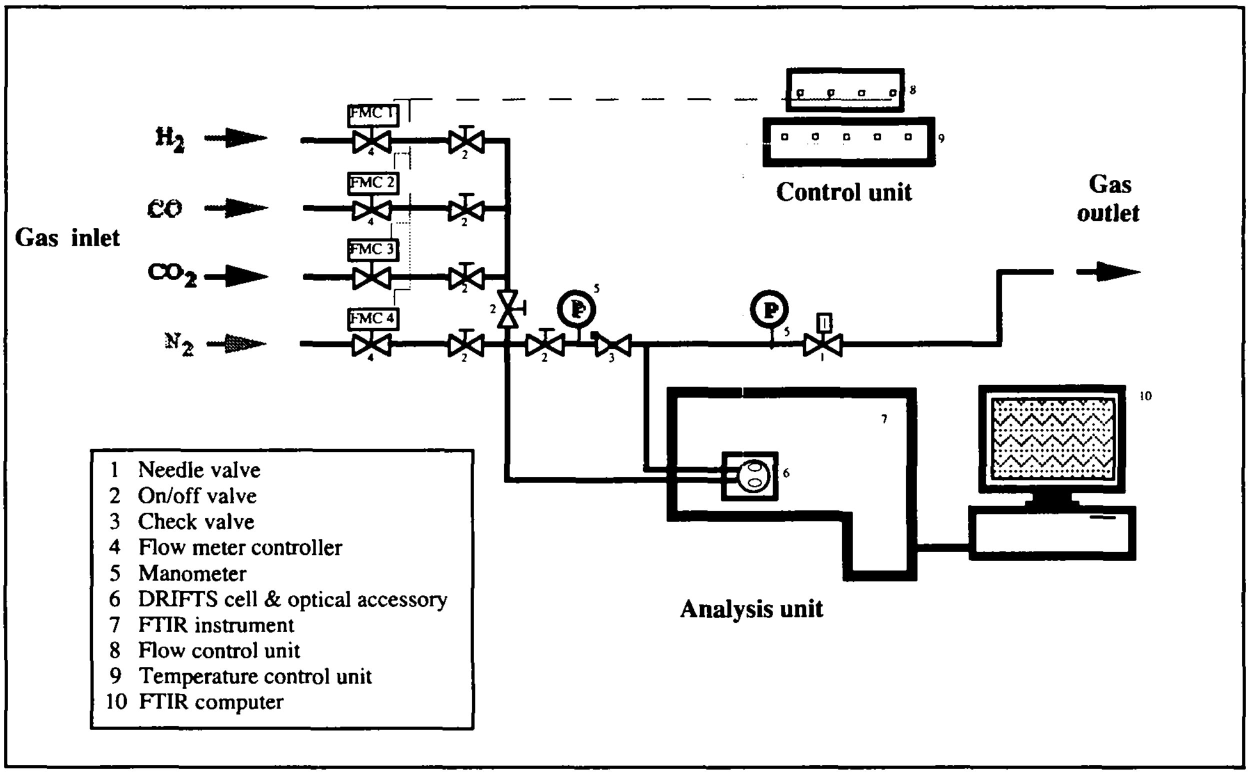
Gas inlet
H₂
CO
CO₂
N₂
FMC 1
FMC 2
FMC 3
FMC 4
Control unit
Gas outlet
Analysis unit
1 Needle valve
2 On/off valve
3 Check valve
4 Flow meter controller
5 Manometer
6 DRIFTS cell & optical accessory
7 FTIR instrument
8 Flow control unit
9 Temperature control unit
10 FTIR computer

Fig. 9: Schematic view of the DRIFTS reactor setup

Catalysts were ground, sieved, and the fraction with diameters from 90 - 150 µm was loaded (~ 50 mg) in the sample holder. For each measurement, new material was used. To ensure that spectra could be reproduced (Yeboah *et al.* 1984), the sample particles were packed under a constant pressure (1 MPa) (Weigel 1996).

The precise running conditions are given in the corresponding chapter (chapter 5) where the different results are discussed.

2.3.3. The modulation reactor

The reactor was a plug-flow fixed bed type (see appendix A.3.3.). It consisted of a stainless steel tube (l = adjustable to catalyst bed height, ID = 21 mm) in which the dead volume could be minimized by adjusting the reactor length to the catalyst bed height (see appendix A.3.3.). The reactor was placed in a vertically mounted furnace (Carbolite MTF 10/38/130, Sheffield, England) and the temperature was feedback-regulated (within ± 0.5 °C, in the isothermal zone). Three additional thermocouples were used for precise temperature measurement in the center of the catalyst bed. Gas reactants were supplied from pre-calibrated electronic flow-meter controllers (FMC series F, Bronkhorst Hi-Tec, Ruurlo, The Netherlands). A carrier gas was used to compensate each change in mass flows of the reaction gases. Pressure was adjusted by a needle valve located after the cell. Pure gases (Carbagas, Rümlang, CH), CO_2 (99.99 %), H_2 (99.995 %) and N_2 (compensation gas) (99.99 %) were used for the synthesis. The reactor and plumbing were found to be leak-tight up to 25 bar. The exit stream from the reactor was analyzed by a FTIR spectrometer (Bruker IFS 55 S Equinox, Rheinstetten, Germany) equipped with a multi-pass absorption cell (path length: 3.2 m, volume: 120 ml; Infrared Analysis Inc., Anaheim, USA). The rapid scan modus (scanner velocity = 150 kHz) of the spectrometer made it possible to record a spectrum of 8 scans at 4 cm^{-1} resolution within 0.5 s. Normally the instrument was operated at a scan speed of 7 $scan.s^{-1}$ at 4 cm^{-1}.

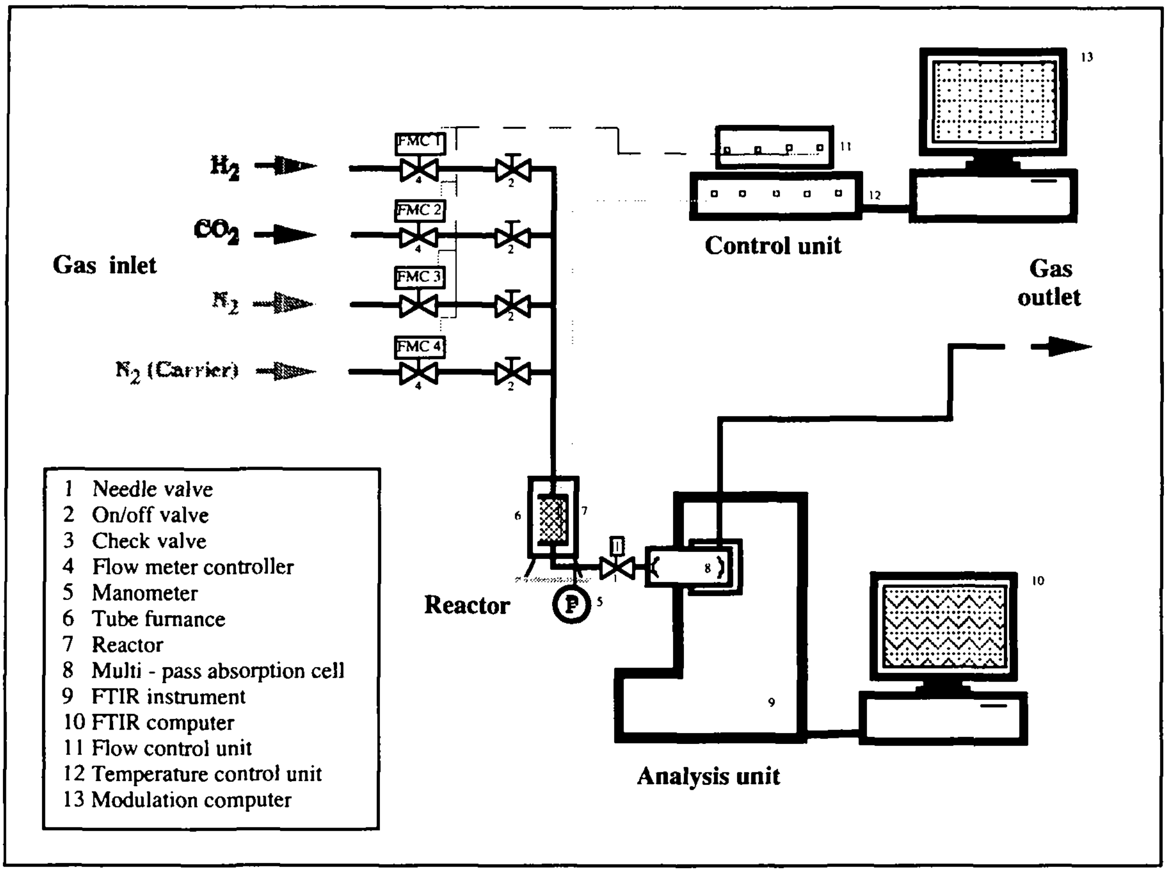
Gas inlet
H_2
CO_2
N_2
N_2 (Carrier)
FMC 1
FMC 2
FMC 3
FMC 4
4
2
11
12
13
Control unit
Gas outlet
6
7
8
5
Reactor
9
10
Analysis unit
1 Needle valve
2 On/off valve
3 Check valve
4 Flow meter controller
5 Manometer
6 Tube furnance
7 Reactor
8 Multi - pass absorption cell
9 FTIR instrument
10 FTIR computer
11 Flow control unit
12 Temperature control unit
13 Modulation computer

Fig. 10: Schematic view of the modulation reactor setup

The catalyst was ground, sieved, and the fraction with diameters from 90 - 125 μm was loaded (~ 2 g) to fill the isothermal zone of the reactor. To eliminate the influence of the reactor walls on the flow pattern, the catalyst particle diameter was at least 10 times smaller than the reactor diameter. To minimize axial gradients, the ratio of the catalytic bed length to the particle diameter was in a range between 5 - 50 (Baiker *et al.* 1989, Dautzenberg 1988, Horàk *et al.* 1978, Thomas *et al.* 1967). Sample activation was done according to section 2.2.2.. Representative steady-state sampling was verified by allowing pre-equilibration for at least 30 minutes at the desired experiment conditions. After recording the background spectrum (1024 scans at 4 cm^{-1} resolution) a modulation experiment was started by varying the inlet mass flow of one reaction gas sinusoidally using the desired modulation frequency. Each change in the mass flow of the reaction gas was compensated by the inverse change in the N_2 (compensation gas) mass flow. Therefore pressure and overall mass flow was constant during the experiments[2]. After waiting at least three modulation periods to enable adjustment of the system to the external perturbation, we started recording spectra by triggering the spectrometer at the starting time of the following modulation period. A set of 60 spectra was recorded during nearly two modulation periods. Modulation frequency limits of $\omega = 1.39 \cdot 10^{-4}$ Hz (period of 2 h) and $\omega = 3.33 \cdot 10^{-2}$ Hz (period of 30 s) were given by the experimental setup. The lower limit is due to the instability of the background, and the upper limit is determined by the dead volume of the system. The phase shift ϕ between the different reactants and products was deduced by determining the arithmetic average of one-phase shift of peak maxima and one-phase shift of peak minima. Examination of a contour plot of the spectra is a convenient way to determine ϕ.

---

[2] A computer (modulation computer) equipped with the Labview software and the corresponding interfaces allowed process monitoring, control and data storage.

The precise experimental conditions are given in the corresponding chapter (chapter 5) where the different results are discussed.

3. Testing of methanol synthesis catalysts

3.1. Scope

Three catalysts are evaluated for use in methanol synthesis from pure carbon dioxide and hydrogen. Performance is shown below as a function of temperature, pressure, space velocity and H_2/CO_2 ratio. Only for the most active catalyst tests were carried out with variable $H_2/CO_2/CO$ mixtures. All experiments were performed under identical process conditions using the tubular reactor.

3.2. Introduction

In industrial processes, methanol is synthesized from combinations of CO, CO_2 and H_2. Typical feeds contain ca 5 % vol. of CO_2 in addition to CO/H_2 (Bart *et al.* 1987). The fundamentals[3] of methanol synthesis by CO_2 hydrogenation and its practical[4] applications have received considerable attention recently. Fundamental interest focuses on the ability of CO_2 to promote methanol synthesis from CO (Bart *et al.* 1987, Chinchen *et al.* 1988, Klier 1982). A small amount of CO_2 in the feed (generally around 5 % vol.) boosts the reaction. Practical application is of interest as the reaction has been recognized as a promising process for the utilization of CO_2 and for reducing global warming caused by the greenhouse gases (CO_2, CH_4, ...) (Eliasson 1993, Eliasson 1994). Although catalysts composed of $CuO/ZnO/Al_2O_3$ are highly effective for $H_2/CO/CO_2$ feeds, they are not necessarily as effective for pure CO_2.

However in recent years a new generation of catalysts has been developed, and these are very active for H_2/CO_2 mixtures. Like the syngas catalysts, they are characterized by an adequate surface area (typically 100 $m^2.g_{cat}^{-1}$, 50 Å particles) of copper and zinc oxide that allow chemisorption for catalysis, and a finely dispersed (20 Å) refractory support (Al_2O_3) to counteract thermally induced sintering. Chain-growth mechanism (higher alcanes, higher alcohols, ...) and early deactivation or poisoning (sulfur and halogen) have also been minimized. Catalyst characterization is of great importance to ascertain the relative performance of these catalysts. It provides a basis for understanding the interrelationship between activity and selectivity and its physical and chemical properties. But as comparison of catalysts' performance is not always straight-forward, because of considerable variation in the reaction conditions (pressure, temperature, feed gas composition, etc.), it seemed reasonable to perform comparative tests under identical and well-defined process conditions.

---

[3] More than 1000 publications over the methanol synthesis from pure CO_2 and/or CO since 1990 (see literature statistics in the bibliography chapter).

[4] ICI Katalco (England) runs a commercial plant which effectively reacts only H_2 and CO_2 to methanol.

3.3. Apparatus

The experiments presented in this chapter were performed in the tubular reactor setup described in paragraph 2.3.1.. Samples of 6 to 8 g were charged into the reactor. The effect of one parameter (temperature, pressure, ...) was studied by varying its value while the other parameters were kept constant. The system was allowed to stabilize for 30 minutes at each parameter value. Some of the measurements were repeated at random to verify that the steady-state was attained.

3.4. Catalysts activation

Catalysts were reduced according to the procedure described in paragraph 2.2.2..

3.5. Results and discussion

3.5.1. Temperature variation

a) Products distribution

The influence of temperature on the mole fractions is given in figure 11 for catalyst C and the standard measurement ($P = 20$ bar, H_2/CO_2 ratio = 3, $Q_{total} = 600$ Nml.min^{-1} and gas hourly space velocity[5] $S_v = 4500$ h^{-1}).

---

[5] See Appendix A.2. for parameter definition.

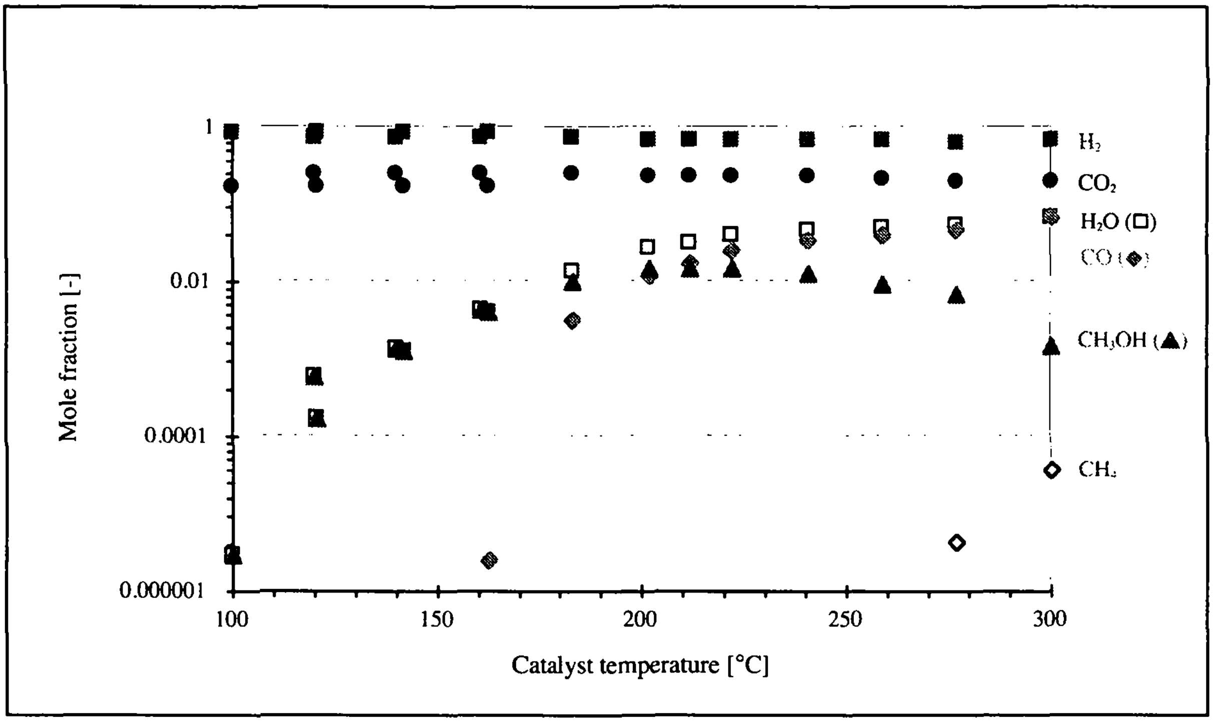

Fig. 11: Products distribution (mole fraction)
(catalyst C, P = 20 bar, H_2/CO_2 = 3, S_v = 4500 h^{-1})

As applies in almost all chemical reactions, temperature is an important factor. Product selectivity and activity, as well as catalyst activity, are largely dependent on this parameter. For all three catalysts, the three main products resulting from CO_2 hydrogenation are methanol, carbon monoxide and water. Methane is also formed at higher temperatures (190 °C for catalyst A and above 270 °C for catalysts B & C) but the amount produced is negligible (at 300 °C: ~ 2.5 ‰ for catalyst A and ~ 60 ppm for catalysts B & C). No other products are detected under these experimental conditions although high temperatures favor the formation of light alcanes, dimethyl ether and esters. CO, H_2O and CH_4 concentrations increase as the temperature is raised. CH_3OH concentration is greatest at about 220 °C. Typical selectivities for catalyst C (P = 20 bar, H_2/CO_2 = 3, S_v = 4500 h^{-1}) are given in table 6.

Table 6: Results of methanol synthesis from pure CO_2 (catalysts C)

		Selectivity		
Temperature [°C]	**CO_2 conversion** [%]	**CH_3OH** [%]	**CO** [%]	**CH_4** [%]
220	16.2	37.6	62.3	0.0
300	28.3	2.1	97.2	0.7

The influence of temperature on the experimental CO_2 conversion is given in figure 12 Thermodynamic values are also plotted (based on the equations given in appendix A.1.).

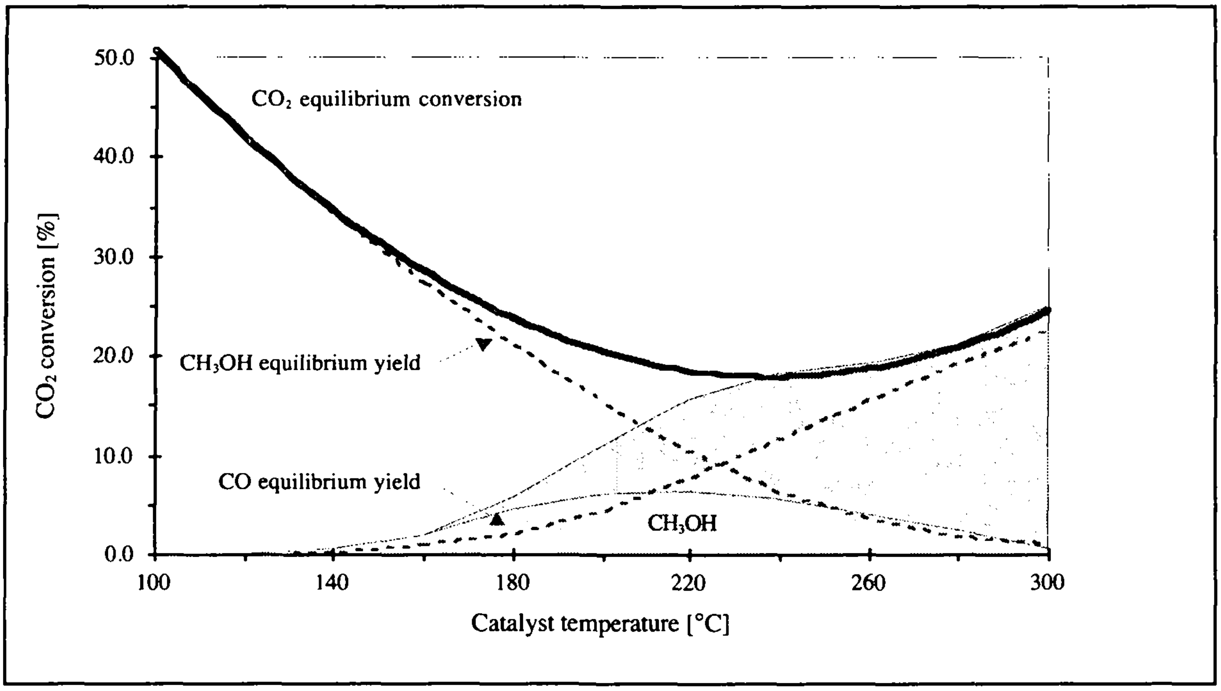

Fig. 12: Experimental CO_2 *conversion and yield in comparison to equilibrium conversion and yield (catalyst C,* $P = 20$ *bar,* $H_2/CO_2 = 3$*,* $S_v = 4500\ h^{-1}$*)*

The graph shows that temperature has a considerable effect on the conversion of CO_2, as well as on the products' selectivity.

Above 130 °C the methanol fraction starts to increase, reaching a maximum at 220 °C, and then decreases as expected for an exothermic reaction. Equilibrium yield (dashed line) is reached at 250 °C. In contrast, the CO fraction increases linearly with temperature above 150 °C. It also reaches equilibrium values at temperatures above 240 °C. Small fractions of CH_4 (not visible on the figure) are formed at temperatures above 280 °C.

The experimental CO_2 conversion increases as temperatures rise and becomes equilibrium-limited at temperatures above 240 °C. Unfortunately at these temperatures, the CO_2 is mainly converted to CO. However figure 12 clearly shows that high levels of CO_2 conversion can also be achieved at temperature below 240 °C (as expected in an exothermic reaction) and in particular when CH_3OH is the main product (as expected for the equilibrium calculations). In order to enhance the equilibrium conversion, the reaction may need to be carried out at lower temperatures and with a more effective catalytic system.

The parallel reaction to the methanol synthesis reaction is the reverse water-gas shift reaction:

$$CO_2 + H_2 \leftrightarrow CO + H_2O_{(g)} \qquad (14)$$

and figure 12 shows that it starts to take place as soon as temperatures rise above 150 °C. This complicates understanding of methanol synthesis as the forward/reverse water-gas shift reaction also proceeds very actively with the same catalyst.

Standard measurements (P = 20 bar, $H_2/CO_2 = 3$ and $S_v = 4500\ h^{-1}$) were taken with the three catalysts. Temperature influence on methanol yield is given in figure 13.

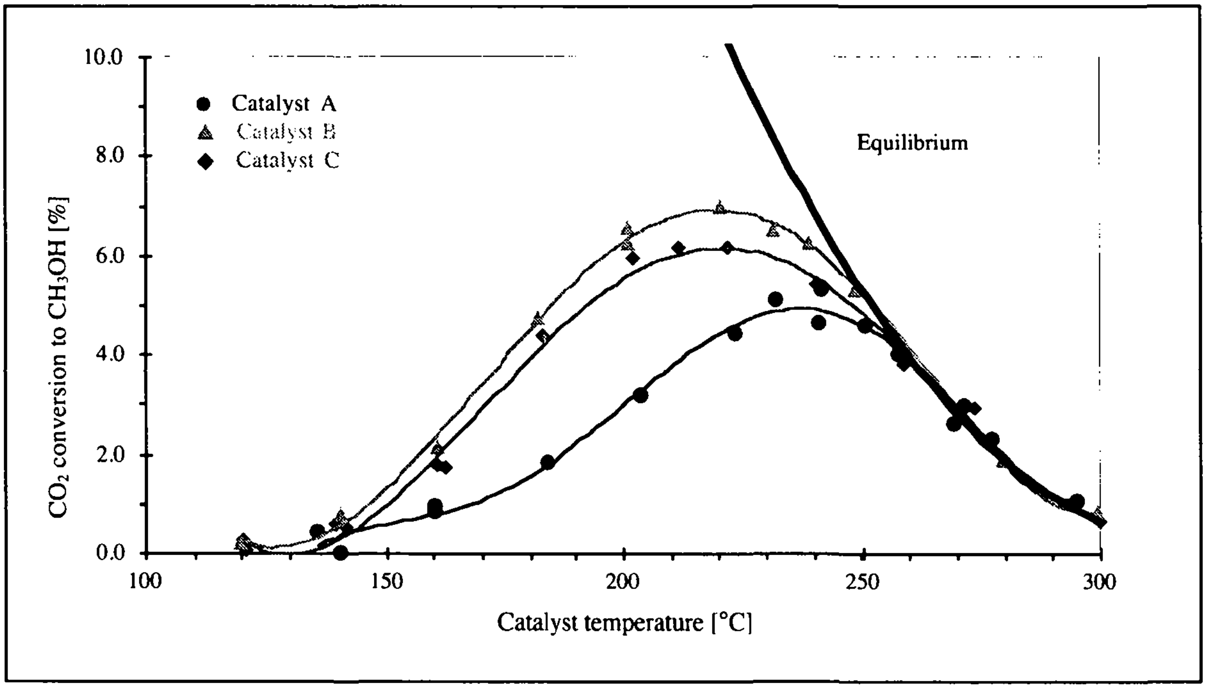

Fig. 13: CO_2 conversion to methanol as a function of temperature
($P = 20$ bar, $H_2/CO_2 = 3$, $S_v = 4500\ h^{-1}$)

When the methanol yield is plotted against the temperature the trend is similar for all three catalysts. Catalyst B gives the highest methanol yield (7.1 %) and has the lowest optimum temperature (222 °C). Catalyst C gives a lower yield (6.1 %) reached at a slightly higher optimum temperature (224 °C). In the case of catalyst A, the optimum temperature is shifted to a higher value (238 °C) and the methanol yield is much lower (4.8 %). Table 7 summarizes the catalysts' performance.

Table 7: Summary of the best methanol yield results ($P = 20$ bar, $H_2/CO_2 = 3$, $S_v = 4500\ h^{-1}$)

	Optimum temperature	**CO_2 conversion** [%]		**CH_3OH selectivity** [%]	
Catalyst	[°C]	Measured	Equilibrium	Measured	Equilibrium
A	238	12.5	18.1	38.4	37.0
B	222	17.2	18.2	43.8	54.9
C	224	16.3	18.1	38.0	52.6

As previously mentioned, all three catalysts give equilibrium yields when the temperature reaches 250 °C.

b) Apparent activation energy

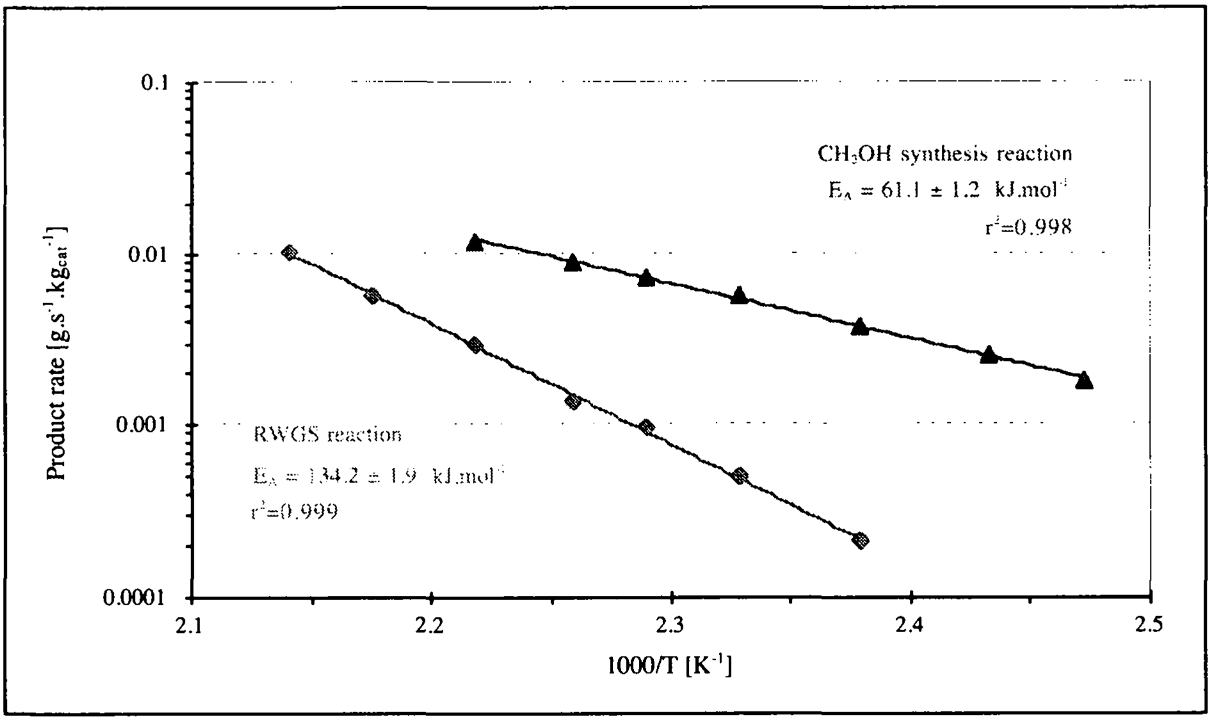

Fig. 14: Arrhenius plot of the methanol synthesis reaction and the RWGS reaction (catalyst B, $P = 20$ bar, $H_2/CO_2 = 3$, $S_v = 4500\ h^{-1}$)

A plot of product rate versus temperature in the Arrhenius form is presented in figure 14 where temperatures range from 130 to 200 °C. According to the results in figure 12, the CO_2 conversion remains below 10 % in this temperature range. From the linear regression, an apparent activation energy of $E_A = 61.1 \pm 1.2$ kJ.mol^{-1} is obtained for the methanol synthesis reaction (eq 4) and a higher value $E_A = 134.2 \pm 1.9$ kJ.mol^{-1} is obtained for RWGS reaction (eq 5) (deduced from the CO formation rate).

Table 8 summarizes a series of apparent activation energy values from the literature (with details of the experimental conditions).

Table 8: Apparent activation energies

	E_A (apparent)		**Experimental conditions**			
Catalyst type	**CH_3OH synthesis** [kJ.mol^{-1}]	**RWGS** [kJ.mol^{-1}]	**Temperature** [°C]	**Pressure** [bar]	**Feed gas** [-]	Ref.
$CuO/ZnO/Al_2O_3$	104.0	109.0	170 - 220	50	H_2/CO_2	(Rozovskii *et al.* 1976)
$CuO/ZnO/Al_2O_3$	65.2	123.4	210 - 245	15 - 50	H_2/CO_2	(Graaf *et al.* 1988)
$CuO/ZnO/Al_2O_3$	54.3	-	200 - 280	60	$H_2/CO_2/CO$	(Le Peltier 1989)
$CuO/ZnO/Al_2O_3$	77.7	125.0	200 - 250	50 - 100	H_2/CO_2	(Höltje 1990)
CuO/ZnO	64.0	121.0	150 - 250	1	H_2/CO_2	(Bardet *et al.* 1981)
CuO/ZrO_2	47.9	93.2	200- 260	17	H_2/CO_2	(Koeppel 1991)

Apparent activation energies (E_{app}) vary widely (typically 50 to 100 kJ.mol^{-1}) for the methanol synthesis reaction. In contrast, E_{app} for the RWGS reaction are much more closely grouped (95 to 125 kJ.mol^{-1}). The disparity between the values can be explained by changes in the reaction mechanism according to the catalysts composition/preparation and by differences in the experimental conditions (Bond 1990, Koeppel 1991). Once again, this clearly indicates that a comparison of catalysts is not straight-forward when measurements are not taken under the same conditions.

3.5.2. Pressure variation

In common with almost all gaseous reactions, the total pressure is an important consideration. Figure 15 shows the effect of pressure variations for the three catalysts at mean temperature[6] ($T_{cat\ A}$ = 240 °C, $T_{cat\ B}$ = 220 °C, $T_{cat\ C}$ = 225 °C). This relationship is particularly apparent for catalyst B, giving the highest methanol yield, 9.5 %, at a pressure of 30 bar. It is much less noticeable for catalysts A & C.

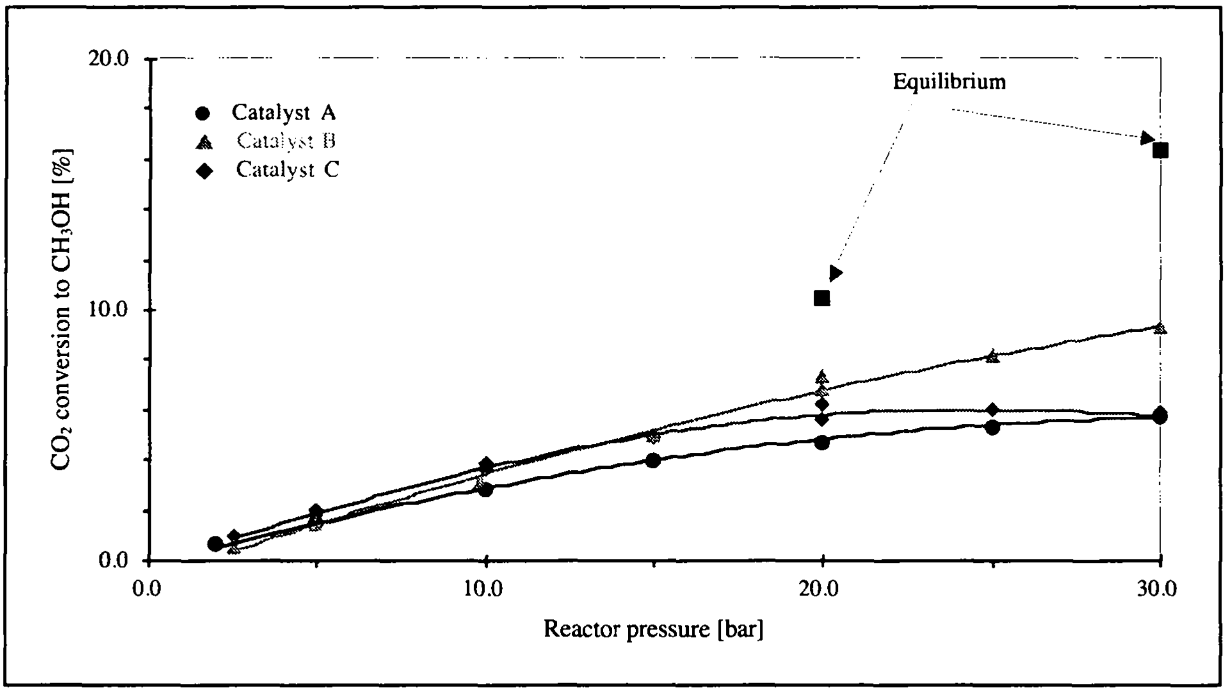

Fig. 15: CO_2 conversion to methanol as a function of the total pressure
($T_{cat\ A}$ = 240 °C, $T_{cat\ B}$ = 220 °C, $T_{cat\ C}$ = 225 °C, H_2/CO_2 = 3, S_v = 4500 h^{-1})

For catalyst B, a methanol yield of 9.5 % is reached at a pressure of 30 bar. This tendency can be explained by Le Chatelier's principle as the methanol synthesis reaction (eq 4) proceeds under a volume contraction. Higher methanol yields are therefore obtained at higher pressures. Table 9 summarizes the catalysts' performance.

---

[6] Indeed when increasing the pressure, the optimum temperature was shifted slightly towards higher values. Therefore a mean temperature was arbitrarily chosen.

Table 9: Summary of the best methanol yield results ($T \approx 220$ °C, $H_2/CO_2 = 3$, $S_v = 4500\ h^{-1}$)

	Mean temperature	**Pressure**	**CO_2 conversion** [%]		**CH_3OH selectivity** [%]	
Catalyst	[°C]	[bar]	Measured	Equilibrium	Measured	Equilibrium
A	240	20	12.5	18.1	38.4	34.8
B	220		17.2	18.2	43.8	57.1
C	225		16.3	18.1	38.0	51.5
A	240	30	16.9	20.7	33.7	53.6
B	220		20.5	22.1	46.3	73.7
C	225		16.0	21.8	37.5	69.6

Fujiwara et al.'s study, performed under similar conditions, gave a methanol yield of 7 % and 11 % at pressures of 20 bar and 30 bar respectively (Fujiwara *et al.* 1994). Lee et al. reported a yield of 4.8 % at 30 bar (Lee *et al.* 1993).

For reversible chemical reactions, their rates are influenced by the reactant and product concentrations. For normal gas solid catalytic reactions, the concentrations in the reactor can be more conveniently substituted by partial pressures (p_i). Assuming ideal gas behavior ($p_i = y_i \cdot P$) and a power law functionality ($R_\alpha = k_\alpha \cdot \left(\Pi\, p_i^{n_i}\right)$), the methanol formation rate is then proportional to:

$$R_{CH_3OH} \ \alpha \ P^{\left(n_{CO_2}+n_{H_2}+n_{CO}+n_{H_2O}+n_{CH3OH}\right)} \qquad (15)$$

where the power terms are to be experimentally determined for CO_2, H_2, CO, CH_3OH and H_2O. For catalyst B, total pressure influence on methanol rate is given in figure 16.

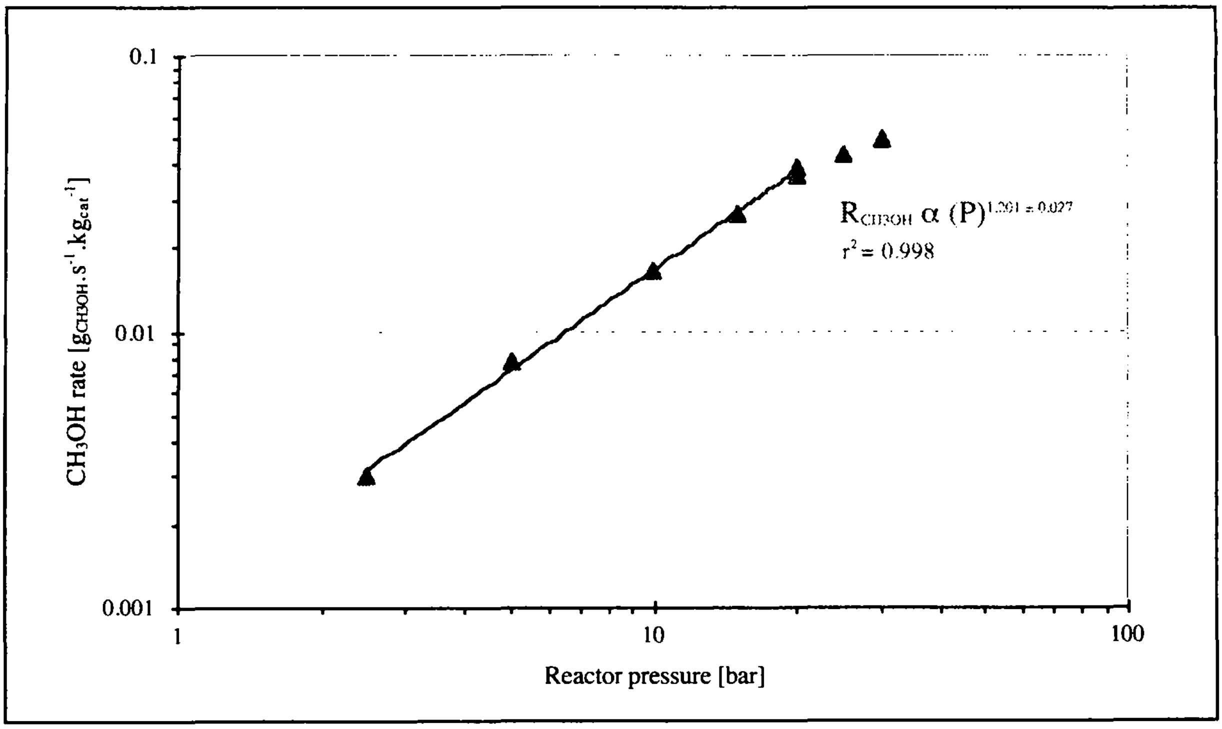

Fig. 16: Methanol rate as a function of the total pressure (catalyst B, T = 220 °C, H_2/CO_2 = 3, S_v = 4500 h^{-1})

For catalyst B, the sum of the average values of the single partial pressures exponent (exponents values are: $\bar{n}_{CO_2} = 0.376$, $\bar{n}_{H_2} = 1.544$, $\bar{n}_{CO} = 0.073$, $\bar{n}_{H_2O} = -0.656$, $\bar{n}_{CH_3OH} = 0.263$; refer to chapter 4) is slightly higher (1.599) than the deduced total pressure exponent 1.201. Nevertheless the correlation rate is satisfactory given that the partial pressures are not constant and the ranges as well as the temperatures are not exactly the same. One possible explanation for this deviation is the positive exponent value for methanol partial pressure. In fact, for very low methanol partial pressures (0.2 - 2 bar), the methanol rate seems to be enhanced.

3.5.3. Space velocity variation

Space velocity influence on methanol yield is given in figure 17. The methanol yield gradually decreases from 1000 to 9000 h^{-1} as space velocity increases (equivalent to a contact time decrease from 3.6 to 0.4 s). This effect is clearly observed for catalysts B and C.

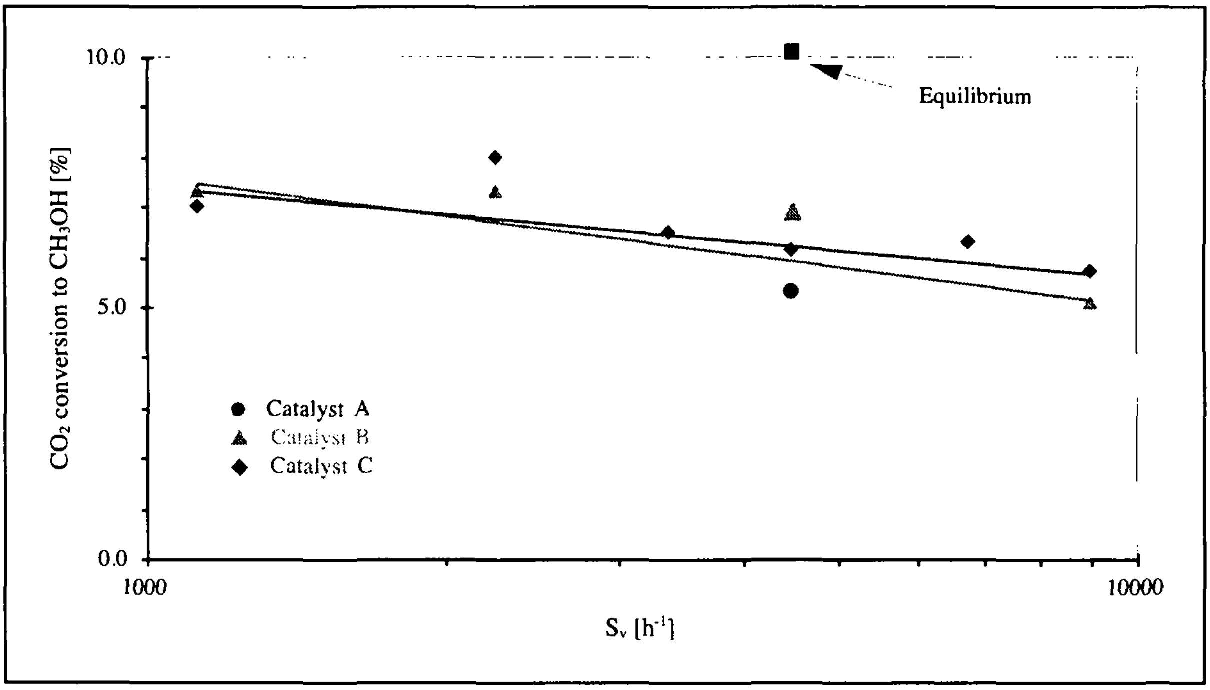

Fig. 17: conversion of CO_2 to methanol as a function of space velocity
($T_{cat\,A}$ = 240 °C, $T_{cat\,B}$ = 220 °C, $T_{cat\,C}$ = 225 °C, H_2/CO_2 = 3, P = 20 bar)

There is a 1.8 % drop in the methanol yield for catalyst B and 1.2 % for catalyst C. The general trend is similar for all the catalysts. The linear decrease of the methanol yield with higher space velocities (above 2250 h^{-1}) indicates the absence of external mass transfer. This state is more evident when expressing the yield in $g_{CH_3OH}.s^{-1}.kg_{cat}^{-1}$ (Fig. 18).

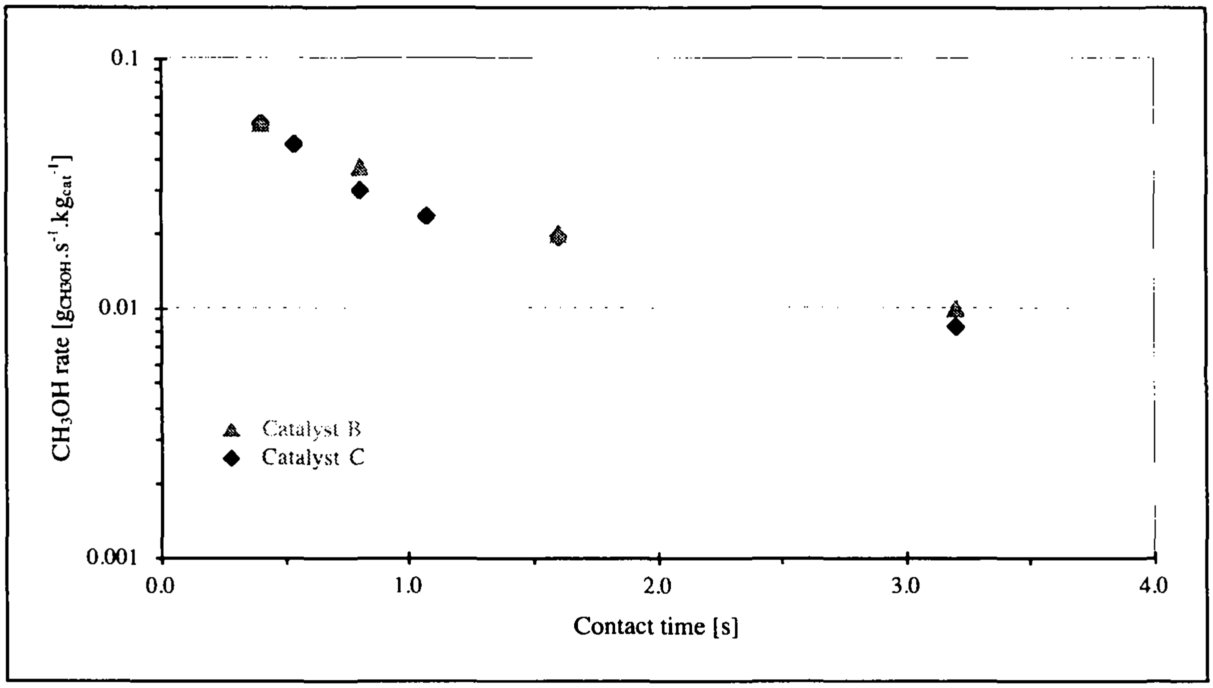

Fig. 18: Methanol activity as a function of the contact time
($T_{cat\,B}$ = 220 °C, $T_{cat\,C}$ = 225 °C, H_2/CO_2 = 3, P = 20 bar)

3.5.4. H_2/CO_2 ratio variation

Feed ratio composition influence on the methanol yield is given in figure 19. CO_2 conversion to methanol is given as a function of the temperature for two different ratios; the stoichiometric ratio and a H_2 rich gas composition. Although the trend is similar, the methanol yield is strongly dependent on the H_2/CO_2 ratio. As shown in chapter 4, hydrogen partial pressure is the dominant influence on the methanol yield. For a H_2/CO_2 ratio of 10 (9.1 % mol CO_2 in the feed), the methanol yield is 18.2 % with catalyst B, and 17.0 % with catalyst C. When compared to the stoichiometric ratio yield it represents an increase of 11.1 % for catalyst B and 10.8 % for catalyst C. Methanol selectivity is also increased when the H_2/CO_2 ratio is higher than 3. Optimum temperature is the same for both ratios and the thermodynamic equilibrium is also obtained before the temperature reaches 250 °C. Höltje (Höltje 1990) reports under similar conditions (P = 50 bar, T = 220 - 240 °C) maximum yields between 15 and 20 % mol CO_2.

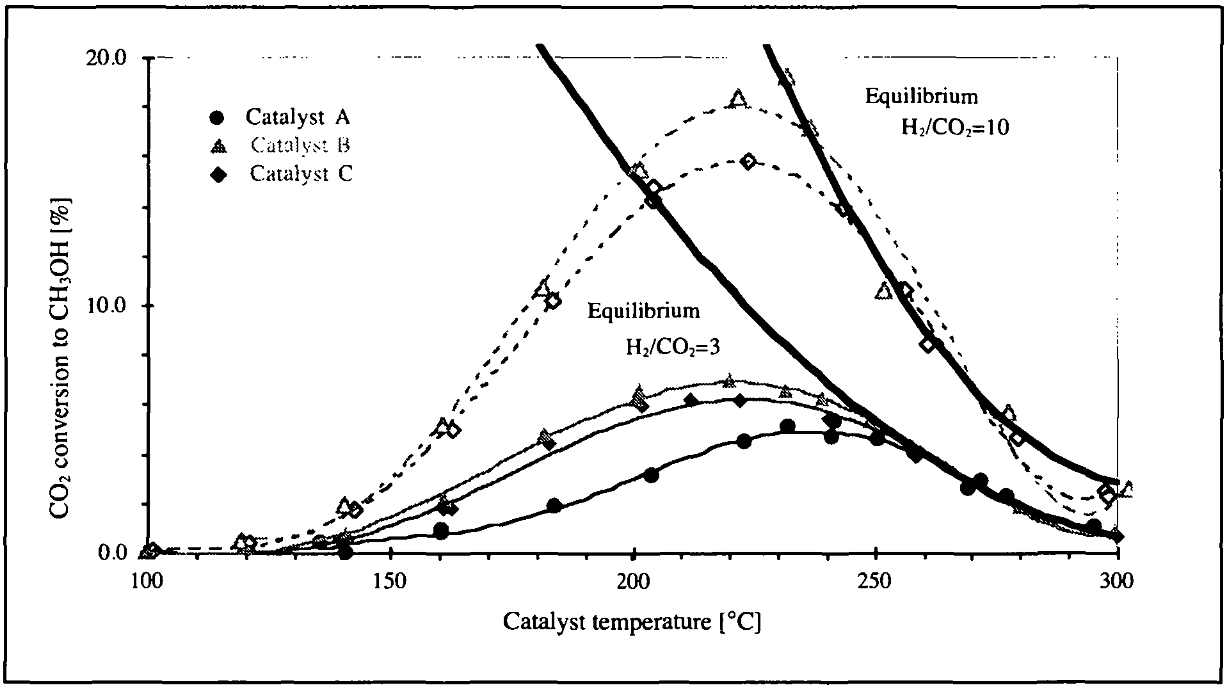

Fig. 19: CO_2 conversion to methanol as a function of feed ratio
($P = 20$ bar, $H_2/CO_2 = 3$, $S_v = 4500\ h^{-1}$)

As a general rule, a certain excess of hydrogen is left in the feed gases to improve the methanol yield (Supp 1990). But the precise feed composition (particularly on the catalyst surface) must always be carefully considered because it will profoundly influence the interplay of the different mechanistic pathways.

3.5.5. CO_2/CO ratio variation

A synergy effect between CO_2 and CO in methanol synthesis has long been recognized and methanol is currently almost exclusively produced from syngas ($CO/CO_2/H_2$ mixture, see paragraph 1.2.2.a)). For this reason a series of measurements with CO_2/CO ratio variation was taken but restricted to the best performing catalyst (catalyst B). CO_2, CO and H_2 partial pressures were adjusted so that the stoichiometric number[7] R remained constant and equal to 2. Temperature was set at 220 °C and total pressure was kept constant at 20 bar (adjusted with He as required).

The CO_2/CO ratio influence on the methanol yield is given in figure 20. When CO_2 is excluded from the reaction ($H_2/CO = 2$), a methanol yield of 2.2 % is obtained. When the reaction takes place in the absence of CO ($H_2/CO_2 = 3$, 25 % vol. CO_2) a value of 6.6 % is recorded. A maximum yield (14.1 %) is obtained when the CO_2 content in the syngas mixture is between 2.5 and 5.0 % vol..

When the CO_2 content of the synthesis gas is rising, the net CO conversion goes up to a maximum (14.9 %) and then drops steeply. CO_2 conversion, on the other hand, reaches an initial maximum (11.7 %), then passes through a minimum (5.2 %) before increasing again to 11.6 %. This behavior is, in part, due to the RWGS reaction that produces CO from CO_2 and H_2, thereby lowering the net CO conversion and increasing CO_2 conversion.

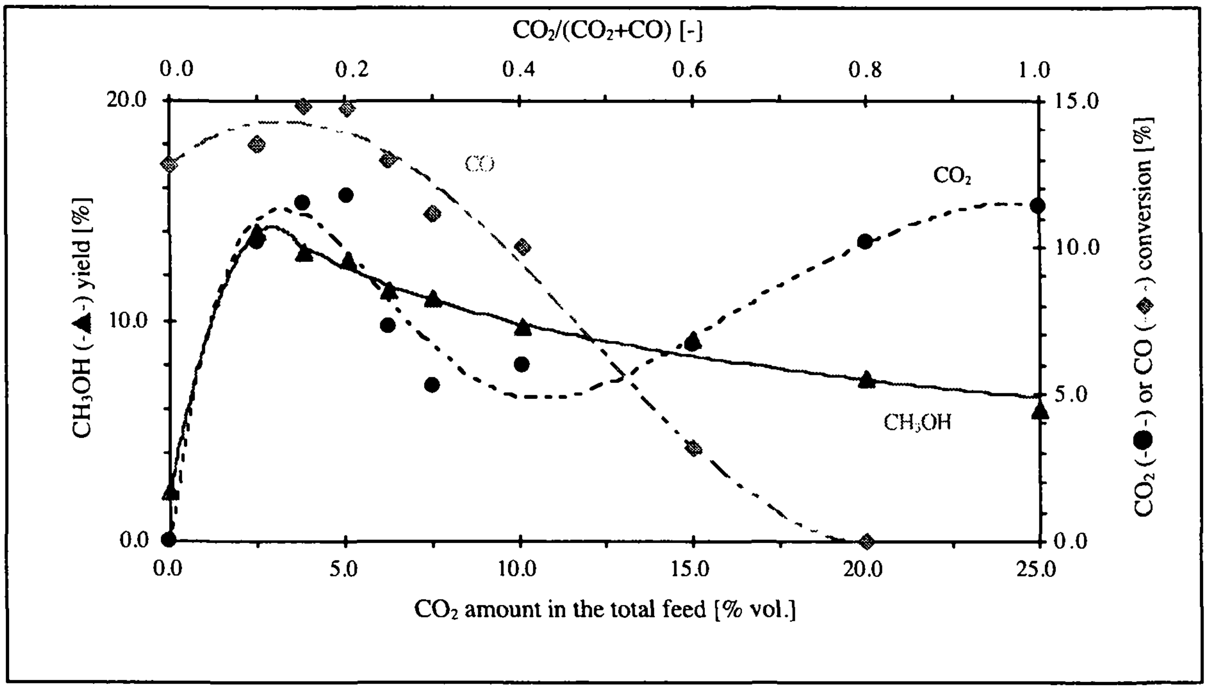

Fig. 20: Methanol yield, CO and CO_2 conversion as a function of the feed gas composition (catalyst B, $P = 20$ bar, $R = 2.0$, $T = 220$ °C, $S_v = 4500\ h^{-1}$)

---

[7] Synthesis gas mixtures are characterized by the stoichiometric number: $R = (H_2 - CO_2)/(CO + CO_2)$ where H_2, CO_2, and CO represent the respective concentrations [% mol]. An R value of 2 signifies a stoichiometric or balanced gas for the methanol synthesis.

Selectivities for particular conditions are summarized in table 10 (P = 20 bar, R = 2.0, T = 220 °C, Q_{total} = 600 Nml.min^{-1}, S_v = 4500 h^{-1}).

Table 10: Results of methanol synthesis from various C-sources (catalyst B)

Feed composition **H_2/CO/CO_2/He**	**R** [-]	**Carbon conversion** [%]	**CH_3OH selectivity** [%]
75.0/0.0/25.0/0.0	2	17.2	38.4
52.5/22.5/2.5/22.5	2	23.9	59.5
66.6/33.3/0.0/0.0	2	12.6	17.5

The methanol synthesis from CO_2 and CO can be summarized for a CO_2/CO ratio of unity in equation form:

$$CO_2 + CO + H_2 \leftrightarrow 2CH_3OH(g) + H_2O(g) \tag{16}$$

The stoichiometric number for this reactant composition is equal to 2. Sizgek et al. (Sizgek *et al.* 1994) compared methanol yields from syngas mixtures, in which the $H_2/(CO+CO_2)$ ratio was kept fixed at 5.66 and best results were obtained at a CO_2/CO ratio less than 1. The high methanol activity, indicated by a low level of CO_2 in the feed, is closely related to the copper metal surface area (Chinchen *et al.* 1988, Rasmussen *et al.* 1994a, Rasmussen *et al.* 1994b, Skrzypek *et al.* 1994, Spencer 1995) and to the ability of the support (oxide phase: ZnO, Al_2O_3) to store active hydrogen species (Bailey *et al.* 1995, Le Peltier *et al.* 1996). About 30 % of the initial copper surface area of a typical industrial catalyst is covered with adsorbed oxygen under working conditions (Chinchen *et al.* 1986b). A balance between a clean and a covered copper surface is required to achieve the optimum effect. The CO_2/CO ratio in the system determines the exact percentage.

To give complementary information, measurements were also performed (only for catalyst B) with pure CO. The temperature influence on the methanol yield is given in figure 21. When using CO as the sole C-source, the maximum methanol yield (4.8 %) is reached at a temperature of 265 °C. When compared to measurements using pure CO_2, the yield is slightly smaller and comes at a temperature 45 °C higher. Experiments that took place over a lesser number of days (~ 250 h^{-1}) also indicate a faster catalyst deactivation for pure CO.

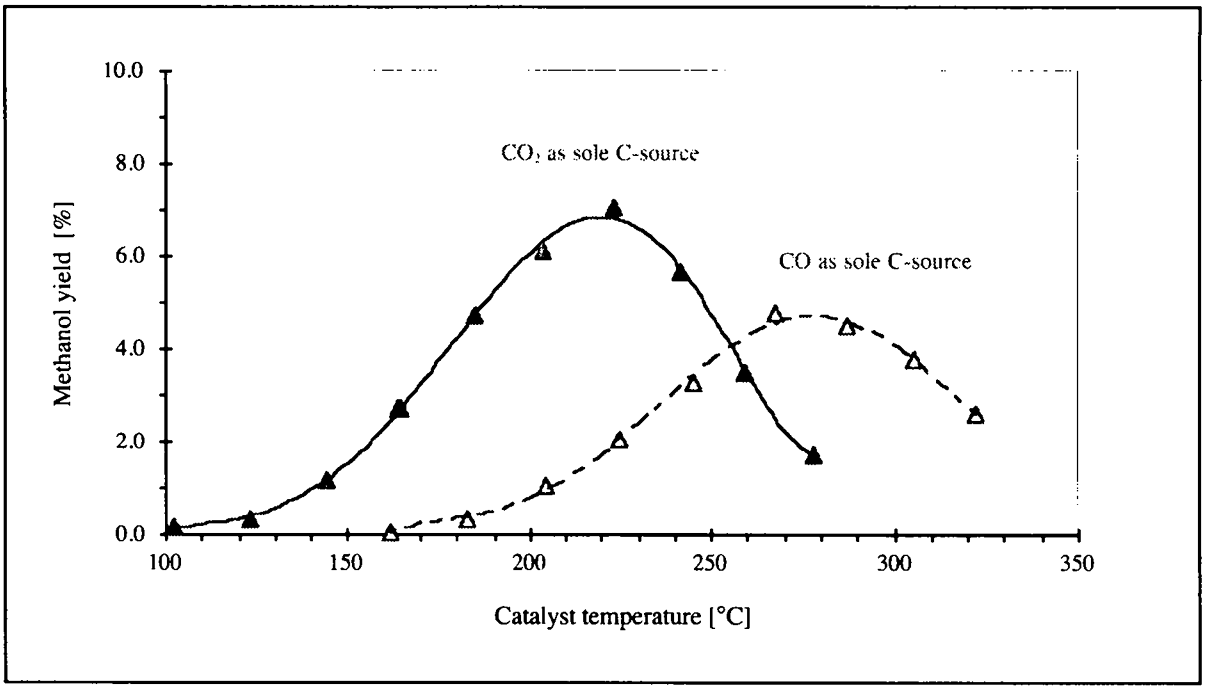

Fig. 21: Methanol yield for different C-sources as a function of the temperature (catalyst B, $H_2/CO = 2$ or $H_2/CO_2 = 3$, $P = 20$ bar, $S_v = 4500\ h^{-1}$)

Table 11 summarize the optimum conditions for catalyst B ($P = 20$ bar, $S_v = 4500\ h^{-1}$).

Table 11: Results of methanol synthesis from pure CO_2 and pure CO (catalyst B)

	Optimum temperature	**Carbon conversion**	**CH_3OH selectivity**
Feed composition	[°C]	[%]	[%]
pure CO_2	222	17.2	38.4
pure CO	265	14.3	33.4

4. Gas phase kinetics

4.1. Scope

Methanol formation rate dependence on the partial pressure of carbon dioxide, hydrogen, water, methanol and carbon monoxide is studied using catalyst B, the most active of the evaluated catalysts. Results are used to derive a possible Langmuir-Hinshelwood formulation for the methanol rate, and parameters are fitted with a non-linear regression. The derived rate expression is compared to the power law rate expression. The carbon monoxide formation rate is qualitatively discussed.

4.2. Introduction

Whenever a reactive process is considered, the kinetics are very important for the scale-up. Various theories have been proposed from which kinetic equations may rationally be developed. When heterogeneous catalytic reactions take place, various mechanistic steps are involved (external mass transfer, pore diffusion, chemisorption, intrinsic reaction, ...), the slowest step predominating in the global rate constant. Using an appropriate reactor to take measurements (see appendix A.3.1.), physical diffusion to and within the particle can be overcome so that, finally, the surface reactions remain relevant for the rate constant. For reactions taking place on an active site on the surface of a catalyst, they are usually found to occur successively in three steps. Initially molecules are adsorbed onto the surface and attached to an active site, and they then react with the molecule on the adjacent site and/or undergo further transformations. Finally, products are desorbed from the surface, thus liberating the sites (Levenspiel 1962).

According to Yang et al. (Yang *et al.* 1950), rate expressions, supposing a rate determining step, can all be written in the form:

$$\text{Rate} = \frac{(\text{Kinetic term})\cdot(\text{Potential term})}{(\text{Adsorption term})^{n}} \tag{17}$$

To prove that a rate equation is correct, it must be shown that this rate equation fits the data better than any alternative rate equation of any other postulated mechanism. Although advanced statistical methods are employed, rate expressions obtained for different mechanisms often have a very similar mathematical form (Boudart 1982, Carberry 1976), and therefore a number of alternative mechanisms may fit the data equally well. Differences in fit may also be so small that they can be explained by experimental error alone. For this reason the selected equation should only be considered as a good fit and not an accurate expression of reality. In fact, one can only recall the simplest precepts on which the Langmuir isotherm rests (monolayer adsorption, no interaction between adsorbed molecules, a constant heat of adsorption and lack of dependence on the surface coverage) and it is very surprising that the isotherm and rate equations based on it are so successful, when the conditions for their validity are so seldom fulfilled (Boudart 1986).

It must be emphasized that knowledge of the kinetics of a reaction does not in itself define the whole mechanism controlling the reaction. Other techniques are always required to establish the validity of the surface reaction (see chapter 5). There may be elementary steps intervening rapidly between reactants and products, but as they do not determine the rate, their existence is not revealed by the rate expression. Knowledge of these steps is necessary but not sufficient to describe the mechanism.

Another important aspect to consider when measuring the kinetic rate is that the experiments must be carried out at temperatures, pressures and concentrations that are relevant to the needs of industry. More often than not, reactions are carried out at ambient pressures with values extrapolated to much higher pressures with considerable loss of accuracy in the results. This is an inappropriate use of the information.

Kinetics measurements on "real world" catalysts are applied to the methanol synthesis reaction from pure CO_2. The methanol synthesis reaction is characterized by the methanol formation rate (R_{CH_3OH}), and the reverse water-gas shift reaction is qualitatively characterized by the CO formation rate (R_{CO}).

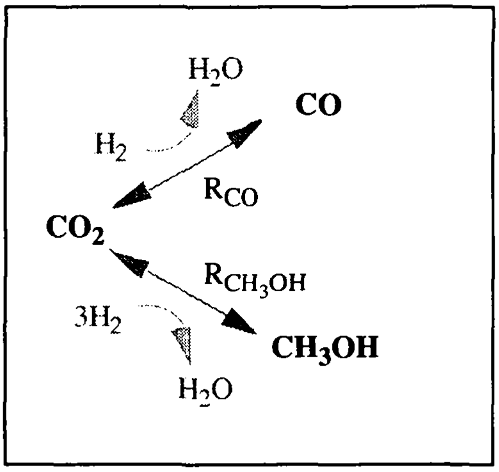

Fig. 22: Schematic diagram of the methanol reaction and the RWGS reaction

Changes in the composition of the feed are applied to the methanol synthesis reaction in order to develop a rate equation and to gain insight into the reaction scheme.

4.3. Apparatus

The experiments presented in this chapter were performed in the tubular reactor setup described in paragraph 2.3.1.. Samples of 500 mg were charged into the reactor to avoid mass and heat influences as well as radial and axial dispersion effects (Dautzenberg 1988, Horàk *et al.* 1978). Temperature was adjusted close to 200.0 °C (± 0.5). The effect of the partial pressure of one component was studied by varying its value while the other partial pressures were kept constant. Helium was used to compensate for pressure changes so that the total pressure remained constant at 20.0 bar (± 0.1). The system was allowed to stabilize for 30 minutes at each parameter value. Some measurements, chosen at random, were repeated to confirm that a steady-state had been achieved. Conversions were kept below 5 % to ensure differential mode (Baiker *et al.* 1989).

4.4. Results and discussion

4.4.1. Carbon dioxide partial pressure variation

The influence of CO_2 partial pressure on the methanol rate is shown in figure 23 for various H_2 partial pressures at a temperature of 200 °C.

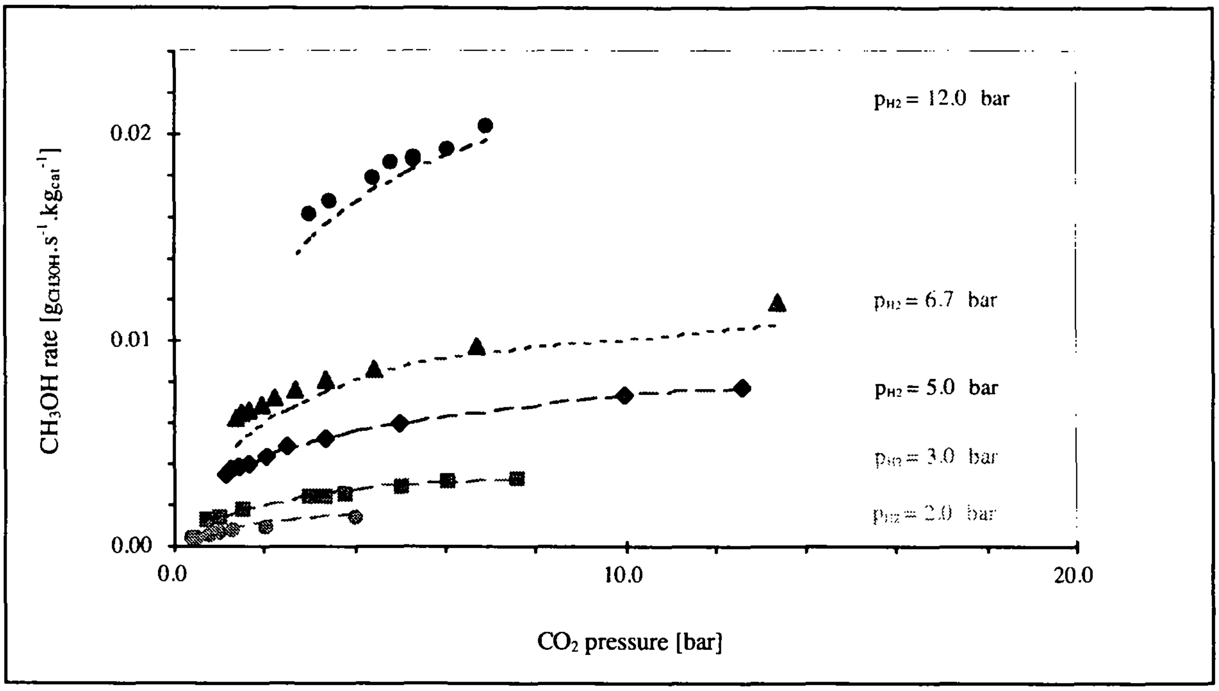

Fig. 23: Experimental (points) CO_2 partial pressure influence on the methanol rate in comparison to the developed model (dashed lines)
($P = 20.0 \pm 0.1$ bar (adjusted with He), $T = 203.1 \pm 0.5$ °C, $S_v = 4500\ h^{-1}$)

For a given H_2 concentration, the methanol rate initially increases with higher CO_2 partial pressures before stabilizing. All curves reveal a similar trend. Moreover as ulteriorly discussed, the estimated methanol formation rate from the developed model fits the experimental data. The thermodynamic calculations indicate that the reaction is not equilibrium limited. The CO_2 concentration above which the methanol rate remains constant is different for each partial pressure of hydrogen. Moreover as the curve shapes are unchanged at higher H_2 partial pressures, it is reasonable to assume a noncompetitive adsorption between H_2 and CO_2.

On $CuO/ZnO/Al_2O_3$ catalysts, CO_2 is found to be adsorbed in two forms: reversibly adsorbed (in equilibrium with the gaseous phase), and irreversibly adsorbed (can not be removed at a given temperature by decreasing the gas pressure) (Dennison *et al.* 1989, Dybkjær *et al.* 1981, Fujita *et al.* 1992, Jackson 1989, Kinnaird *et al.* 1987, Kinnaird *et al.* 1988). In addition to these two forms, CO_2 can be dissociatively adsorbed according to:

$$CO_2(g) \leftrightarrow CO_{(a)} + O_{(a)} \tag{18}$$

The heat of adsorption of CO_2 is found to be dependent on the coverage. It decreases from 50 to 30 $kJ.mol^{-1}$ with the coverage increasing from 0.2 to 0.6.

It is also difficult to separate the role of CO_2 from the roles of H_2O and CO due to the forward/reverse water-gas shift reaction (eq 5) and because they compete for the same active sites (Skrzypek *et al.* 1994). The ratio between the adsorption coefficients of CO_2 and H_2O can be estimated from other measurements. Assuming the reaction rate to be dependent on the active free sites (adsorption following a Langmuir isotherm) and considering a competitive adsorption between H_2O and CO_2 (see paragraph 4.4.4.), one can write:

$$R_{CH_3OH} = k_{CH_3OH} \cdot \frac{K_{CO_2} \cdot p_{CO_2}}{(1 + K_{CO_2} \cdot p_{CO_2} + K_{H_2O} \cdot p_{H_2O})} \cdot f(H_2) \quad \text{(at a given temperature)} \tag{19}$$

Given the selected conditions, the CO partial pressure remains a factor of 10 less than the CO_2 partial pressure so that, to a first approximation, the term $K_{CO} \cdot p_{CO}$ may be omitted. To a second approximation, for CO_2 partial pressures corresponding to a methanol rate limitation, the number 1 in the denominator may also be omitted. So at a given temperature and at a fixed hydrogen partial pressure, one can write:

$$R_{CH_3OH} = k_{CH_3OH} \cdot \frac{1}{\left(1 + \frac{K_{H_2O}}{K_{CO_2}} \cdot \frac{p_{H_2O}}{p_{CO_2}}\right)} \tag{20}$$

An estimation of the $\frac{K_{H_2O}}{K_{CO_2}}$ ratio can easily be deduced when plotting $\frac{1}{R_{CH_3OH}}$ as a function of $\frac{p_{H_2O}}{p_{CO_2}}$ (respecting the two assumptions). Typical values are given in table 12.

Table 12: Results of the K_{H_2O}/K_{CO_2} ratio (catalyst B, T = 203.1 ± 0.5 °C)

H_2 partial pressure [bar]	K_{H_2O}/K_{CO_2} [-]
3.0	10.8
5.0	13.6
6.7	14.3

Values increase with higher H_2 partial pressures. As the hydrogen concentration increases, the methanol synthesis rate is strongly enhanced (see paragraph 4.4.2.). More methanol is produced, and more water too, increasing the competition between H_2O and CO_2 for the same adsorption sites. Results agree closely with previous study results in the literature (Tagawa *et al.* 1987). Le Peltier (Le Peltier 1989) reported a ratio of 18, for a $CuO/ZnO/Al_2O_3$ catalyst (T = 215 °C and a H_2 partial pressure of 37 bar).

The apparent order (relative to CO_2) for the methanol rate can be deduced from a log-log plot (Fig. 24) over a wide feed ratio range ($0.5 \leq H_2/CO_2 \leq 6.0$). It is always positive and varies from 0.267 to 0.587.

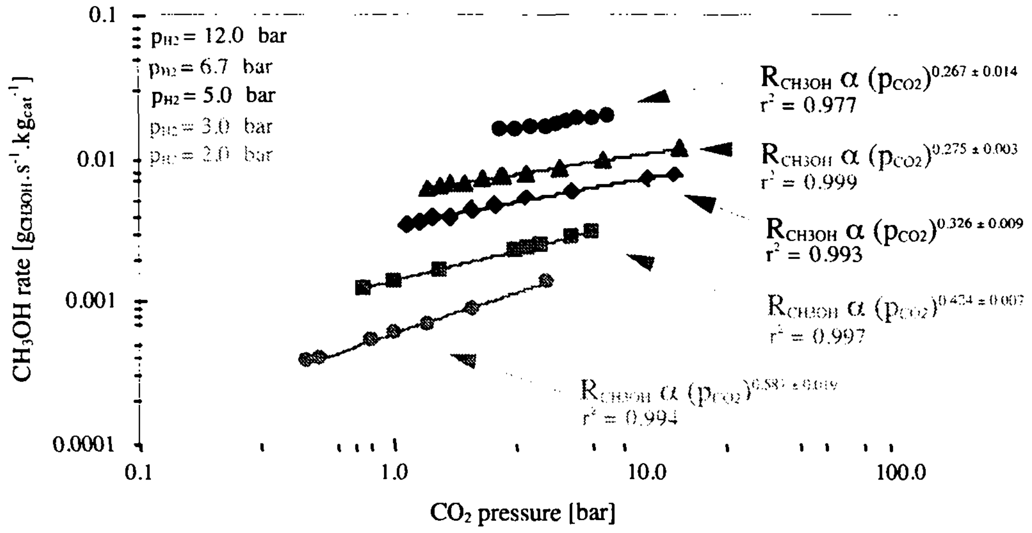

Fig. 24: CO_2 partial pressure variation (log-log plot)
(P = 20.0 ± 0.1 bar (adjusted with He), T = 203.1 ± 0.5 °C, S_v = 4500 h^{-1})

The CO rate is slightly slower particularly at higher CO_2 concentrations. The apparent order, for the same range of CO_2 pressures, varies from 0.395 to 0.446. This indicates that the CO rate is less dependent on CO_2 than the methanol rate.

4.4.2. Hydrogen partial pressure variation

The influence of H_2 partial pressure on the methanol rate is shown in figure 25 for various CO_2 partial pressures at a temperature of 200 °C. For a selected CO_2 concentration, the methanol rate increases linearly with higher H_2 partial pressures. Again all curves show a similar trend and the thermodynamic calculations indicate that the reaction is not equilibrium limited. CO_2 partial pressures have little influence on the methanol rate. As the curve shapes are unchanged at higher CO_2 concentrations, the absence of competitive adsorption between H_2 and CO_2 can be confirmed.

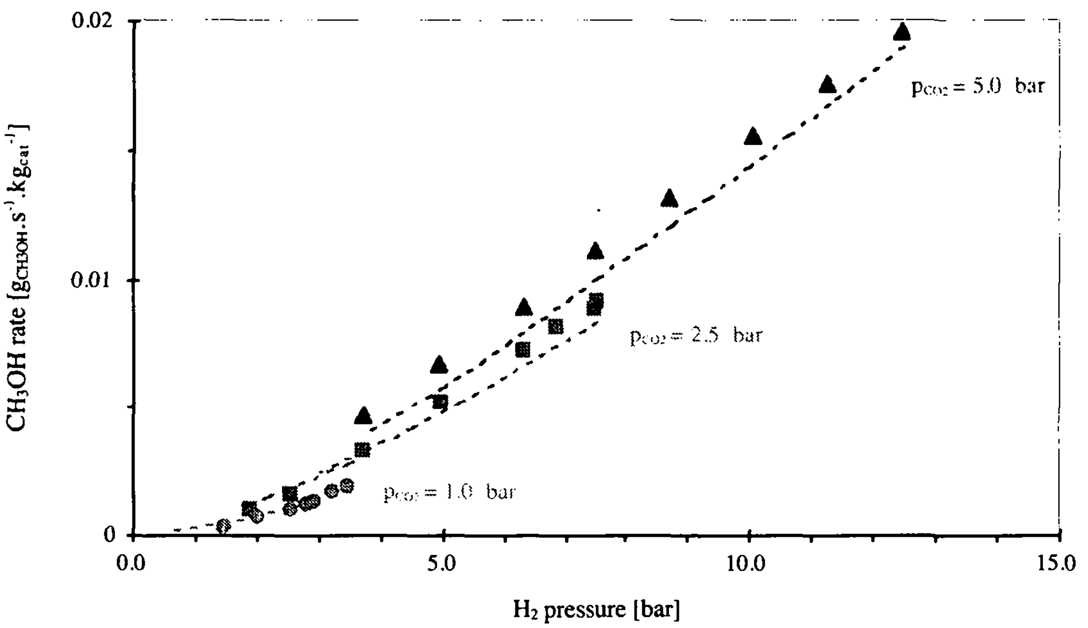

Fig. 25: Experimental (points) H_2 partial pressure influence on the methanol rate in comparison to the developed model (dashed lines)
($P = 20.0 \pm 0.1$ bar (adjusted with He), $T = 202.5 \pm 0.3$ °C, $S_v = 4500\ h^{-1}$)

The apparent order (relative to H_2) for the methanol rate is positive and varies from 1.142 to 2.131 over a wide feed ratio range ($0.5 \leq H_2/CO_2 \leq 4.0$) (Fig. 26). The methanol rate is thus significantly more dependent on the H_2 partial pressure than on CO_2. A higher order dependence on H_2 is also valid with regard to CO, H_2O and CH_3OH (see following paragraphs).

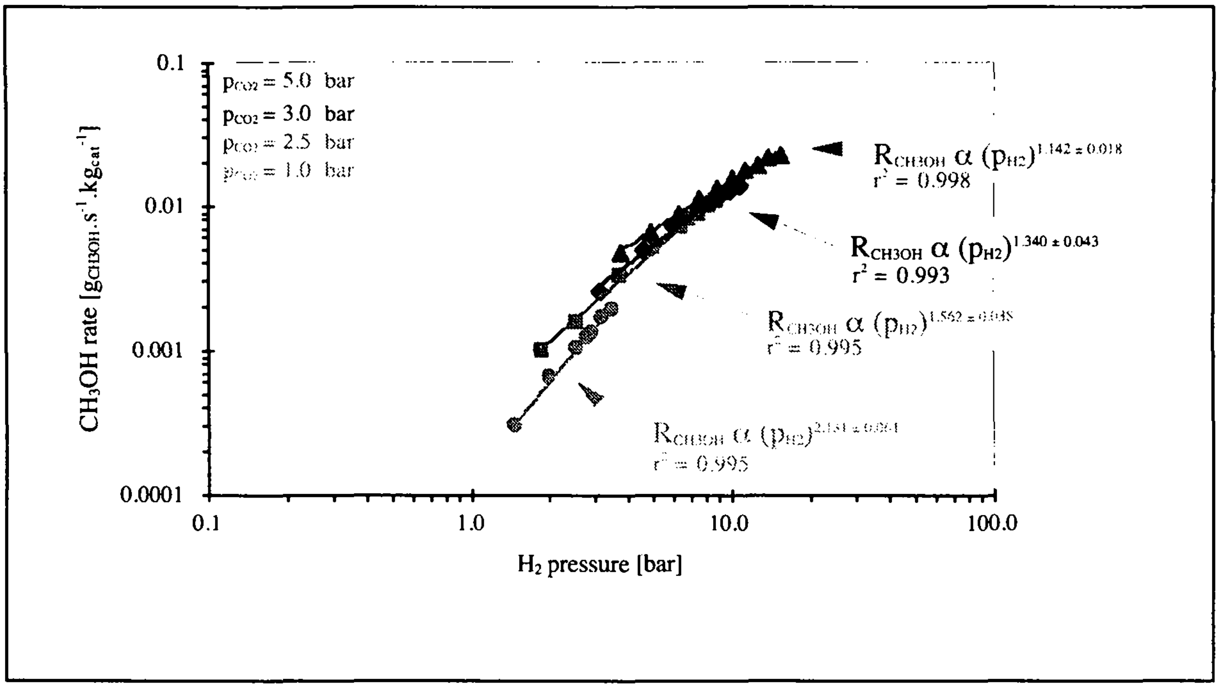

Fig. 26: H_2 partial pressure variation (log-log plot)
($P = 20.0 \pm 0.1$ bar (adjusted with He), $T = 202.5 \pm 0.3$ °C, $S_v = 4500\ h^{-1}$)

For CO_2 and H_2, this is very well illustrated by a 3D plot (Fig. 27).

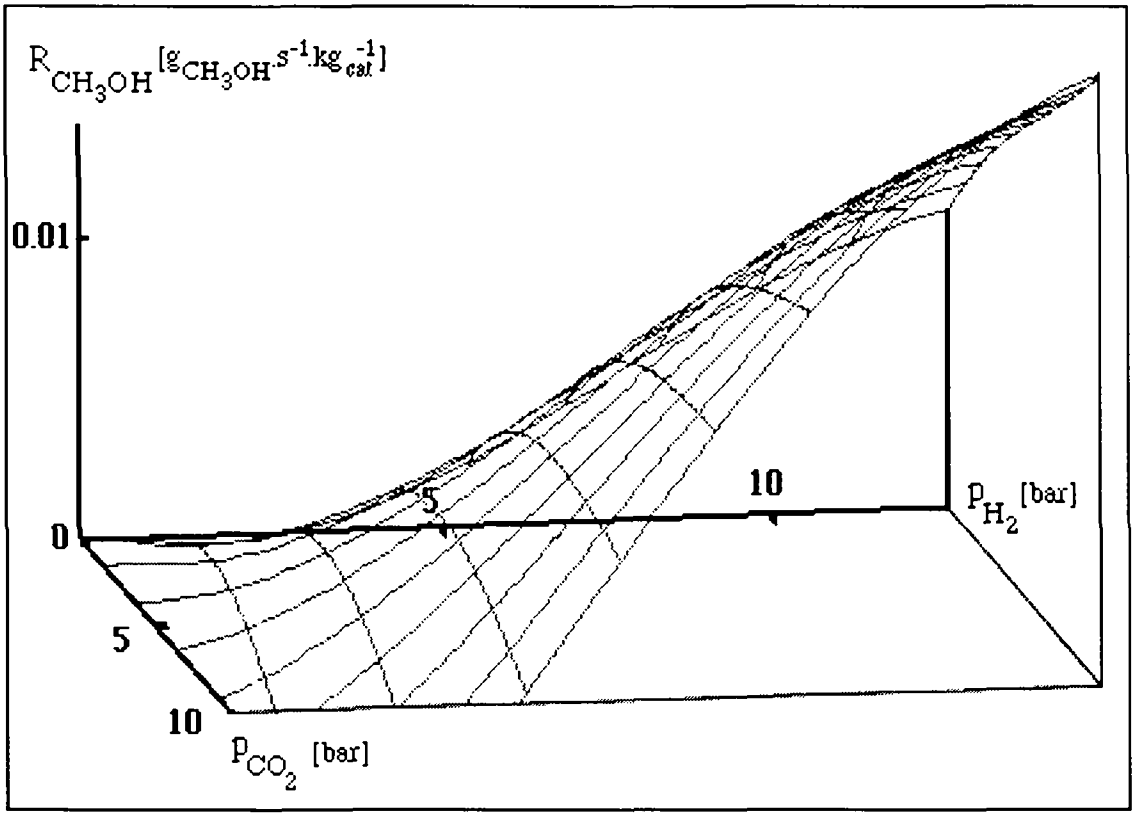

Fig. 27: Methanol rate as a function of the H_2 and CO_2 partial pressures
($P \approx 20.0$ bar (adjusted with He), $T \approx 200.0$ °C, $S_v = 4500\ h^{-1}$)

H_2 adsorption on $CuO/ZnO/Al_2O_3$ catalysts is dissociative (Dennison *et al.* 1989, Suzuki *et al.* 1971). Heat of adsorption is typically 45 kJ.mol^{-1} (Skrzypek *et al.* 1994). Chemisorption of H_2 is an activated process with an activation energy equal to about 60 kJ.mol^{-1}. It has also been found that part of the adsorbed hydrogen diffuses into the bulk of the catalyst (Sloczynski *et al.* 1991, Wrobel *et al.* 1987).

Given the same experimental conditions, the CO rate is slightly slower. The apparent order, for the same range of H_2 pressures, varies from 0.256 to 0.287. This indicates that hydrogen has less influence on the CO rate than on the methanol rate. This is in agreement with the stoichiometric coefficients of hydrogen in the methanol synthesis reaction ($CO_2 + 3H_2 \leftrightarrow CH_3OH_{(g)} + H_2O_{(g)}$) and the reverse water-gas shift reaction ($CO_2 + H_2 \leftrightarrow CO + H_2O_{(g)}$).

4.4.3. Carbon monoxide partial pressure variation

Although carbon monoxide does not appear as a component in the methanol synthesis reaction, when CO_2 is used as the sole C-source (eq 4), it can influence the methanol rate. Indeed CO appears in the parallel reverse water-gas shift reaction (eq 5) and it can lead to the formation of methanol (eq 3).
The influence of CO partial pressure on the methanol rate is shown in figure 28 for various H_2 and CO_2 partial pressures at a temperature of 200 °C. The H_2/CO_2 ratio was kept constant and equal to 3. In each case, the CO partial pressure has a negligible influence on the methanol rate. Only the initial H_2 and CO_2 concentrations are found to influence the methanol rate. In both cases a greater initial concentration results in a higher methanol rate.

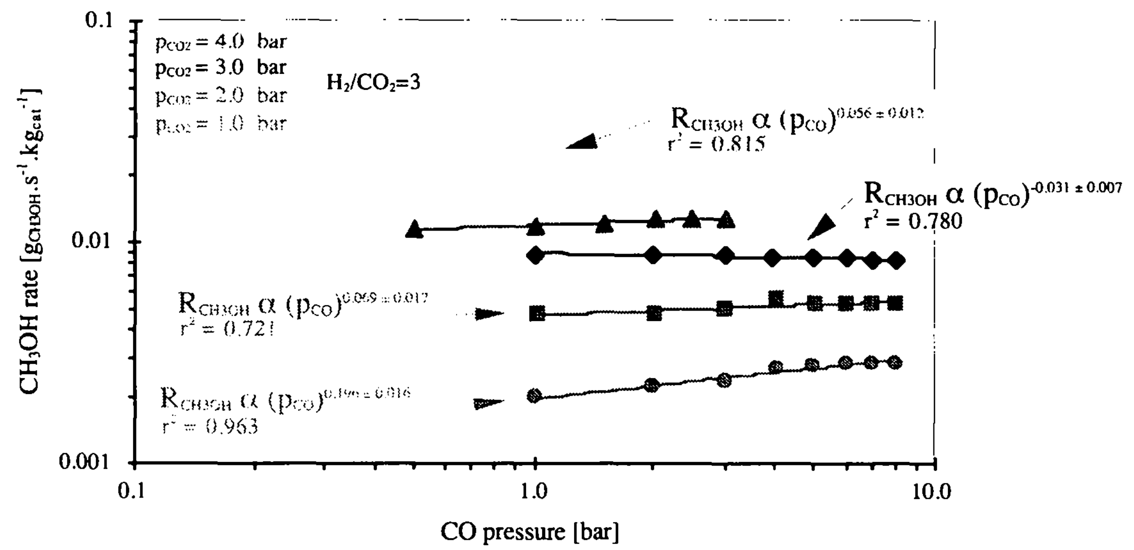

Fig. 28: CO partial pressure variation (log-log plot)
(P = 20.0 ± 0.1 bar (adjusted with He), T = 203.6 ± 0.4 °C, S_v = 4500 h^{-1})

The apparent order (relative to CO) for the methanol rate is close to zero. It varies, over a wide range of CO feed concentrations ($2.5 \leq$ CO in the feed ≤ 40.0 % vol.), from -0.031 to 0.056.

Two assumptions may be made, based on these results. Either the CO_2 partial pressure is sufficiently high not to limit the methanol formation from pure CO_2, or the CO hydrogenation occurs extremely slowly under these experimental conditions.

CO is chemisorbed on the surface of the $CuO/ZnO/Al_2O_3$ catalyst. The heat of adsorption of CO is also found to be dependent on the coverage. It typically decreases from 65 to 45 $kJ.mol^{-1}$ as the coverage increases from 0.2 to 0.6 (Skrzypek *et al.* 1994). In addition to reversible adsorption a separate irreversible adsorption may take place (consisting of less than a few percent of the total amount adsorbed) (Parris *et al.* 1986, Sloczynski *et al.* 1991).

Given the same experimental conditions, the CO_{reac}[8] rate is much slower. The apparent order, for the same range of CO pressures, varies from -2.183 to -0.535. This means that carbon monoxide slows down the reverse water-gas shift reaction (eq 5). In the next paragraph, a detailed explanation is given.

4.4.4. Water partial pressure variation

The influence of water partial pressure on the methanol rate is shown in figure 29 for various H_2 and CO_2 partial pressures at a temperature of 200 °C.

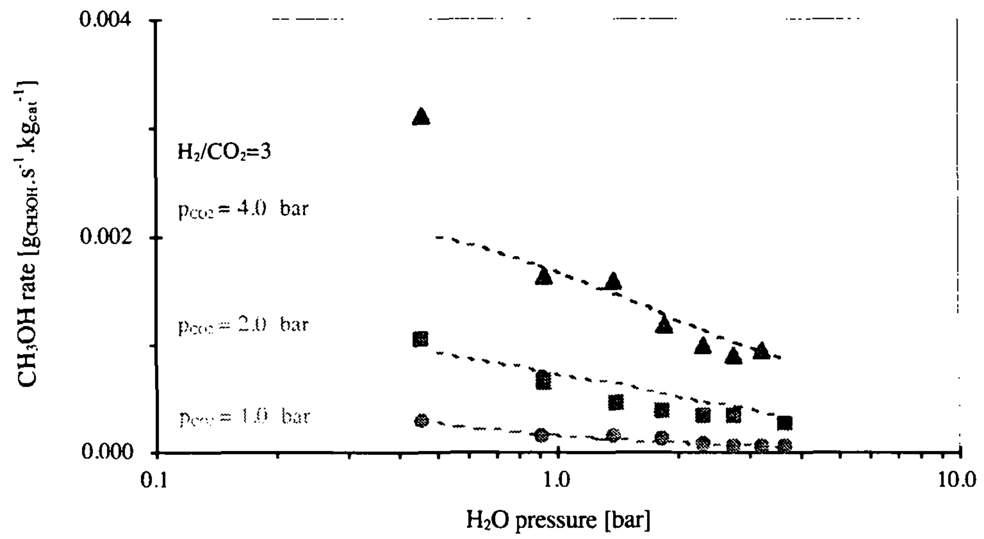

Fig. 29: Experimental (points) H_2O partial pressure influence on the methanol rate in comparison to the developed model (dashed lines)
($P = 20.1 \pm 0.1$ bar (adjusted with He), $T = 202.0 \pm 0.4$ °C, $S_v = 4500\ h^{-1}$)

---

[8] CO concentration was deduced from a mass balance for the gas phase, plug flow reactor, under steady state conditions: $CO_{input} - CO_{output} + CO_{reaction} = 0$ (no accumulation)

The apparent order (relative to water) for the methanol rate is always negative and varies, over a wide range of water feed concentrations (2.5 ≤ H_2O in the feed ≤ 17.5 % vol.), from -0.518 to -0.827 (Fig. 30).

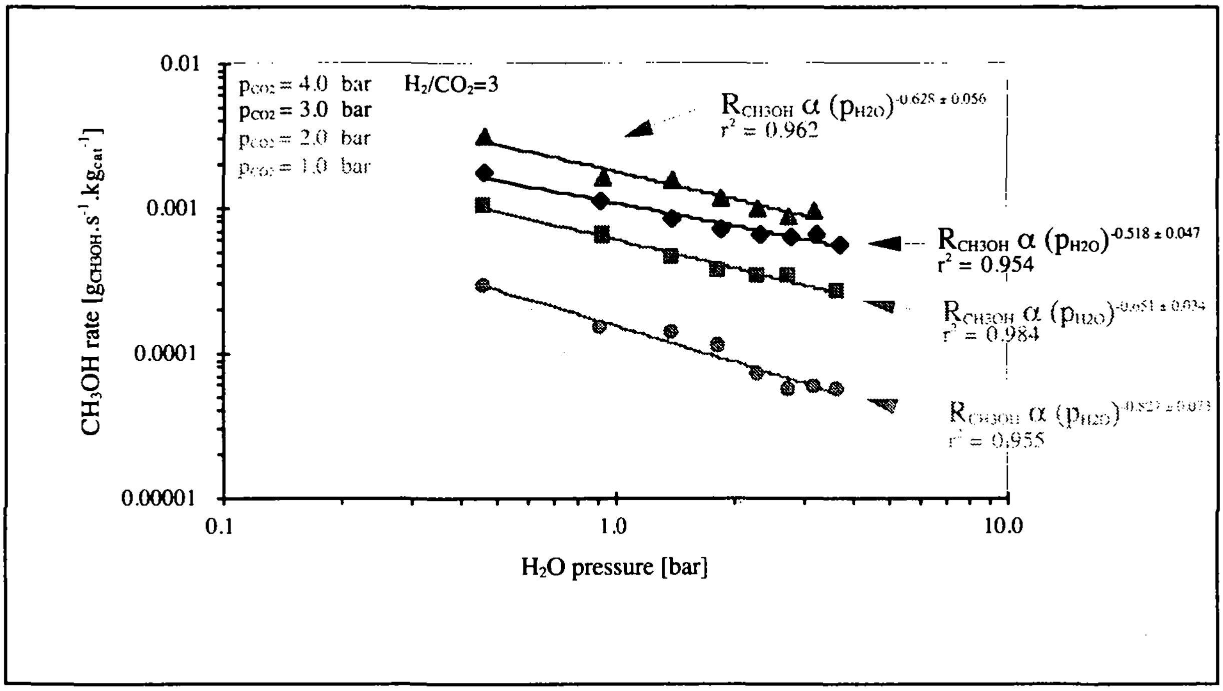

Fig. 30: H_2O partial pressure variation (log-log plot)
($P = 20.1 \pm 0.1$ bar (compensated with He), $T = 202.0 \pm 0.4$ °C, $S_v = 4500\ h^{-1}$)

This inhibition is due to the strong competitive adsorption of H_2O on the catalyst surface (especially on CO_2 adsorption sites, see paragraph 4.4.1.). Skrzypek et al. (Nowak *et al.* 1991) have also observed an inhibitory effect caused by water over a composite $CuO/ZnO/Al_2O_3$ catalyst.

However the mechanism of inhibition is quite complex because of the forward/reverse water-gas shift reaction (eq 22), making it difficult to separate the roles of H_2O from those of CO_2.

$$CO_2 + 3H_2 \leftrightarrow CH_3OH(g) + H_2O(g) \tag{21}$$

$$CO + H_2O(g) \leftrightarrow CO_2 + H_2 \tag{22}$$

Indeed, an increase in the water concentration inhibits the methanol synthesis rate (eq 21). But at the same time, water enhances the rate of the forward water-gas shift reaction thus increasing the CO_2 content in the reactor. An increase in CO_2 concentration enhances the methanol rate again. This reasoning is not only applicable for CO_2 but also, similarly, to CO. The relative contribution of the promoting/inhibiting effect of water may vary widely, depending on the conditions under which the synthesis is carried out. Klier et al. (Vedage *et al.* 1984) observed a maximum methanol yield at low water concentrations and a strong inhibition at higher concentrations. The optimum concentration of water was found to vary with temperature. At 225 °C, the water content promoting the methanol rate

was 2.2 % mol whereas, at 210 °C, it was only 0.7 %. Lee et al. (Lee 1990) also reported a maximum for the methanol rate within the range of water concentrations studied (0.1 to 0.2 %) at a temperature of 237 °C. The optimal concentration of water within the reactor is then determined by balancing the methanol and CO rates. This kind of optimum depends not only on the temperature, but also on the feed gas composition which favors the formation of the critical intermediate.
According to Sloczynski (Sloczynski *et al.* 1991), H_2O is adsorbed on $CuO/ZnO/Al_2O_3$ catalysts in a reversible form (20 % of the coverage) and an irreversible form (remaining surface). The water chemisorbed irreversibly binds strongly to the surface blocking the adsorption sites of other reactants. The heat of adsorption of H_2O is found to be dependent on the coverage. It decreases from about 67 to 20 $kJ.mol^{-1}$ as the coverage increases from 0.0 to 0.7.

Given the same experimental conditions, the CO rate is much faster. The apparent order, for the same range of water pressures, varies from -1.074 to -0.280. This indicates that water does not inhibit the CO rate as strongly as it inhibits the methanol rate. It also suggests that H_2O might block some sites where H_2 is adsorbed. As was mentioned in paragraph 4.4.2., hydrogen has a greater influence on the methanol rate than on the CO rate. Therefore blocking H_2 adsorption sites would have a greater effect on the methanol rate than on the CO rate.

4.4.5. Methanol partial pressure variation

The influence of methanol pressure on the CH_3OH_{react}[9] rate is shown in figure 31 for various H_2 and CO_2 partial pressures at a temperature of 200 °C. The H_2/CO_2 ratio was kept constant and equal to 3. In each case, the methanol rate increases slightly with higher methanol partial pressures. Only the initial H_2 and CO_2 concentrations have the same influence on the methanol rate as their influence on the CO_2, CO and H_2O partial pressures variations.

---

[9] CH_3OH concentration was calculated using the same formula as for the CO concentration.

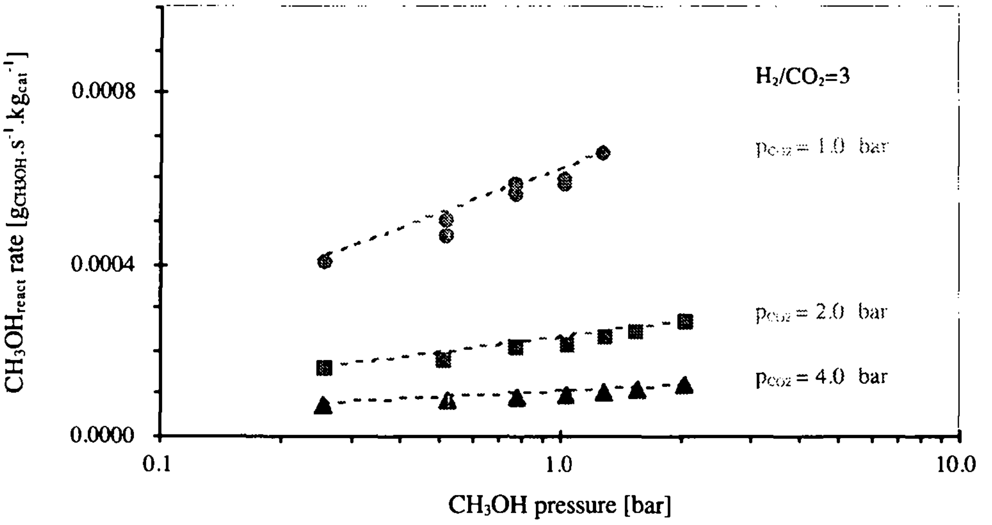

Fig. 31: Experimental (points) CH_3OH partial pressure influence on the methanol rate in comparison to the developed model (dashed lines)
($P = 19.9 \pm 0.2$ bar (compensated with He), $T = 202.4 \pm 0.3$ °C, $S_v = 4500\ h^{-1}$)

The apparent order (relative to methanol) for the methanol rate is slightly positive and varies, over the range of methanol feed concentrations ($1.2 \leq CH_3OH$ in the feed ≤ 10.0 % vol.), from 0.234 to 0.299 (Fig. 32). This observation is only valid within the given experimental conditions. For higher methanol partial pressures, the methanol rate would become negative (Graaf *et al.* 1988, Höltje 1990).

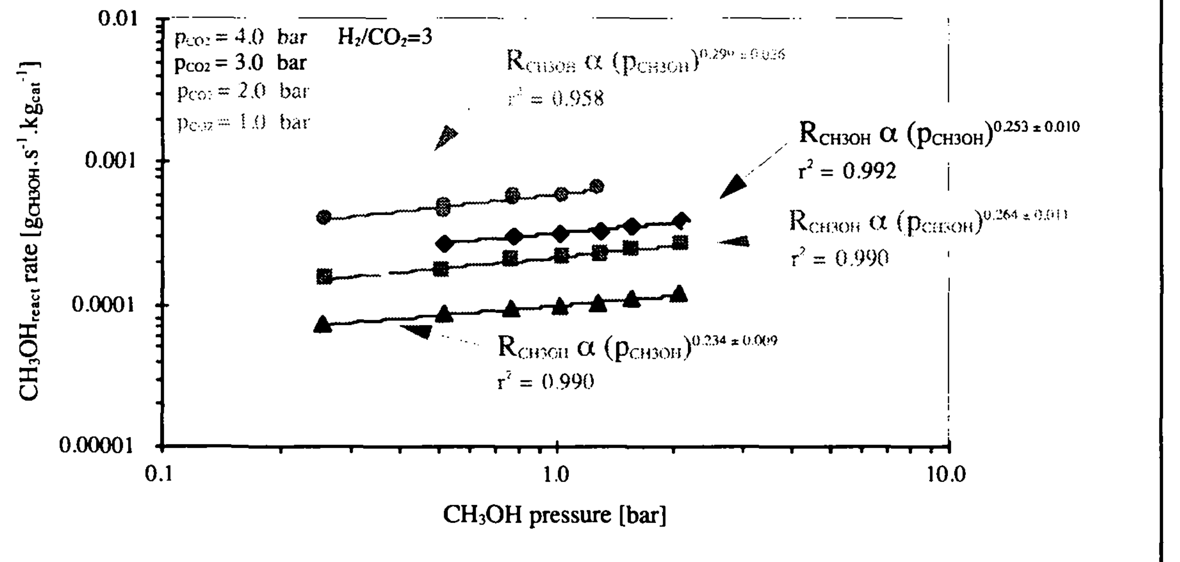

Fig. 32: CH_3OH partial pressure variation (log-log plot)
($P = 19.9 \pm 0.2$ bar (compensated with He), $T = 202.4 \pm 0.3$ °C, $S_v = 4500\ h^{-1}$)

This promoting effect can only be explained by an increase in adsorption of the reaction components on the surface of the catalyst. According to Höltje et al (Höltje 1990), it enhances the dissociative adsorption of hydrogen.

CH_3OH is both reversible (weakly bound), and irreversible (dissociated) on the surface of $CuO/ZnO/Al_2O_3$ catalysts (Le Peltier 1989, Sloczynski *et al.* 1991). The heat of adsorption does not depend on the coverage, and is about 46 kJ.mol^{-1} (Sloczynski *et al.* 1991).

Given the same experimental conditions, the CO rate is much faster. The apparent order, for the same range of methanol pressures, varies from 0.287 to 0.439. Methanol enhances CO formation.

4.4.6. Kinetic model at moderate pressure and temperature

a) Model development

A full kinetic model coupled to the forward/reverse water-gas shift reaction is beyond the scope of this thesis. A complete overview of the kinetics models for the methanol synthesis reaction can be found in the review papers of Klier et al. (Klier 1982), Bart et al. (Bart *et al.* 1987), as well as in the book of Skrzypek et al. (Skrzypek *et al.* 1994). This thesis only attempts to cover the main features of the observed methanol synthesis rate.

The rate equation can be expressed, at a given temperature, as a function of the surface concentration of H_2 and CO_2:

$$R_{CH_3OH} = k_{CH_3OH} \cdot \theta_{CO_2} \cdot \theta_{H_2} \tag{23}$$

A simple kinetic model can be developed by assuming the following conditions:

- □All the species (reactants, products, adsorbed intermediates) are in equilibrium and the reverse reaction rate of the rate limiting reaction is negligible. This assumption is reasonable, since the amount of methanol formed during the synthesis is linear to the exposure time (see paragraph 3.5.3.) (Rasmussen 1993).
- The ideal gas law is appropriate for the selected conditions (P = 20 bar and T = 200 °C). Fugacity coefficients are set to 1 and components partial pressures are directly used. Maximum deviation is only about 3 %.
- CO_2 and H_2 molecules are adsorbed on distinct sites (Skrzypek *et al.* 1994) on the catalyst surface.

Based on an approximation of the Langmuir isotherm (introducing n_{CO_2} and n_{H_2} exponents), the reaction rate is given by:

$$R_{CH_3OH} = k_{CH_3OH} \cdot \left(\frac{K_{CO_2} \cdot p_{CO_2}}{1 + K_{CO_2} \cdot p_{CO_2}} \right)^{n_{CO_2}} \cdot \left(\frac{K_{H_2} \cdot p_{H_2}}{1 + K_{H_2} \cdot p_{H_2}} \right)^{n_{H_2}} \tag{24}$$

- According to Skrzypek et al. (Skrzypek *et al.* 1994), only the following pairs are competitively adsorbed: H_2O/CO_2, H_2O/H_2. This is a reasonable assumption although one has to be aware that other pairs are also competitively adsorbed: H_2O/CO, H_2O/CH_3OH as well as CO/H_2O, CO/CO_2, CO/CH_3OH and CO_2/CH_3OH, but in their cases the competition is much weaker.

The reaction rate can be written as:

$$R_{CH_3OH} = k_{CH_3OH} \cdot \left(\frac{K_{CO_2} \cdot p_{CO_2}}{1 + K_{CO_2} \cdot p_{CO_2} + K_{\frac{H_2O}{CO_2}} \cdot p_{H_2O}} \right)^{n_{CO_2}} \cdot \left(\frac{K_{H_2} \cdot p_{H_2}}{1 + K_{H_2} \cdot p_{H_2} + K_{\frac{H_2O}{H_2}} \cdot p_{H_2O}} \right)^{n_{H_2}} \tag{25}$$

The rate equation is extended by including a term representing methanol's very slight positive influence (see paragraph 4.4.5.):

$$R_{CH_3OH} = k_{CH_3OH} \cdot \left(\frac{K_{CO_2} \cdot p_{CO_2}}{1 + K_{CO_2} \cdot p_{CO_2} + K_{\frac{H_2O}{CO_2}} \cdot p_{H_2O}} \right)^{n_{CO_2}} \cdot \left(\frac{K_{H_2} \cdot p_{H_2}}{1 + K_{H_2} \cdot p_{H_2} + K_{\frac{H_2O}{H_2}} \cdot p_{H_2O}} \right)^{n_{H_2}} \cdot \left(p_{CH_3OH} \right)^{n_{CH_3OH}} \tag{26}$$

b) Model evaluation

A thorough estimation of study parameters was carried out by fitting the experimental results (92 experiments measuring partial pressure variation) with a non-linear regression. Calculations to minimize the residual sum of square rate[10] were carried out using the STARPAC program from NIST. The results of the developed model are shown in figure 33.

A comparison to the power rate law (see also paragraph 3.5.2.):

$$R_{CH_3OH} = k_{CH_3OH} \cdot \left(p_{CO_2} \right)^{n_{CO_2}} \cdot \left(p_{H_2} \right)^{n_{H_2}} \cdot \left(p_{CO} \right)^{n_{CO}} \cdot \left(p_{H_2O} \right)^{n_{H_2O}} \cdot \left(p_{CH_3OH} \right)^{n_{CH_3OH}} \tag{27}$$

is also given.

These rate equations are valid at temperatures of 200 °C and in the concentration range of the experimental results. Values of calculated parameters are given in tables 13 and 14.

---

[10] $RSS = \sum \left(R_i - R_{i,c} \right)^2$

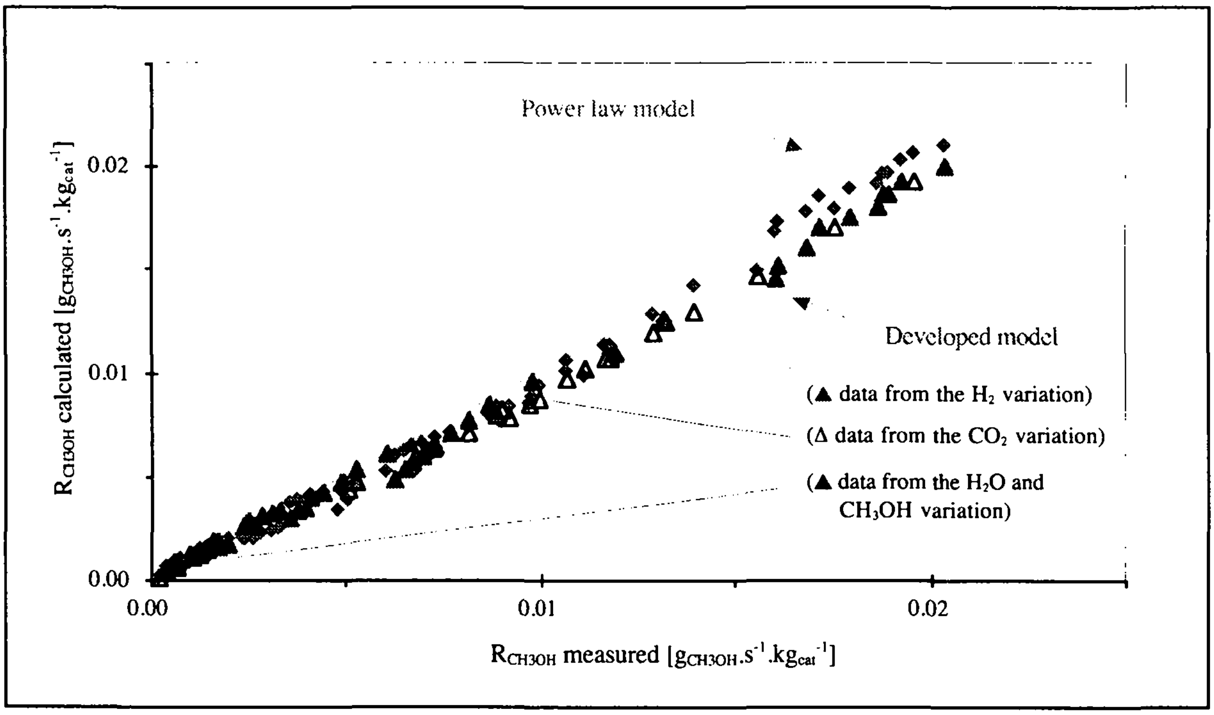

Fig. 33: Comparison between the measured steady-state reaction rates and those calculated with the developed model and with the power law rate expression
($P \approx 20$ bar, $T \approx 200$ °C, $S_V = 4500\ h^{-1}$)

Rate values of the power law model show a satisfactory correlation ($R_M^2 = 0.9848$)[11] with the data points aligned along the diagonal.

Table 13: Parameter values of the power law model (catalyst B, $T \approx 200$ °C)

	Power law model						
	R_M^2 [-]	$\bar{n}_{CO_2}$	$\bar{n}_{H_2}$	$\bar{n}_{CO}$	$\bar{n}_{H_2O}$	$\bar{n}_{CH_3OH}$	k_{CH_3OH}
Values	0.9848	0.376	1.544	0.073	-0.656	0.263	$2.5 \cdot 10^{-4}$
STDEV	-	(± 0.134)	(± 0.427)	(± 0.094)	(± 0.128)	(± 0.027)	(± $1.9 \cdot 10^{-6}$)

However a positive shift is observed for higher rates. Rates predicted by the power law are slightly overestimated (15 %). Such a model (eq 14) should only be used over a limited range because the pressure exponents are not always constant. In particular they may depend upon the range over which the pressures are varied, the values of the pressures held constant and the temperature.

---

[11] $R_M^2 = 1 - \frac{\sum (R_i - R_{i,c})^2}{\sum (R_i - \bar{R})^2}$ with $\bar{R} = \frac{1}{n} \cdot \sum R_i$

A better correlation ($R^2_M = 0.9955$) is obtained with the developed model, particularly for the higher rates.

Table 14: Parameter values of the developed model (catalyst B, T ≈ 200 °C)

	Developed model								
	R^2_M [-]	n_{CO_2}	K_{CO_2} [-]	$K_{\frac{H_2O}{CO_2}}$ [-]	n_{H_2}	K_{H_2} [-]	$K_{\frac{H_2O}{H_2}}$ [-]	n_{CH_3OH}	k_{CH_3OH}
Values	0.9955	1.21	$7.7 \cdot 10^{-2}$	1.28	1.43	$7.6 \cdot 10^{-3}$	0.00	$1.0 \cdot 10^{-2}$	$2.1 \cdot 10^{-4}$

These values indicate that for the experimental conditions, the methanol synthesis rate can be described by a modified Langmuir-Hinshelwood rate expression. High methanol rates especially are much better correlated. The main advantage of the developed model is to enable to describe the methanol formation rate based on constant parameters. It to avoid the varying exponents which are unsatisfactory.

Unfortunately, at present there is a remarkable lack of data, especially in the case of CO_2. Methanol synthesis rate expressions for the industrial $CuO/ZnO/Al_2O_3$ catalyst are traditionally for CO-rich syngas, in which a function was added to allow a rate enhancement due to the small CO_2 addition (Andrew 1980).

Nevertheless, it is generally agreed that hydrogen has a greater effect on the rate than the effect of carbon dioxide. In both models hydrogen exponents are higher than the others; reaction rates are of the order ~ 1.5 on hydrogen partial pressure. These results agree closely with other experimental results in the literature where hydrogen reaction orders are reported to vary between 1.0 and 2.0 (Chinchen *et al.* 1988).

As regards the CO_2 exponent, the values are lower than for those obtained for hydrogen. Moreover they differ greatly between the two models. For the power law rate expression a mean value of 0.376 was recorded and a value of 1.21 reported for the developed model. Although this latter value appears to be very high, the CO_2 influence term $\left(\frac{K_{CO_2} \cdot p_{CO_2}}{1 + K_{CO_2} \cdot p_{CO_2} + K_{\frac{H_2O}{CO_2}} \cdot p_{H_2O}}\right)^{n_{CO_2}}$ is lowered by the introduction of the inhibitory term for the water. At this stage, it is appropriate to point out that water has a strong inhibitory effect on the methanol rate. Water "covers" the surface active sites available for the methanol synthesis. Inhibition is even more important at high methanol rates as water is then also produced in larger amounts.

Using a similar model, Le Peltier (Le Peltier 1989) reports on a n_{CO_2} value of 1 and a n_{H_2} value ranged of between 1.5 and 2.0, depending on the experimental conditions.

The ratio $K_{\frac{H_2O}{CO_2}} / K_{CO_2}$ gives a value of 16.6 which agrees closely with the value (~ 12) found by a similar approximation in paragraph 4.4.1. The value of zero for the parameters $K_{\frac{H_2O}{H_2}}$ reveals that water is not competing with hydrogen.

The fact that gaseous CO does not enter into the methanol forming step, is nicely borne out by the straightforward power law fit where the corresponding exponent is zero (within the experimental accuracy).

Rate coefficient terms are in good agreement and their values are close to the values reported by Höltje et al. ($k_{CH_3OH} = 2.1 \cdot 10^{-4}$) (Höltje 1990). Unfortunately, a comparison to the Graaf et al. (Graaf *et al.* 1988) results is not straightforward as Graaf's values contain the adsorption equilibrium constant of hydrogen. The other kinetic equations which have been expressed are in arbitrary units (Le Peltier 1989) and coefficients remain the property of the industrial organization.

5. Identification of the surface species and reaction scheme

5.1. Scope

Carbon dioxide hydrogenation over the most active catalyst is investigated by infrared techniques. The catalyst surface is analyzed by in situ Diffuse Reflectance Fourier Transform Infrared Spectroscopy (DRIFTS). The identification and evolution of intermediates leads to information improving understanding of the methanol synthesis mechanism.

Responses of sine shape variation applied to the reactants are analyzed by FTIR spectroscopy. Results of the oscillations may have identified the elementary steps of the overall reaction.

5.2. Introduction

In the study of heterogeneously catalyzed reactions, an understanding of the mode of action of the catalyst, (i.e. knowledge of adsorbed intermediates and their formation rate), is fundamental in postulating a mechanism.

a) Identification of the surface species

An in situ observation of the catalyst surface is required to obtain information about the mechanism controlling the reaction(s) occurring on its surface. Techniques such as DRIFTS enable to "take a closer look" at the adsorbed species and intermediates. It allows measurements of the molecular vibrational and rotational energy levels, while the catalyst is operating under, or close to, industrial conditions (Coudurier *et al.* 1994, Griffiths *et al.* 1986, Highfield *et al.* 1991, Suzuki *et al.* 1986).

The first part of this chapter looks at the use of DRIFTS to study the surface of catalyst B the during methanol synthesis reaction. Results are compared to measurements taken with catalyst A. A study of this type inevitably benefits from the wealth of infrared spectra data in the literature covering reactants and likely intermediates (formates, carbonates, ...) on single compounds (copper single crystal, polycristalline copper, ...), binary compounds (CuO/ZnO, ...) or ternary compounds (CuO/ZnO/Al_2O_3 catalysts) (Arakawa *et al.* 1992, Bailie *et al.* 1995, Chafik *et al.* 1995, Fröhlich 1993, Fujita *et al.* 1995, Millar *et al.* 1992a, Millar *et al.* 1992b, Millar *et al.* 1995, Schild 1991, Weigel 1996, Weigel *et al.* 1996, Wokaun *et al.* 1994). Tables 15 and 16 present the main data on the characteristic IR adsorption bands (precise data about the adsorbents is given in the references).

Table 15: IR adsorption bands (cm^{-1}) of gas phase molecules

	For gas phase molecules		
Molecule	**Vibration type**	**Wavenumber** [cm^{-1}]	Ref.
CO_2	ν_{as} (C-O)	2349	(Welti 1970)
CO	ν (C-O)	2144	
H_2O	δ (OH)	1600 - 1595	
H_2CO	ν (C-O)	1744	
	ν_s (C-H)	2780	
	ν_{as} (C-H)	2874	
CH_3OH	ν (C-O)	1060, 1029	
	ν_s (C-H)	2844 - 2825	
	ν_{as} (C-H)	2977 - 2935	
CH_4	δ (CH)	1307	
	ν_{as} (C-H)	3018	
C_nH_{2n+2} for $2 \leq n \leq 4$	δ (CH)	1469 - 1466	
	ν_s (C-H)	2895 - 2880	
	ν_{as} (C-H)	2977 - 2966	

Table 16: IR adsorption bands (cm^{-1}) of surface species

Molecule	Vibration type	For adsorbed molecules Wavenumber on CuO/ZrO$_2$ [cm^{-1}]	on CuO/ZnO/Al$_2$O$_3$ [cm^{-1}]	Ref.
CO$_3$ – (monodentate) (carbonate)	ν_s (C-O)	1400 - 1350	1383 (Cu)	(Bailey et al. 1995, Schild 1991, Skrzypek et al. 1994)
		1450 - 1400	1466, 1415 - 1410 (Cu)	
	ν (C=O)	1680 - 1630	1530 (Cu)	
(bidentate)	ν_{as} (C-O)	1300 - 1220	1332 (Cu)	
(polydentate)			1522 (ZnO)	
HCO$_3$ – (hydrogenocarbonate)			1635, 1424 (ZnO)	
CH$_2$O – (π - bounded formaldehyde)	ν (C-O)	1165 - 1140		
	ν_s (C-H)	2830 - 2820		
CH$_3$O – (methoxy)	ν (C-O)	1065 - 1050	1095, 1080 (ZnO)	
			990 (Cu)	
	ν_s (C-H)	2830 - 2820	2840	
	ν_{as} (C-H)	2950 - 2930	2950	
HCO – (formyl)	ν (C-O)	1700	1611, 1340	
	ν (C-H)		2743	
HCO$_2$ – (formate) (monodentate)	ν_s (C-O)	1380	1304	
	ν_{as} (C-O)	1580	1600, 1583 (ZnO)	
(bidentate)	ν_s (C-O)	1360	1381, 1364, 1360 (ZnO)	
	ν_{as} (C-O)	1600	1604 - 1600, 1957, 1577, 1560, 1350 (ZnO)	
HCO$_2$ – (formate)	ν (C-O) + δ (C-H)	2750		
	ν (C-H)	2880 - 2870	2700	
	ν_{as} (C-O) + δ (C-H)	2960		
– OH (isolated) (hydroxyl)	ν (O-H)	3780 - 3670		
CO (adsorbed)	ν (C-O)	2100 - 1750	2100 - 2070 (Cu)	
			2184 (ZnO)	
(singly bound)	ν (C-O)	2100 - 2000		
(doubly bound)	ν (C-O)	2000 - 1900		
(triply bound)	ν (C-O)	1900 - 1800		
H$_2$O (adsorbed)	δ (O-H)	1620		
CO$_2$ (adsorbed)			1370 (ZnO)	

b) Periodic experiments

Reaction mechanisms can be derived from steady-state and transient rate measurements. Steady-state experiments are often unable to accurately describe the dynamics of heterogeneously catalyzed reactions. In particular they cannot predict the transient behavior and the optimum regulation parameters for catalytic reactors with changing input conditions. Transient experiments are more sensitive to the elementary step rate constants. Experiments usually consist of a either step-up or step-down changes in the feed composition. A further step is reached by exposing the system to repeated consecutive step-up and step-down composition changes (periodic operation) (Marwood 1995, Noda 1989, Noda 1990, Noda *et al.* 1993). An alternative approach is to vary the reactants concentration according to the shape of a sine wave (Kritzenberger *et al.* 1997). In all cases, forced oscillation of the reactor parameters, such as concentration of the reactants in the feed, flow rate and temperature can significantly alter the behavior of continuous chemical reactors. The dynamic behavior of the reactor and the individual steps making up the overall reaction can be exploited to obtain performances and selectivities which cannot be accomplished in steady-state operation under comparable conditions. This is based on the fact that in the transition state, following a reaction parameter change, the coverage of the catalysts surface with reactants and products may assume values different from those of steady-state operation (Renken 1984).

In the second part of this chapter, sine shaped modulations of CO_2 or H_2 are applied to the methanol synthesis reaction.

5.3. Apparatus

The experiments presented in this chapter were performed in the DRIFTS reactor (described in paragraph 2.3.2.) and in the modulation reactor (described in paragraph 2.3.3.). Experimental notes, relevant to this particular chapter are given below for each of the two reactors.

a) The DRIFTS reactor

Measurements were taken using catalyst B. A single measurement was also taken using catalyst A for comparison. The sample was exposed to a flow of hydrogen and nitrogen ($Q_{total} = 4$ Nl.h^{-1}) for at least 15 minutes. Subsequently all the nitrogen was replaced by CO_2, setting a H_2/CO_2 ratio equal to 3. Similar step-up experiments were carried out with CO ensuring that the H_2/CO ratio was equal to 2. The experiments were performed at a pressure of 4 bar and at a temperature of 200 °C. The time was noted at the precise moment the carbon source valve was opened, with the surface spectra taken thereafter at defined intervals.

When CO_2 was used as a reactant, the signal of gaseous CO_2 at 2349 cm^{-1} was cut off in the resulting DRIFT spectra. This ensured that this band would not dominate in the presented spectra.

b) The modulation reactor

Modulation of CO_2 and H_2 concentrations was investigated for catalyst B. For the standard frequency ($\omega = 1.67\ 10^{-2}$ Hz, corresponding to a period of 60 s), experiments were performed at pressures of 5, 10 and 20 bar and at temperatures of 200, 220 and 260 °C. A set of 18 spectra is shown in figure 34.

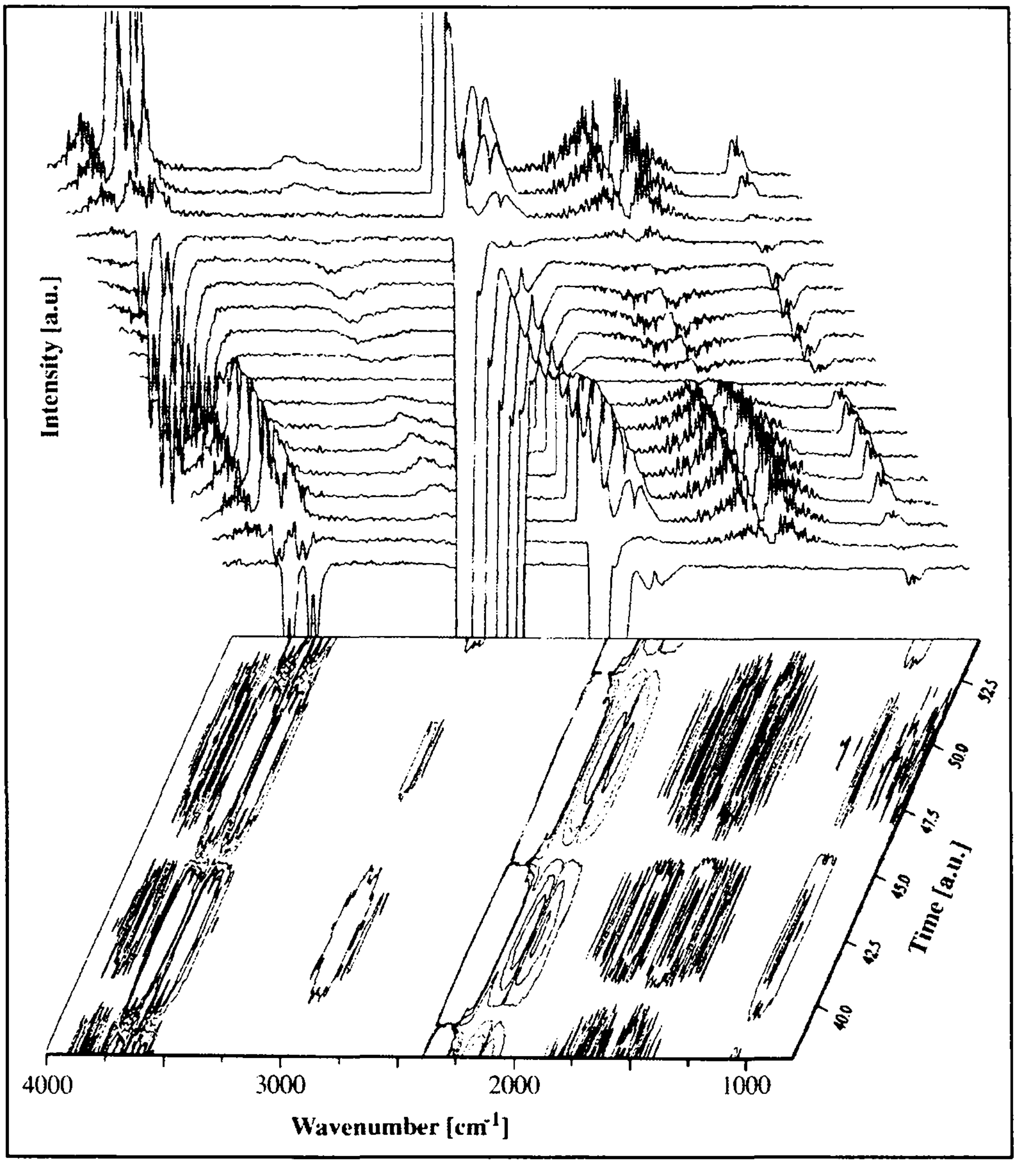

Fig. 34: Set of 18 spectra of a typical CO_2 modulation experiment (top). Peak maxima were deduced from the contour plot (bottom).

($P = 5$ bar, $T = 220$ °C, $Q_{CO_2} = 50 \pm 25$ Nml.min^{-1}, $Q_{H_2} = 580$ Nml.min^{-1}, $Q_{tot} = 2$ Nl.min^{-1}, (compensation with N_2))

A series of modulation experiments were performed, at a pressure of 5 bar and temperature 200 °C, using different modulation frequencies, i.e. $3.33\ 10^{-2}$ to $8.33\ 10^{-4}$ Hz, corresponding to periods varying between 30 and 1200 s.

5.4. Results and discussion

5.4.1. Identification of the surface species

Infrared spectra obtained at different times, after a continuous flow of H_2/N_2 (3:1) was switched to a stoichiometric H_2/CO_2 mixture, are shown in figure 35.

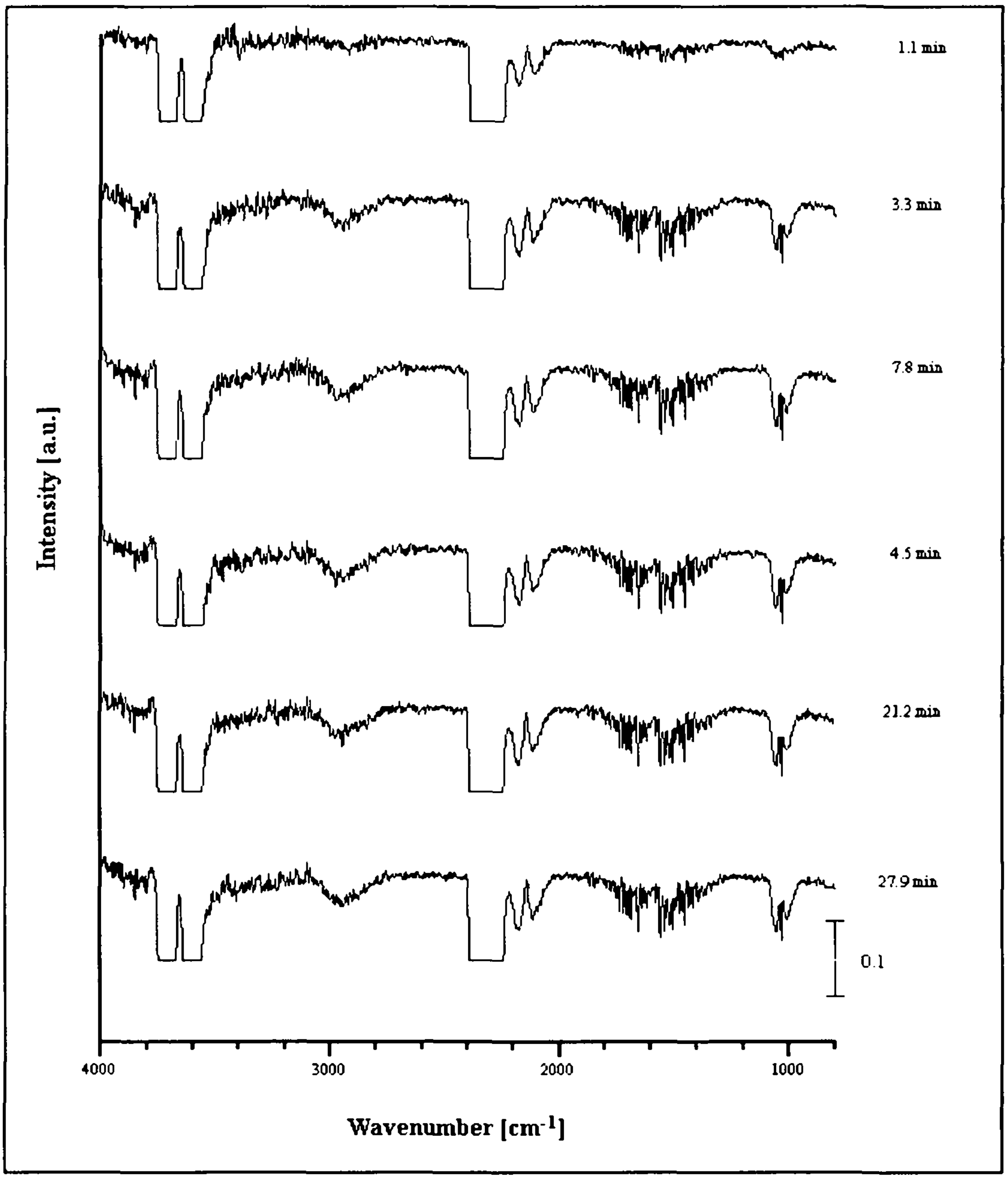

Fig. 35: CO_2 hydrogenation over catalyst B
($P = 10$ bar, $T = 200$ °C, $Q_{CO_2} = 2.5$ Nl.min^{-1}, $Q_{H_2} = 7.5$ Nl.min^{-1})

Intense CO_2 signals (2349, 3609, 3716 cm^{-1}) can be observed immediately . Gaseous CO (2144 cm^{-1}) is detected in less than 1 minute, and the signal at around 1600 cm^{-1} indicates that water is also formed. These products result from the reverse water-gas shift reaction.

The first traces of gas phase methanol (1005, 1029, 1060 cm^{-1}) are visible. Peak intensities increase for approximately 7 minutes, after which no further changes are observed.

According to table 16, the region between 1300 - 1600 cm^{-1} contains a wealth of information on the morphology of the molecules adsorbed on the surface of the catalyst. Unfortunately, the strong signal from water (a multiplet) around 1600 cm^{-1} leaves this region unresolved. Changing experimental conditions to slow down the reaction rate did not resolve the problem (figures not shown). A measurement was taken using catalyst A, under identical conditions, to ensure correct experimental settings (Fig. 36).

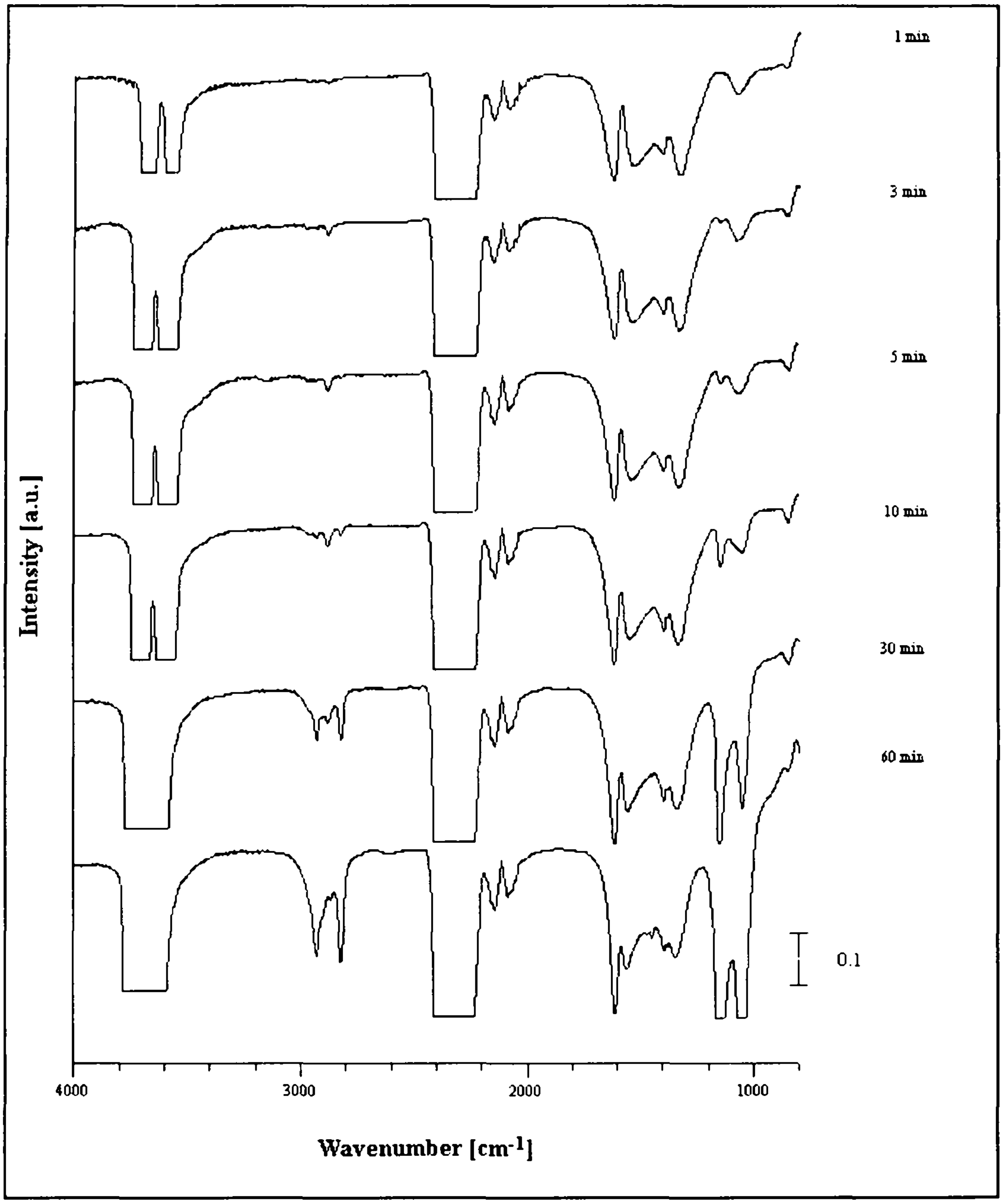

Fig. 36: DRIFT spectrum of catalyst A

(P = 10 bar , T = 200 °C, $Q_{CO_2} = 2.5\ Nl.min^{-1}$, $Q_{H_2} = 7.5\ Nl.min^{-1}$*)*

Results agree closely with the various spectra reported by Weigel (Weigel 1996). The formation of carbonates and formates (broad bands between 1600 and 1200 cm^{-1}) as well as gaseous CO (2144 cm^{-1}), occurs rapidly. After three minutes, methoxy species (2930, 2830, 1150 and 1050 cm^{-1}) are observed, with intensities increasing strongly as a function of the reaction time. The surface of the formate species remained constant during the same time interval, whereas the intensities due to the surface carbonates decreased. No other significant changes are detectable after 60 minutes (spectra not shown).

Detection of surface species can easily be achieved on catalyst A due to a slower methanol formation rate, even given real-world conditions. Measurements were taken using catalyst B diluted with 90 % w. KBr. This dilution is necessary to enable surface species to be identified.

Experiments using KBr showed that none of the bands observed derived from KBr. Infrared spectra obtained at different times, after a continuous flow of H_2/N_2 (3:1) was switched to a stoichiometric H_2/CO_2 mixture, are shown in figure 37.

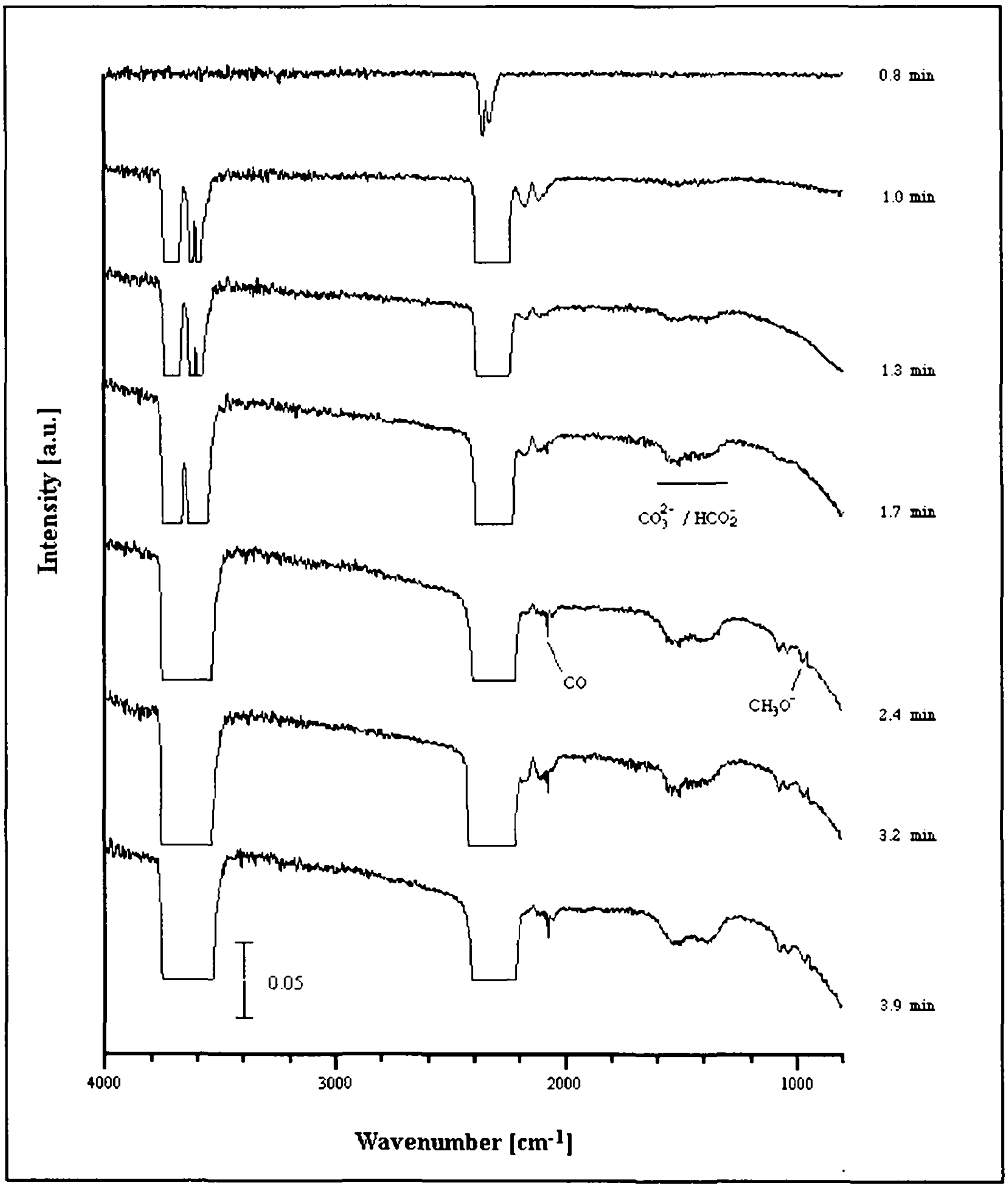

Fig. 37: CO_2 hydrogenation over catalyst B (10 % w. in KBr)
($P = 4$ bar, $T = 200$ °C, $Q_{CO_2} = 2.5$ Nl.min^{-1}, $Q_{H_2} = 7.5$ Nl.min^{-1})

CO_2 signals (2349, 3609, 3716 cm^{-1}) are immediately observed.

The product of the reverse water-gas shift reaction, gaseous CO (2144 cm^{-1}), is apparent soon after the reaction starts (approximately 60 seconds) and then its concentration decreases slightly. After 1.7 minutes, a peak begins to develop located at 2076 cm^{-1}. According to Saussey et al. it can be assigned to CO adsorbed on Cu (111) (Saussey *et al.* 1982). Peaks between 1600 and 1300 cm^{-1} are also observed that prove complex to interpret. Indeed, consultation of table 16 shows that they contain the C-O stretches of carbonates and formates species together with hydrogenocarbonates. Further specification of the adsorbed species requires thermal desorption analysis data. According to Bailey et al. (Bailey *et al.* 1995), the species producing peaks in this region derives solely from carbonates and formates adsorbed on the copper component of the catalyst.

Gas phase methanol is represented by peaks at 1060 and 1029 cm^{-1} which are detected slightly later than carbonates and formiates. After 3.2 minutes, within acceptable accuracy limits for figure 37 data, a peak is observed at 978 cm^{-1} which can be assigned to methoxy adsorbed on the Cu component of the catalyst (Ryberg 1985).

As already reported by Weigel (Weigel 1996), no significant changes are detectable during a 25 minutes period under static conditions (spectra not shown).

5.4.2. Periodic experiments

a) Carbon dioxide modulation

Modulation experiments were first performed using different modulation frequencies.

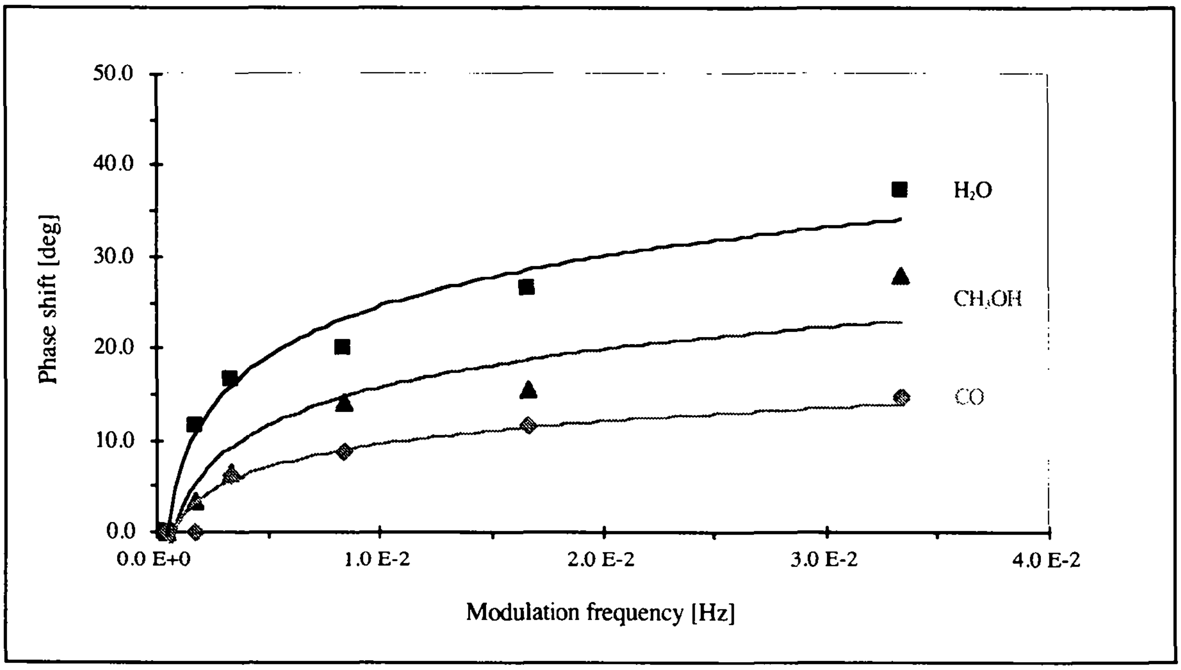

Fig. 38: Phase shift ϕ (relative to the CO_2 signal) for different modulation frequencies (modulation frequencies from $4.17 \cdot 10^{-4}$ Hz to $3.33 \cdot 10^{-2}$ Hz corresponding to periods of 20 min and 30 s, $P = 5$ bar, $T = 200$ °C, $Q_{CO_2} = 50 \pm 25$ Nml.min^{-1}, $Q_{H_2} = 580$ Nml.min^{-1}, $Q_{tot} = 2$ Nl.min^{-1}, (compensation with N_2))

The phase shifts between the products' signal and the CO_2 signal versus the modulation frequency are shown in figure 38. No phase shifts are detected at low modulation frequencies ($\omega \leq 4.17 \cdot 10^{-4}$ Hz). Products are formed "immediately"[12] following any change in the CO_2 inlet concentration. As modulation frequencies are raised, phase shifts slowly become greater with values in the order $\phi_{H_2O} > \phi_{CH_3OH} > \phi_{CO}$. These phase shifts indicate that rate limiting steps are involved in the reaction scheme.

The highest phase shifts ($\phi_{CO} = 15$ °, $\phi_{CH_3OH} = 28$ °, $\phi_{H_2O} = 37$ °) are obtained for the largest modulation frequency employed, i.e. $3.33 \cdot 10^{-2}$ Hz. For this defined set of experimental conditions, CO formation occurs much more quickly than CH_3OH and H_2O following changes in the CO_2 inlet concentration. Similar time shifts are observed in CO_2 step-up experiments (paragraph 5.4.1.) where CO(g) always appears prior to gaseous CH_3OH and H_2O.

---

[12] External perturbation (change in the concentration) occurs within a time range where its influence on the system is not detected.

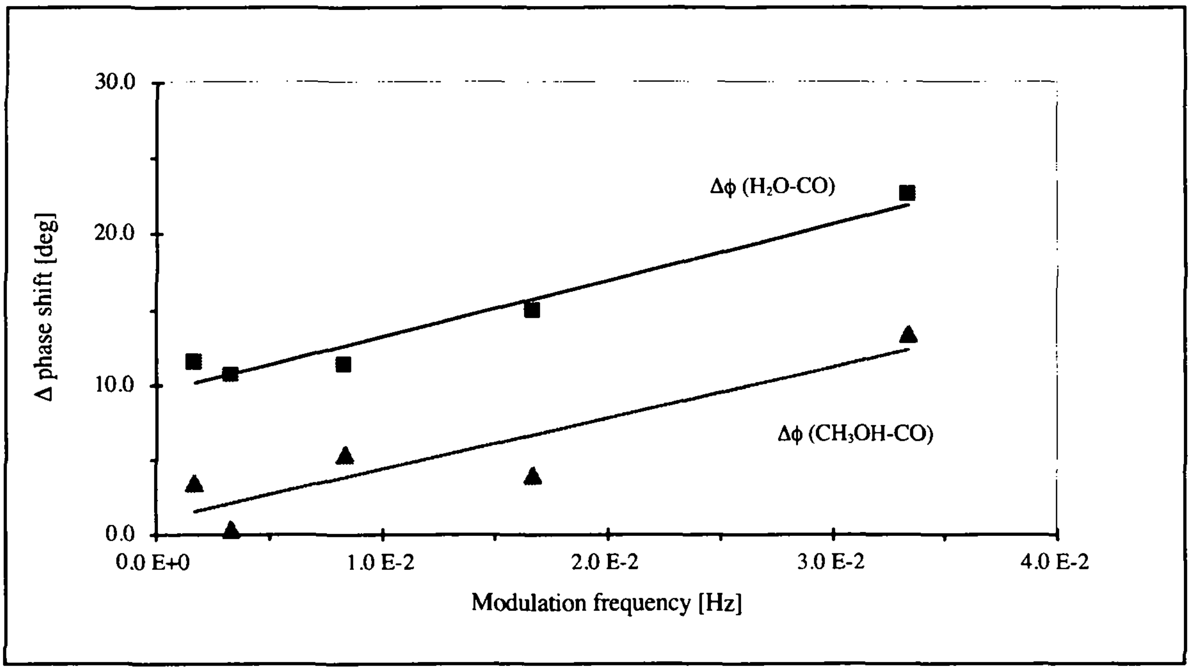

Fig. 39: Phase shift difference $\Delta\phi$ $(\phi_i - \phi_{CO})$ *for different modulation frequencies (experimental conditions are described in figure 38)*

Phase shift differences (relative to CO) lead to the results shown in figure 39.
The similar curve gradients might indicate that identical reaction steps are involved (hydrogenation of an intermediate), in the formation of methanol and water.

Experiments were also performed using different pressures at the standard modulation frequency ($\omega = 1.66 \cdot 10^{-2}$ Hz). The phase shifts (relative to CO_2) versus the total pressure is shown in figure 37. Pressure dependence is different regarding the product which is formed. ϕ_{CO} increases slightly and ϕ_{CH_3OH} decreases slightly as the pressure increases. In contrast, ϕ_{H_2O} strongly decreases with increasing pressure. The interesting finding, for the selected experimental conditions, is that the ϕ_{CO} and ϕ_{CH_3OH} curves intersect. Above 18 bar the methanol phase shift becomes smaller than the CO phase shift. This indicates that CO is formed faster than CH_3OH.

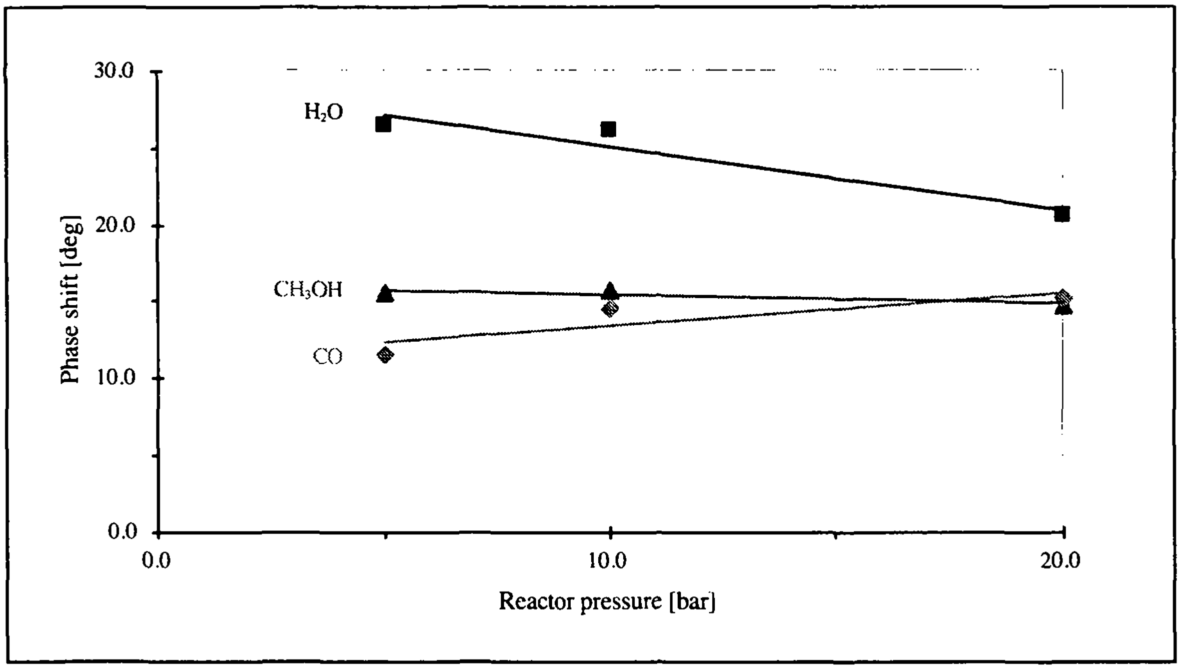

Fig. 40: Phase shift ϕ (relative to the CO_2 signal) for different pressures ($\omega = 1.67 \cdot 10^{-2}$ Hz, $T = 200$ °C, $Q_{CO_2} = 50 \pm 25$ Nml.min^{-1}, $Q_{H_2} = 580$ Nml.min^{-1}, $Q_{tot} = 2$ Nl.min^{-1}, (compensation with N_2))

The relationship of temperature, pressure and the phase shifts is given for CO (Fig. 41), CH_3OH (Fig. 42) and H_2O (Fig. 43). From the observation it follows that temperature has a stronger influence than pressure on the phase shifts. For all products, increasing the temperature leads to a significant decrease in the phase shifts. In the cases of CO and CH_3OH, given these experimental conditions, increasing the temperature from 200 to 260 °C reduces the phase shifts to zero. In other words CO and CH_3OH are formed much faster at higher temperatures. This is due to the fact that the rate coefficient increase with higher temperatures.

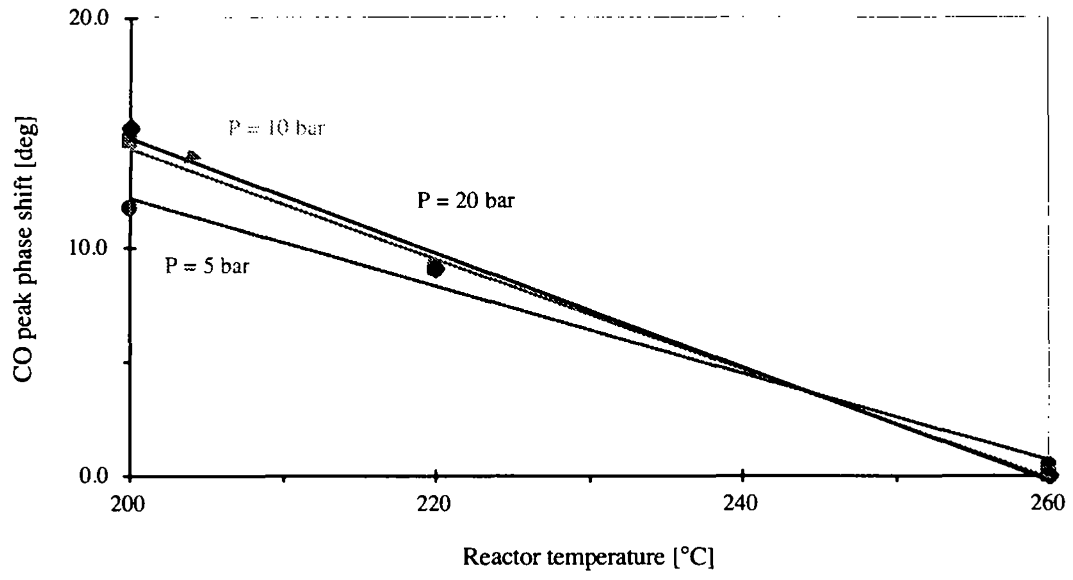

Fig. 41: CO phase shift ϕ (relative to the CO_2 signal) for different pressures and temperatures ($\omega = 1.67 \cdot 10^{-2}$ Hz, $Q_{CO_2} = 50 \pm 25$ Nml.min^{-1}, $Q_{H_2} = 580$ Nml.min^{-1}, $Q_{tot} = 2$ Nl.min^{-1}, (compensation with N_2))

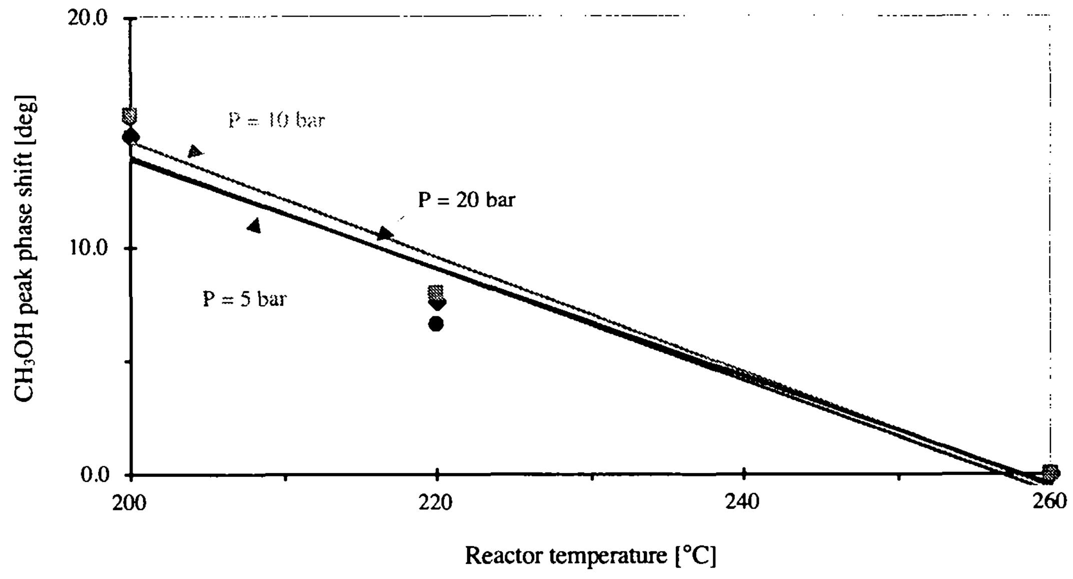

Fig. 42: CH_3OH phase shift ϕ (relative to the CO_2 signal) for different pressures and temperatures ($\omega = 1.67 \cdot 10^{-2}$ Hz, $Q_{CO_2} = 50 \pm 25$ Nml.min^{-1}, $Q_{H_2} = 580$ Nml.min^{-1}, $Q_{tot} = 2$ Nl.min^{-1}, (compensation with N_2))

In the case of water, temperature has the same general influence but does not reduce the phase shifts to zero. The phase shift is close to 10 ° at a temperature of 260 °C and at a pressure of 20 bar. Water formation is slightly delayed, in comparison to CO and CH_3OH.

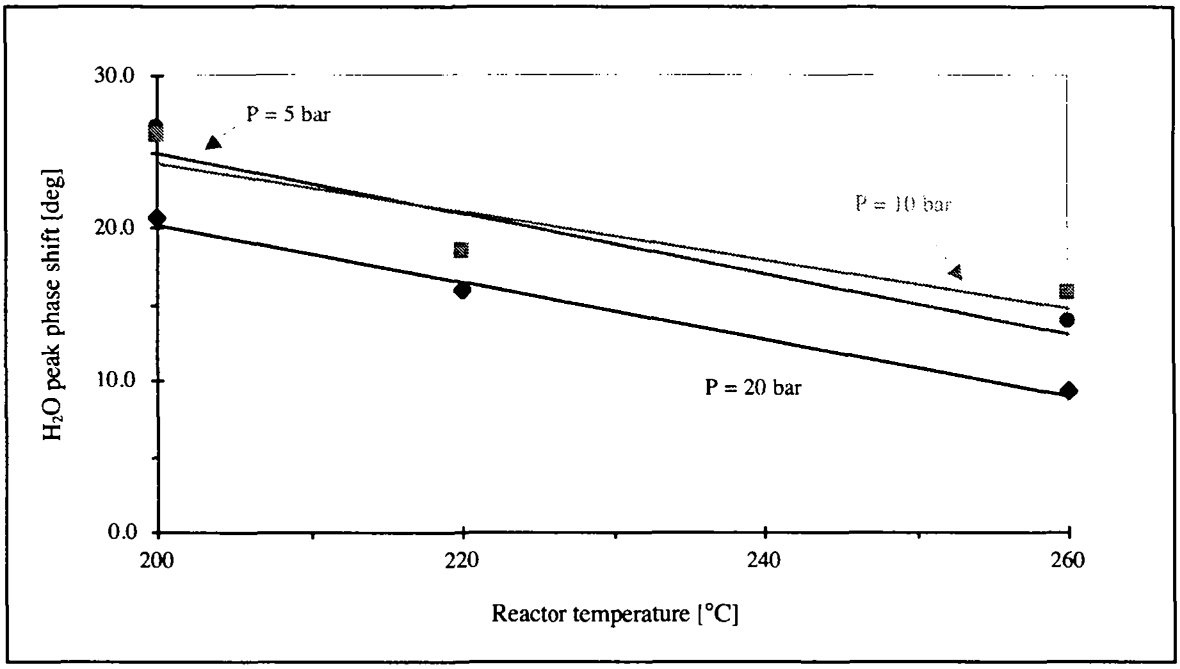

Fig. 43: H_2O phase shift ϕ (relative to the CO_2 signal) for different pressures and temperatures ($\omega = 1.67\cdot10^{-2}$ Hz, $Q_{CO_2} = 50 \pm 25$ Nml.min^{-1}, $Q_{H_2} = 580$ Nml.min^{-1}, $Q_{tot} = 2$ Nl.min^{-1}, (compensation with N_2))

b) Hydrogen modulation

The measurements taken for CO_2 are now repeated for H_2. Phase shifts are relative to the H_2 modulation signal set by the modulation computer (see paragraph 2.33.). Due to the fact that H_2 does not show a detectable IR-signal, the uncertainty in the shift values is significantly greater compared to the CO_2 modulation experiments.

The phase shifts versus the H_2 modulation frequency are shown in figure 44. For a very short modulation frequency ($\omega = 1.39\cdot10^{-4}$ Hz) no phase shifts are detected for H_2O and CH_3OH. For CO_2 a characteristic phase shift of 180 °C is reported. Indeed as the H_2 concentration increases, more CO_2 is consumed in the reaction thus decreasing its concentration in the reactor. Due to uncertainty concerning the phase shifts for CO, the latter values are considered too inaccurate for conclusion. When increasing the modulation frequency, phase shifts become greater and values recorded are in the order $\phi_{CO_2} > \phi_{CH_3OH} \approx \phi_{H_2O}$. Maximum phase shifts ($\phi_{H_2O} = 58$ °, $\phi_{CH_3OH} = 60$ °, $\phi_{CO_2} = 239$ °) are obtained for a modulation frequency of $3.33\cdot10^{-2}$ Hz.

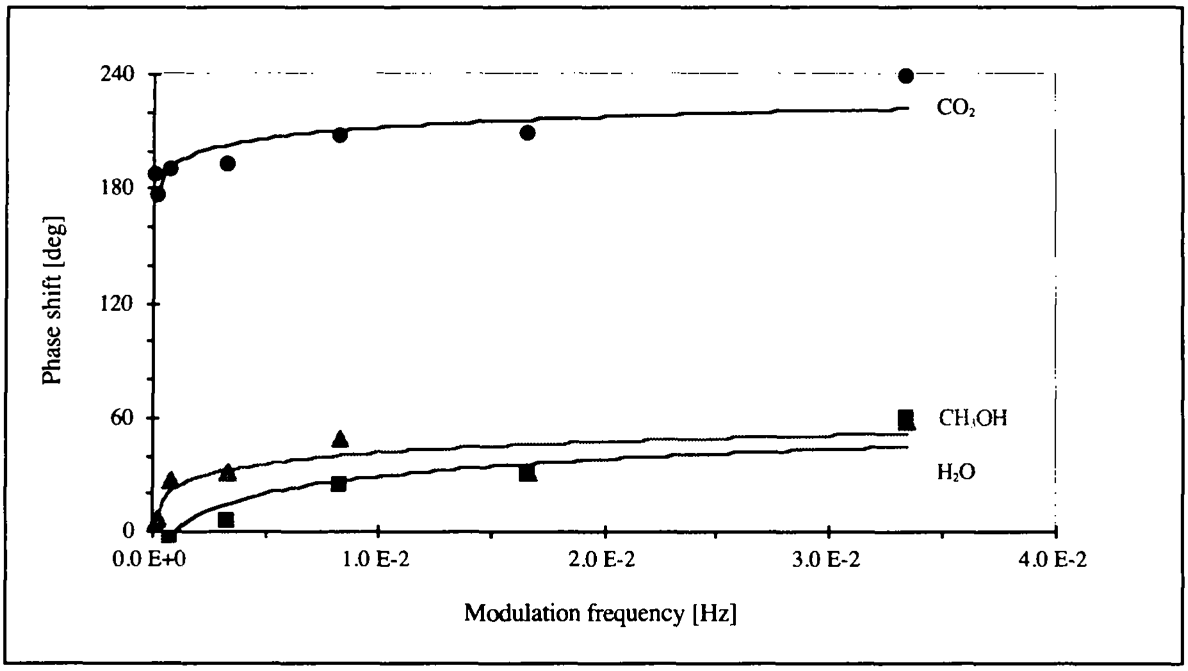

Fig. 44: Phase shift ϕ *(relative to the* H_2 *signal) for different modulation frequencies (*$P = 5$ *bar ,* $T = 200$ *°C,* $Q_{H_2} = 390 \pm 100$ *Nml.min*$^{-1}$*,* $Q_{CO_2} = 50$ *Nml.min*$^{-1}$*,* $Q_{tot} = 2$ *Nl.min*$^{-1}$*, (compensation with* N_2*))*

In general, phase shifts for the H_2 modulation experiments are much larger than for the CO_2 modulation experiments. These results clearly indicate that H_2 has a much larger influence than CO_2 on the reaction rate. The methanol formation rate is found to agree closely with the gas phase kinetic measurements (see paragraph 4.4.1 & 4.4.2.) which indicate a higher apparent order for the dependence on H_2 (1.543) than on CO_2 (0.323). Water responds slightly more quickly than methanol to changes in the H_2 inlet concentration. Compared to the results of the CO_2 modulation experiments ($CH_3OH < H_2O$) the order of the phase shifts is now reversed $H_2O < CH_3OH$. It can be assumed that water has a different dependence on H_2 than on CO_2.

Experiments were also conducted at the standard modulation frequency ($\omega = 1.66 \cdot 10^{-2}$ Hz) at different pressures. The phase shifts (relative to H_2) versus the total pressure is shown in figure 45. ϕ_{H_2O} and ϕ_{CH_3OH} increase slightly, and ϕ_{CO_2} decreases slightly, as the pressure increases.

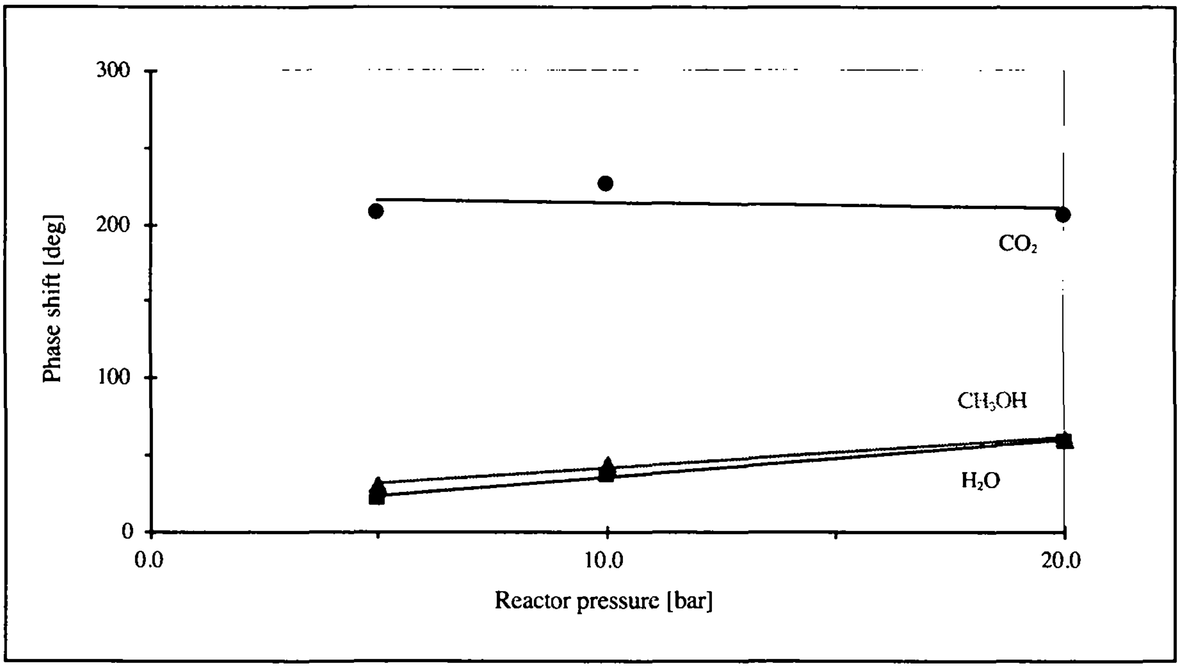

Fig. 45: Phase shift ϕ *(relative to the* H_2 *signal) for different pressures*
$(\omega = 1.67\cdot10^{-2}\ Hz, T = 200\ °C, Q_{H_2} = 390 \pm 100\ Nml.min^{-1}, Q_{CO_2} = 50\ Nml.min^{-1},$
$Q_{tot} = 2\ Nl.min^{-1}$, *(compensation with* N_2*))*

The influence of temperature on the phase shifts is given for H_2O, CH_3OH and CO_2 in figure 46.

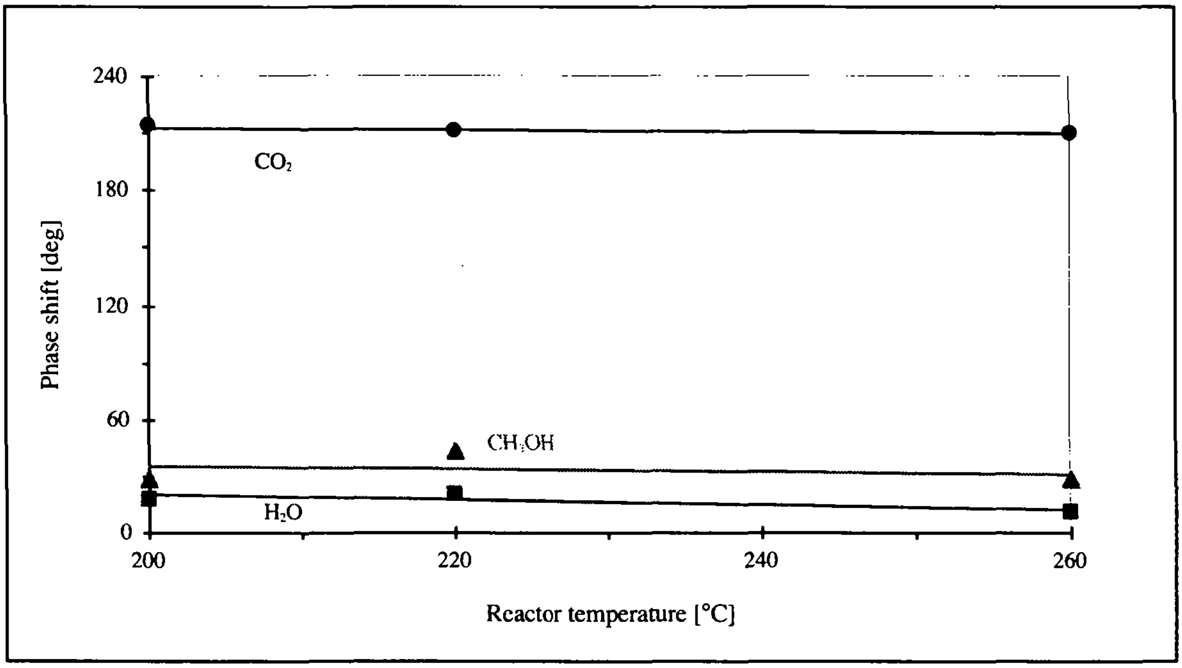

Fig. 46: Phase shift ϕ *(relative to the* H_2 *signal) for different temperatures*
$(\omega = 1.67\cdot10^{-2}\ Hz, P = 5\ bar, Q_{H_2} = 390 \pm 100\ Nml.min^{-1}, Q_{CO_2} = 50\ Nml.min^{-1}, Q_{tot} = 2\ Nl.min^{-1},$
(compensation with N_2*))*

For H_2 modulations, as also applies for CO_2, a rise in temperature greatly reduces phase shifts. Their formation (or consumption in the case of CO_2) occurs faster due to the increase in the rate coefficient at higher temperatures.

5.4.3. Reaction scheme

Considering the adsorbed species detected on catalyst B (carbonates, formates and methoxy) and in agreement with a similar study by Bailey et al. (using a $CuO/ZnO/Al_2O_3$ catalyst) (Bailey *et al.* 1995), the following proposal may be offered. Methanol synthesis proceeds by prior formation of the carbonate on the copper, followed by hydrogenation of the carbonate to the formate and then to methoxy and methanol, as summarized in figure 47.

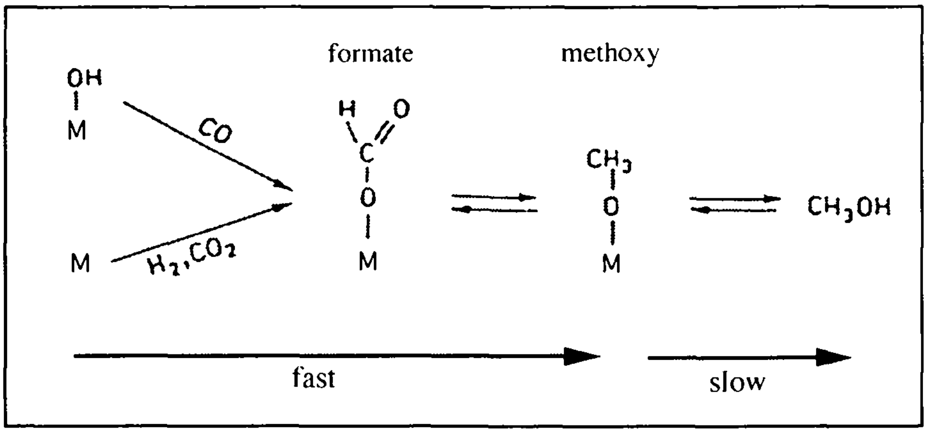
formate
methoxy
OH
M
M
CO
H₂,CO₂
H O C O M
CH₃ O M
CH₃OH
fast
slow

Fig. 47: Reaction scheme for carbon dioxide (and carbon monoxide) hydrogenation reactions for $CuO/ZnO/Al_2O_3$ catalysts

This mechanism has also been proposed by other groups (Bowker *et al.* 1988, Le Peltier *et al.* 1996, Millar *et al.* 1991).

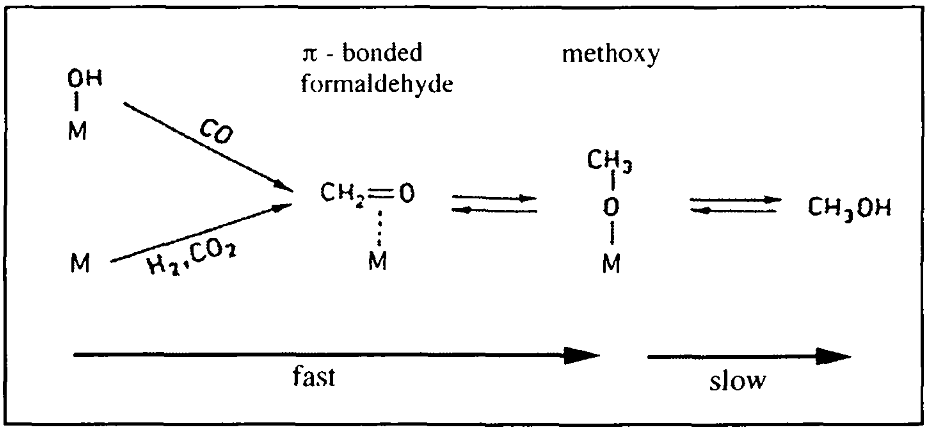
π - bonded formaldehyde
methoxy
OH
M
M
CO
H₂,CO₂
CH₂=O
M
CH₃ O M
CH₃OH
fast
slow

Fig. 48: Reaction scheme for carbon dioxide (and carbon monoxide) hydrogenation reactions for CuO/ZrO_2 catalysts

Regarding CuO/ZrO_2 catalysts (catalyst A), Weigel's conclusions (Weigel 1996) do not support the hypothesis that formate is an intermediate in methanol synthesis. A mechanism involving π - bound formaldehyde is preferred (Fig. 48). Two different methanol synthesis routes exist depending on whether a CuO/ZrO_2 or $CuO/ZnO/Al_2O_3$, catalyst composition applies. The route for the former catalyst is via a π - bound formaldehyde intermediate and for the latter catalyst via a formate species.

Preliminary results from the simulation of the periodic experiments (see appendix A.5.) shows that a pathway with consecutive or consecutive/parallel reactions is prevailing. Unfortunately, it was not possible to predict unambiguously which pathway is the right one. Nevertheless the model with only 2 parallel reactions can be rejected.

6. An alternative approach (A)
Carbon dioxide hydrogenation to methanol in dielectric-barrier discharges

6.1. Scope

Conversion of CO_2 to methanol in dielectric-barrier discharges is investigated. Excitation of CO_2 and H_2 molecules by energetic electrons causes reactions which lead to the formation of new products such as carbon monoxide, methane and methanol.

6.2. Introduction

Dielectric-barrier discharges or barrier discharges (DBDs), also frequently referred to as silent discharges, have been utilized for more than a century. Early investigations, pioneered by Siemens (Siemens 1857) in 1857, studied the ozone generation by a stream of oxygen or air when subjected to the influence of a DBD. Ozone and nitrogen oxide formation in DBDs became an important area of research during the subsequent decades (Andrews *et al.* 1860, Becker 1920, Becker 1923, Briner *et al.* 1930, Devins 1956, Eliasson *et al.* 1987, Filippov *et al.* 1987, Fuji *et al.* 1959, Hautefeuille *et al.* 1881, Kogelschatz 1983, Lunt 1959, Otto 1929, Samoilovich *et al.* 1989, Warburg 1904, Warburg 1925, Warburg *et al.* 1909).

In recent years novel applications of DBDs with respect to CO_2 lasers (Takenaka *et al.* 1991, Yagi *et al.* 1981, Yasui *et al.* 1989), excimer lamps (Eliasson *et al.* 1988, Kogelschatz 1990, Kogelschatz 1991, Kogelschatz 1992, Shuaibov *et al.* 1979, Volkova *et al.* 1984), surface modification (Kanazawa *et al.* 1988, Massines *et al.* 1992, Reitz 1992), flue gas treatment (Chang *et al.* 1991, Chang *et al.* 1992, Chang *et al.* 1996, Sardja *et al.* 1990) and pollution control (Bugaev 1996, Clothiaux *et al.* 1984, Eliasson *et al.* 1991b, Evans 1993, Sheinson *et al.* 1987, Storch *et al.* 1993) have been proposed. Large gas flows, at pressures close to atmospheric pressure, can be subjected to non-equilibrium plasma conditions with only a negligible increase in the enthalpy of the feed gas.

CO_2 hydrogenation in a DBD reactor is investigated as an alternative approach to methanol synthesis in a packed-bed reactor.

6.3. The dielectric-barrier discharge

The dielectric-barrier discharge is a high pressure non-equilibrium discharge which occurs when alternating voltages are applied between two electrodes separated by a non conducting medium. The distance across the discharge gap is normally limited to a few millimeters (at ambient pressure) avoiding applied voltages that are too high. The frequency can vary over a wide range from line frequency to several MHz. A planar configuration is shown in figure 49 but cylindrical geometries are also common using annular discharge gaps. Glass, quartz or ceramics can be used as dielectrics. In this study a thin metal coating is used as an electrode. It is also possible to apply dielectric coatings to a metal electrode, for example enamel layers on steel electrodes.

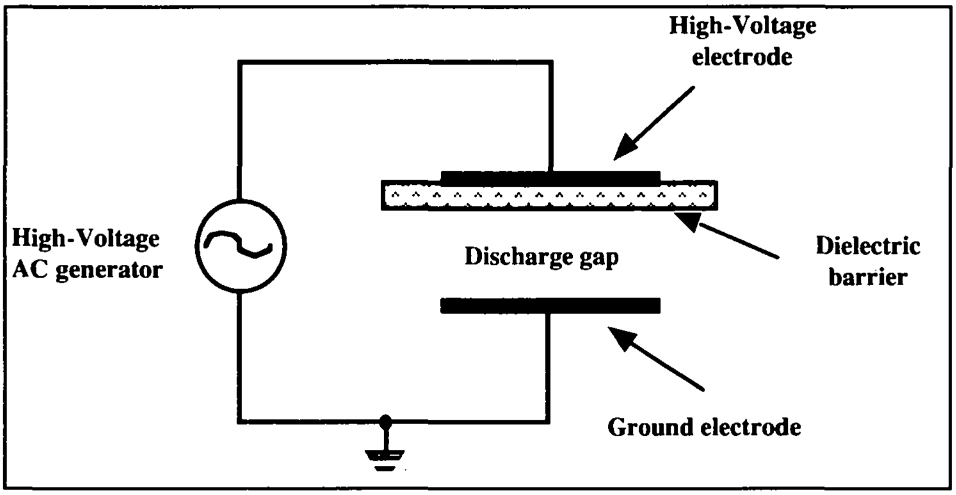

Fig. 49: Schematic view of a dielectric-barrier discharge (planar geometry)

When the amplitude of the applied sinusoidal field rises above a critical value, breakdown is initiated and a current flows from one electrode to the other. This silent discharge consists of a multitude of current filaments of short duration (in the order of 10 ns) which are the so-called micro discharges (Fig. 50). These micro discharges have diameters of the order of 100 μm. As a result of the dielectric barrier, only a short current pulse can propagate. At atmospheric pressures, typical values for electron densities are of the order 10^{21} □m^{-3}, charges transported by individual micro discharges are of the order nC and electron energies of several eV (Eliasson *et al.* 1994).

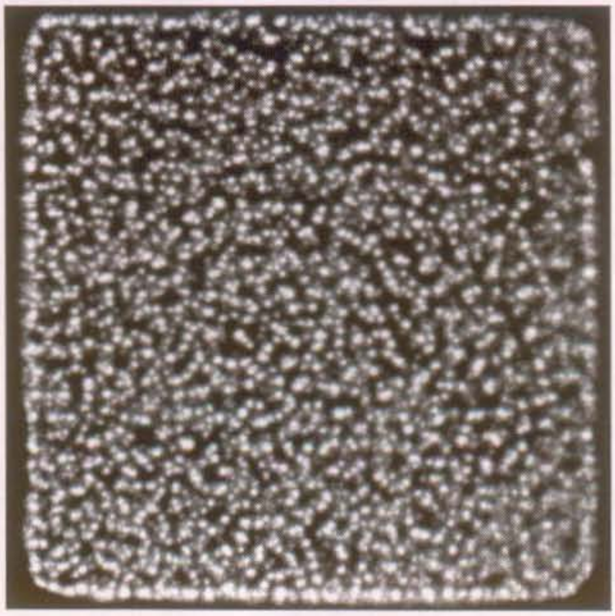

Fig. 50: Photograph of micro discharges in air at atmospheric pressure.
White and gray points are the micro discharges
(photograph taken through a transparent electrode, original size: 6 cm x 6 cm,
exposure time: 20 ms)

Charge accumulation at the dielectric surface results in a local reduction of the electric field. If the external voltage is still rising, additional micro discharges will preferentially strike other locations with higher fields. Thus, the dielectric is certainly the most important feature and serves a dual purpose. It distributes the micro discharges over the entire electrode and, at the same time, limits the amount of charge and energy forming on an individual micro discharge. These micro discharges can leave behind[13] a track of excited and ionized species as well as free radicals with negligible increase in gas temperature. The excited molecules can in turn initiate chemical reactions which lead to the formation of new products.

This process is used to investigate the hydrogenation of CO_2 to methanol. The influence of various parameters for example, temperature, pressure, electrical power, gas composition and flow rate on the methanol synthesis reaction is examined.

6.4. Materials and methods

The experimental configuration is shown in figure 51. The DBD reactor is mounted in a high-pressure cylindrical vessel, which can be run at pressures up to 10 bar and with temperatures controlled up to 350 °C. A silent discharge is maintained in an annular gap of 1 mm formed by an outer steel cylinder of 54 mm internal diameter and an inserted cylindrical quartz tube of 52 mm external diameter and 2.5 mm wall thickness. The length of the discharge gap is 310 mm and the discharge volume is approximately 50 ml. The steel cylinder serves as the ground electrode and an alternating high voltage frequency is applied to a gold coating on the inside of the quartz tube. The power can be measured accurately and regulated between 50 W and 1000 W by a HV power supply (Arcotec HS 15, Mönsheim, Germany). It adjusts the amplitude and the frequency (up to 20 kHz) of the applied voltage automatically.

---

[13] The local breakdown is usually completed within nanoseconds, the current transport takes typically 1-100 ns and chemical reactions can last from nanoseconds to seconds.

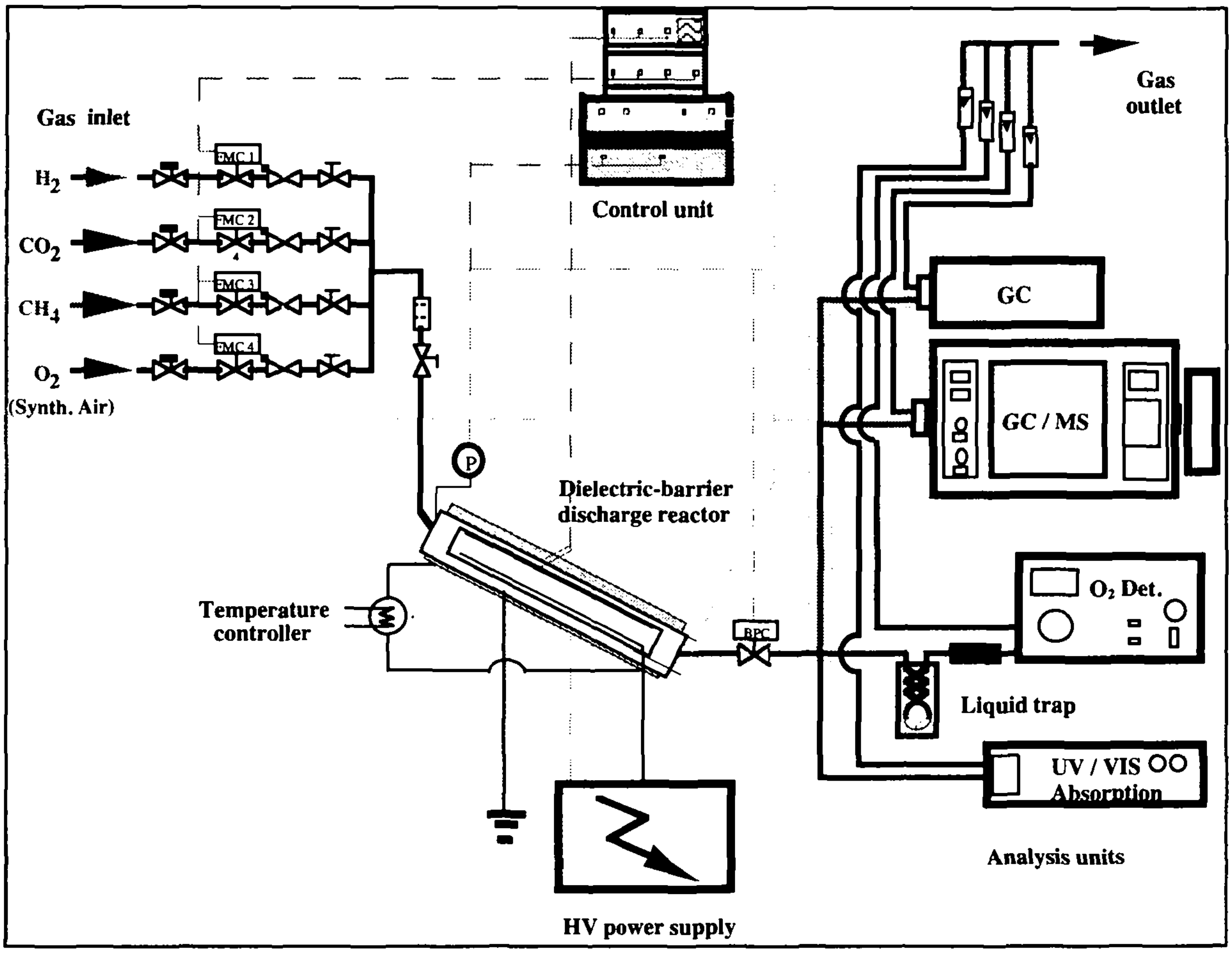
Gas inlet
H_2
CO_2
CH_4
O_2
(Synth. Air)
FMC 1
FMC 2
FMC 3
FMC 4
Control unit
P
Dielectric-barrier discharge reactor
Temperature controller
BPC
HV power supply
Gas outlet
GC
GC / MS
O_2 Det.
Liquid trap
UV / VIS Absorption
Analysis units

Fig. 51: Schematic view of the DBD reactor setup

Different feed gases can be added and mixed before entering the discharge reactor. The individual flow rates are controlled by mass flow controllers (FMC series F, Bronkhorst Hi-Tec, Ruurlo, The Netherlands). Total gas flows can vary from 125 to 4000 Nml.min^{-1}. A regulating valve (Research Control Valve, Badger Meter, Oklahoma, USA) situated at the exit of the reactor controls the discharge pressure. Oil circulates in a closed loop controlled by a thermostat, maintaining the temperature of the reactor at a preset value (Lauda USH 400, Königshofen, Germany). The products are analyzed by two gas chromatographs (Hewlett Packard 5890A, Palo Alto, USA and MTI M 200 H, Fremont, USA) which are connected to the reactor by a heated line. For the HP instrument, a poraplot Q column (25 m, 0.53 mm) is used in connection with TCD and FID detectors. For the MTI instrument, a poraplot Q column (8 m, 0.32 mm) and a molecular sieve 5 A (10 m, 0.32 mm) are used in connection with two TCD detectors. Oxygen concentration is measured by a special oxygen monitor based on paramagnetism (Helox 3, Biel-Benken, CH). Ozone concentration is measured by

UV absorption at 254 nm (Shimadzu UV 120, Kyoto, Japan). In addition, condensable products (water and oxygenated compounds) are collected in a cold trap at a temperature of 0 °C.

6.5. Results and discussion

6.5.1. Temperature variation

a) Carbon dioxide dissociation

Initially, a measurement is taken using pure CO_2 at a pressure of 1 bar and a flow rate of 500 Nml.min^{-1}. The electrical power is set to 200 W. Figure 52 shows a typical distribution of the partial pressures as a function of the temperature.

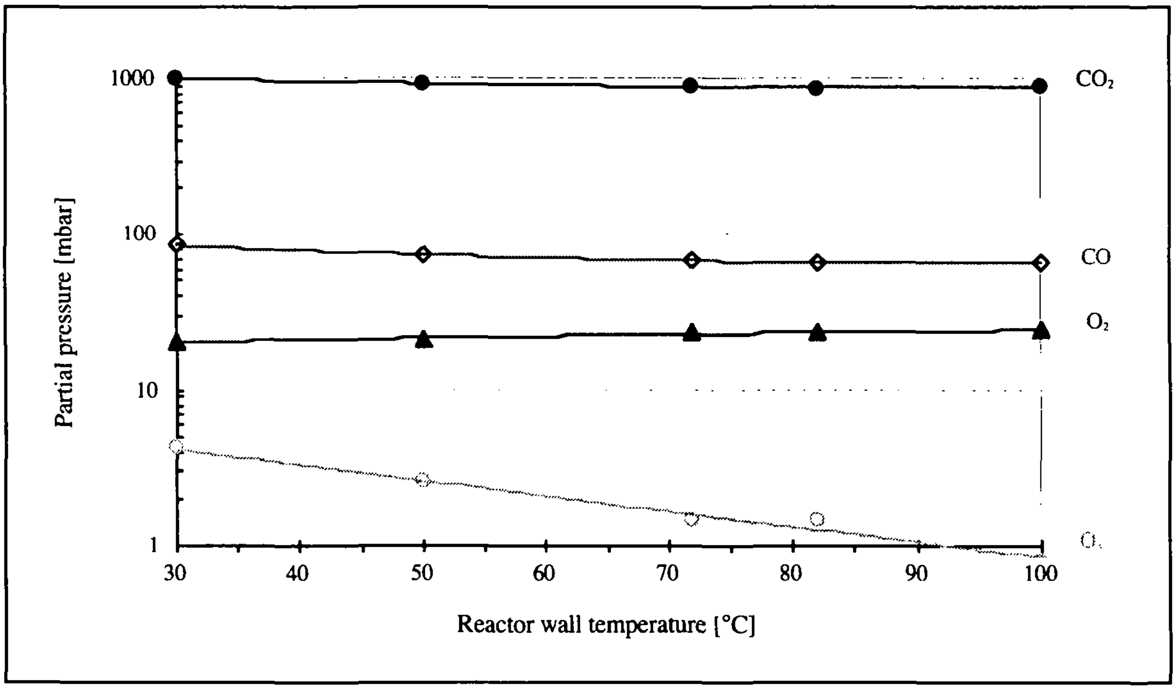

Fig. 52: Products distribution (partial pressures at standard pressure)
(Electrical power = 200 W, P = 1 bar, Q_{CO_2} = 500 Nml.min^{-1})

The graph shows that temperature only has a slight influence on the dissociation of the carbon dioxide molecules and on the formation of carbon monoxide and molecular oxygen. Only the ozone concentration decreases strongly with rising temperature. This behavior is well known and understood from studies on ozone generation in silent discharges (Eliasson *et al.* 1987, Eliasson *et al.* 1991a).
The dissociation of carbon dioxide in the discharge takes place according to the reaction 28:

$$CO_2 + e \rightarrow CO + O + e \tag{28}$$

The oxygen atoms immediately recombine to form molecules according to:

$$O + O + M \rightarrow O_2 + M \tag{29}$$

and

$$O + O_2 + M \rightarrow O_3 + M \tag{30}$$

In these reactions M stands for a third collision partner. It is interesting to note that CO is not oxidized by ozone.

b) Carbon dioxide hydrogenation

Secondly carbon dioxide hydrogenation is studied. A H_2/CO_2 mixture (3:1) is passed through the reactor at a pressure of 1 bar and at a total flow rate of 1 $Nl.min^{-1}$. The electrical power in the reactor is set to 400 W. Figure 53 shows the typical distribution of the partial pressures as a function of the reactor wall temperature.

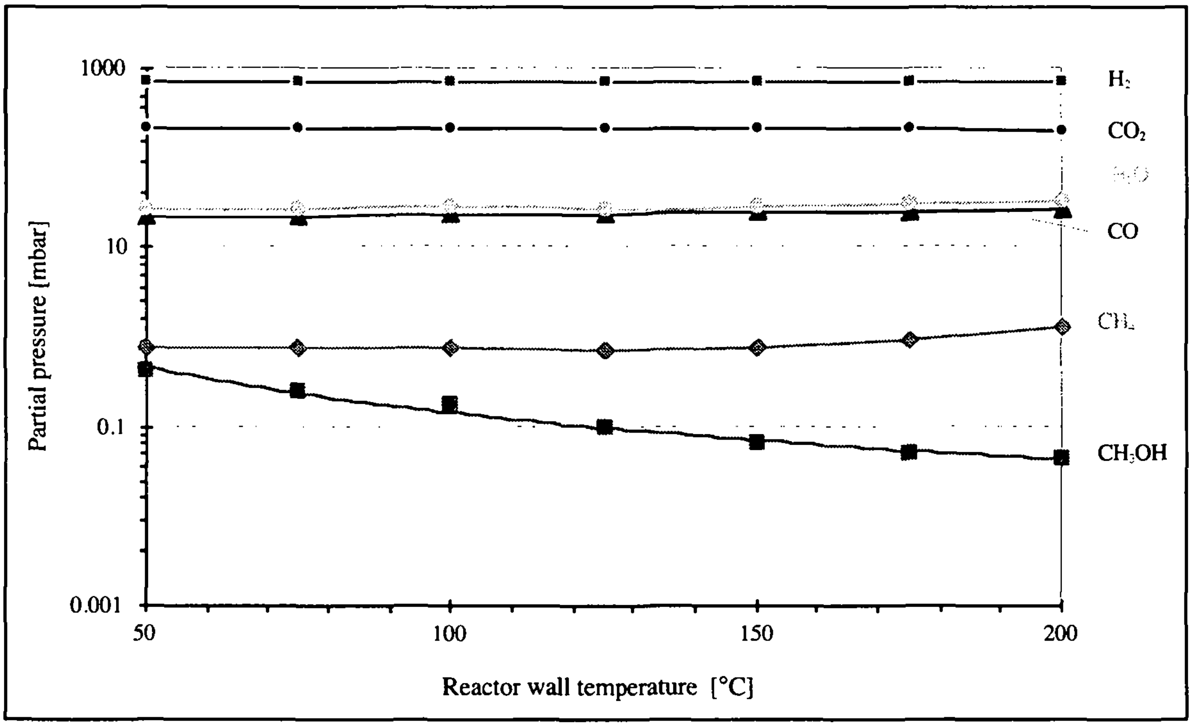

Fig. 53: Products distribution (partial pressures at standard pressure) as a function of the reactor wall temperature
(Electrical power = 400 W, P = 1 bar, H_2/CO_2 = 3, Q_{tot} = 1 $Nl.min^{-1}$)

The graph shows that temperature does not have a very strong influence on the products' selectivity over the investigated temperature range. This is also the case for pure CO_2. The major products are carbon monoxide and water. They are produced in comparable amounts which increase slightly as the temperature rises. Methanol and methane are produced in smaller quantities and their concentrations show different temperature dependencies. Neither oxygen nor ozone are detected in this experiment. CO, CH_4 and CH_3OH yields as a function of the temperature are shown in figure 54.

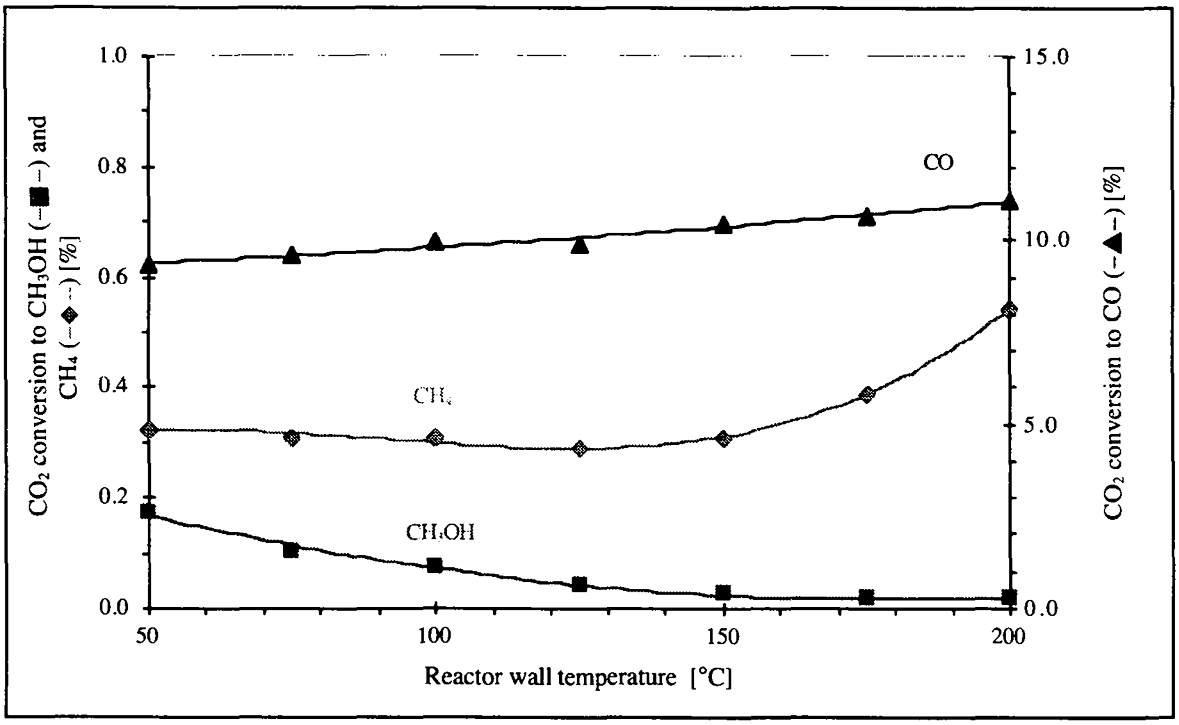

Fig. 54: Products yield as a function of reactor wall temperature
(Electrical power = 400 W, P = 1 bar, $H_2/CO_2 = 3$, $Q_{tot} = 1\ Nl.min^{-1}$*)*

Methanol concentration decreases with higher temperatures as expected for an exothermic reaction (see paragraph 1.3.1.). A maximum CH_3OH yield (0.2 %) is obtained at the lowest investigated temperature (T = 50 °C). Conversely, CO and CH_4 yields increase with rising temperature. Maximal measured values at 200 °C are 11 % and 0.5 % for CO and CH_4 respectively.

6.5.2. Pressure variation

Figure 55 shows the effect of pressure variations on the products' yield. Pressure has little influence on product formation. Maximum values, 13 % and 0.5 % for CO and CH_4 respectively are obtained at 1 bar. As the pressure is increased to 6 bar CO and CH_4 yields gradually decrease. Regarding methanol formation, a slight maximum is observed at approximately 2 bar. Referring to a study by Kogelschatz et al. (Eliasson *et al.* 1991a) a maximum was also observed at 2 bar in the ozone formation DBDs.

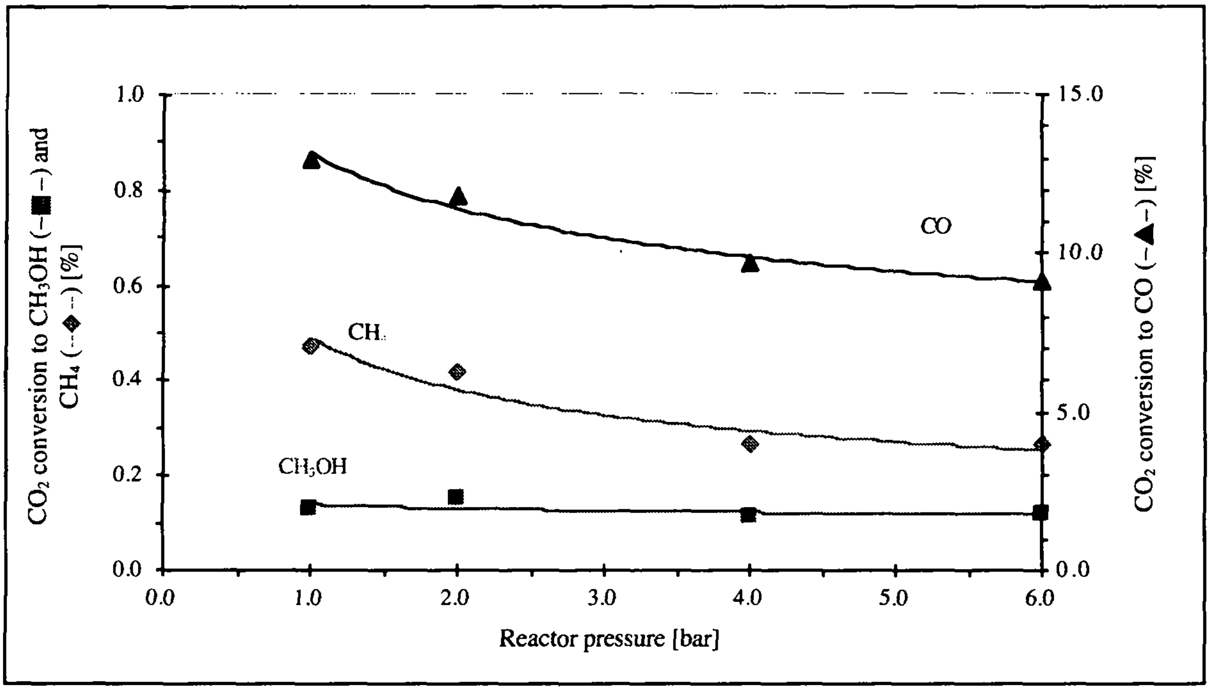

Fig. 55: Products yield as a function of reactor pressure
(Electrical power = 400 W, T = 80 °C, $H_2/CO_2 = 3$, $Q_{tot} = 1\ Nl.min^{-1}$)

6.5.3. Electrical power variation

Carbon dioxide hydrogenation's dependence on electrical power is also investigated and the CO, CH_4 and CH_3OH yields are shown in figure 56. A linear increase in the CO and CH_4 concentrations as a function of the electrical power is observed. As regards methanol, a saturation yield of 0.1 % is obtained at about 400 W which corresponds to a specific energy[14] of 5.5 eV per molecule of the feed gas. Methanol production initially rises with increasing specific energy, and after reaching a maximum begins to decrease again. At energy levels that are too high, the methanol destruction reaction apparently offsets the formation process.

---

[14] The specific energy refers to the amount of electrical energy supplied to the discharge per molecule of feed gas.

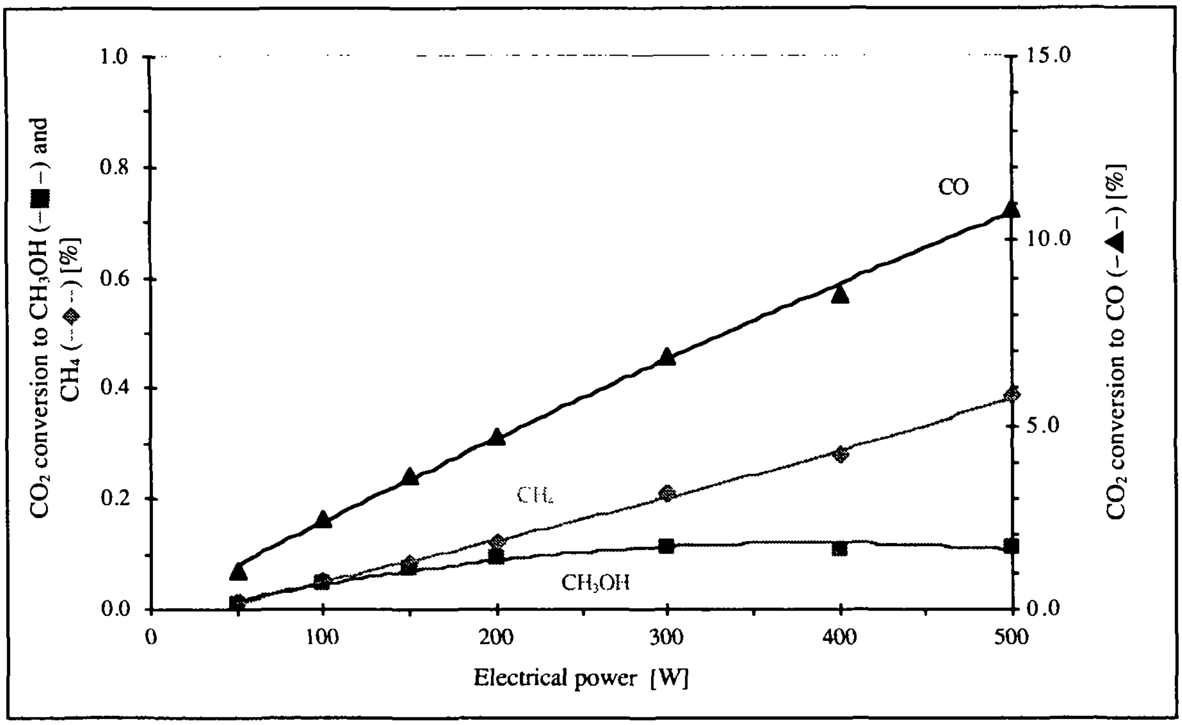

Fig. 56: Products yield as a function of the electrical power
(T = 80 °C, P = 1 bar, $H_2/CO_2 = 3$, $Q_{tot} = 1$ *Nl.min*$^{-1}$*)*

6.5.4. H_2/CO_2 ratio variation

Figure 57 shows a typical distribution of the partial pressures when H_2/CO_2 mixtures of different mixing ratio are used.

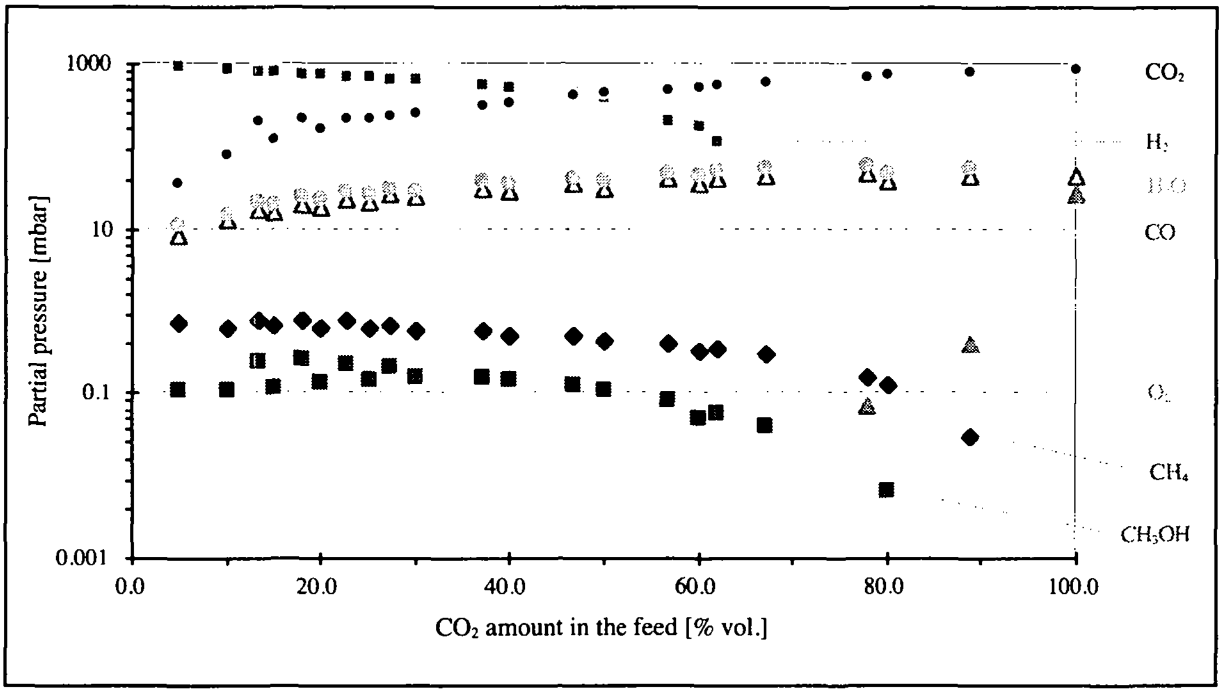

Fig. 57: Mixture of hydrogen and carbon dioxide. Products distribution (partial pressures at standard pressure) as a function of the CO_2 amount in the feed (Electrical power = 400 W, $T = 80$ °C, $P = 1$ bar, $Q_{tot} = 1$ Nl.min^{-1})

Again comparable amounts of CO and H_2O are produced. As an obvious check, we confirmed that H_2O and CO were not formed or detected present, when hydrogen and CO_2 respectively were removed from the feed. CH_4 is again produced in smaller amounts. Its concentration decreases as the amount of CO_2 in the feed increases. Regarding methanol, the experiment shows that a gas feed containing approximately 20 % CO_2 gives the maximum yield. This result is close to theoretical calculations (Eliasson *et al.* 1994).

6.5.5. Residence time variation

Figure 58 shows the products' yield as a function of the total gas flow rate.

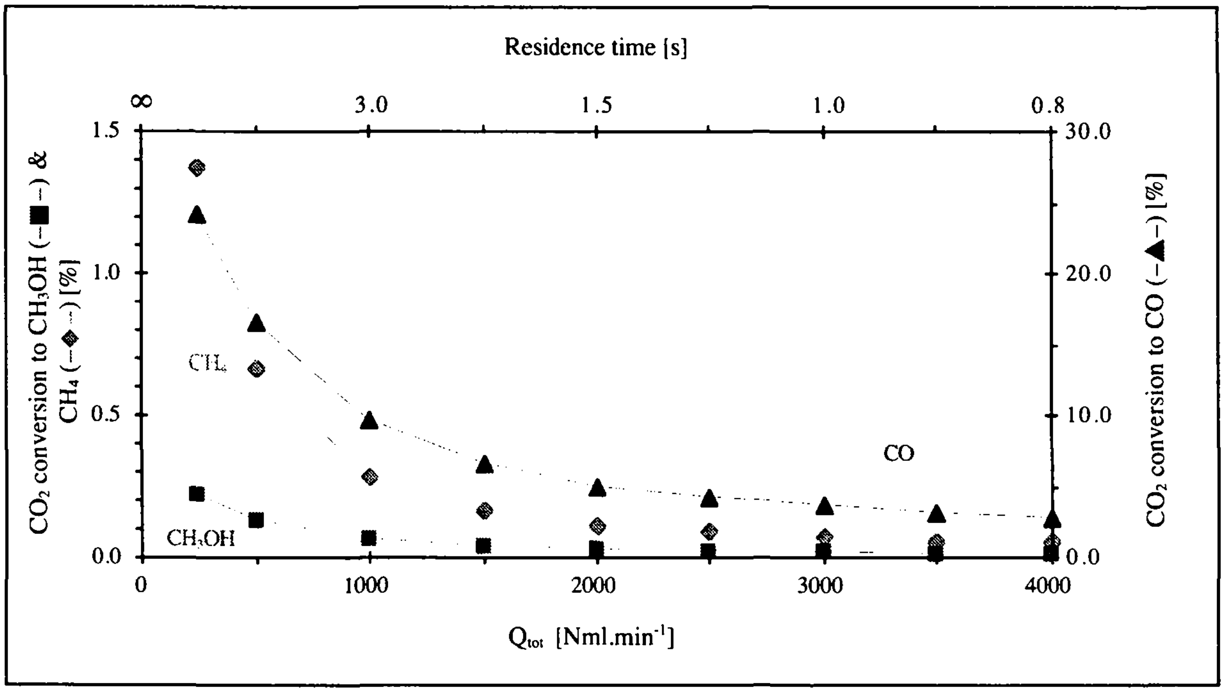

Fig. 58: Products' yield as a function of the total gas flow
(Electrical power = 400 W, T = 80 °C, P = 1 bar, $H_2/CO_2 = 3$)

Yields gradually decrease to zero when increasing the flow rate from 250 $Nml.min^{-1}$ to 4000 $Nml.min^{-1}$. Therefore maximum yields are obtained with the longest residence times. Maximal values of 0.2 %, 1.4 % and 30 % are obtained for methanol, CH_4 and CO respectively . This also correspond to high specific energies.

6.5.6. Measurement with catalyst

It is easy to imagine the simultaneous use of discharges and catalysts. It is quite likely that the combination of a DBD and an appropriate catalyst would improve the performance of the DBD reactor considerably. In particular, there is no reason why a catalyst should not be introduced into the discharge gap does not present a problem. Preliminary measurements show that the methanol yield and selectivity are increased at least ten-fold (Eliasson *et al.* 1997).

6.5.7. Measurement with air

As already reported (Bill *et al.* 1997), a mixture of oxygen and methane (1:19) also leads to the formation of methanol. The methanol concentration saturates at about 1.2 %, after all the oxygen is consumed. Similar results are reported by Okazaki (Okazaki *et al.* 1995) for a pulsed silent discharge reactor.

A final exploratory experiment was performed where methane and air mixtures of different mixing ratios were fed through the reactor. A maximum methanol yield (0.6 %) is obtained at a 30:70 mixture of air and methane. These experiments show that it is possible to synthesize methanol from methane and air at room temperature and 1 bar (ambient) pressure, in a DBD reactor.

6.6. Conclusions

The experiments have shown how electrical breakdown, which leads to the formation of micro discharges in high pressure gases and excited molecules, can be applied to the methanol synthesis.

A summary of the experimental conditions found to maximize the methanol formation is given in table 17.

Table 17: Best results for the methanol synthesis from a H_2/CO_2 (3:1) mixture
Comparison of DBD and packed-bed reactors

	Experimental configurations					
Parameter	**DBD reactor without catalyst**		**DBD reactor with catalyst**		**Packed-bed reactor with catalyst**	
Temperature [°C]	50	100	100	220	100	220
Power [W]	400	500	500	500	-	-
Pressure [bar]	1	8	8	8	8	8
Total flow rate [Nl.min^{-1}]	0.25	0.50	0.50	0.50	0.50	0.50
Methanol yield [%]	0.2	< 0.1	0.8 - 1.0	0.22	0	2.2
Ref.	Paragraph 6.4.5.	(Eliasson *et al.* 1997)	(Eliasson *et al.* 1997)		Paragraph 3.5.2.	

These preliminary experiments do not indicate a viable economic solution. They do however demonstrate that CO_2 conversion in DBDs is possible and may therefore be regarded as a useful step in tackling the problem of CO_2 recycling.

7. An alternative approach (B) **Carbon dioxide electroreduction**

7.1. Scope

Electrochemical reduction of carbon dioxide is investigated by using TiO_2/Ni complex and TiO_2/Ru complex thin film electrodes in solutions containing dissolved carbon dioxide. The use of transition metal complexes means that considerable decreases in overvoltage are achieved together with respectable current densities.

7.2. Introduction

CO_2 electroreduction was investigated as early as 1870 by Royer (Royer 1870). Reduction was carried out on a Zn(Hg) electrode in an aqueous solution leading to the formation of formic acid. Since then, particularly in the last two decades, CO_2 electroreduction has been the subject of many studies, looking at the effects of the electrode materials and electrolyte media on the nature of the products. The most important and interesting aspects are summarized in papers by Silvestri et al. (Silvestri *et al.* 1991), Frese et al. (Frese 1993), Keene et al. (Keene *et al.* 1993) and in a book written by Halmann (Halmann 1993).

Reasonably favorable thermodynamics[15] are observed for the CO_2 reduction leading to the various products given below (see eq 31 to 35):

$$CO_2 + 2H^+ + 2e^- \rightarrow HCOOH \qquad (E^0 = -0.61\ V) \qquad (31)$$

$$CO_2 + 2H^+ + 2e^- \rightarrow CO + H_2O \qquad (E^0 = -0.52\ V) \qquad (32)$$

$$CO_2 + 4H^+ + 4e^- \rightarrow HCHO + H_2O \qquad (E^0 = -0.48\ V) \qquad (33)$$

$$CO_2 + 6H^+ + 6e^- \rightarrow CH_3OH + H_2O \qquad (E^0 = -0.38\ V) \qquad (34)$$

$$CO_2 + 8H^+ + 8e^- \rightarrow CH_4 + 2H_2O \qquad (E^0 = -0.24\ V) \qquad (35)$$

As the energy required for the transfer of each electron is very much less for these multi-electron reactions (eq 34 and 35) than for the monoelectronic reduction of CO_2 to its radical anion $CO_2^{\cdot -}$ ($E^0 = -2.1$ V vs. SCE) (Teeter *et al.* 1954), the application of multi-electron transfer to the reduction of

---

[15] Equilibrium electrode potentials at pH = 7.0 (aqueous media) are given with respect to SHE (Teeter*et al.* 1954).

CO_2 commands considerable interest. In particular, systems without catalysts still present strong kinetic hindrances resulting in very large electrode overpotentials (approximately 1 V) (Hori 1993).

A number of electrode systems have been investigated for the production of methanol by direct electrochemical reduction of carbon dioxide. Some of these systems have high Faradaic efficiencies, but usually they have very low current densities (less than 1 mA.cm^{-2}). On Cu electrodes, the product distribution depends on the electrode potential (Ikeda *et al.* 1991). Using n-GaAs single-crystal electrodes, in CO_2 saturated Na_2SO_4 solution, methanol was produced with a 100 % Faradaic yield, at electrode potentials of -1.2 to -1.4 V (SCE), but at current densities of only 0.2 mA.cm^{-2} (Canfield *et al.* 1983, Frese *et al.* 1984). On molybdenum electrodes, in CO_2 saturated acidic solutions at -0.7 to -0.8 V vs. SCE, methanol was formed as the major product, with Faradaic efficiencies higher than 50 %, and current densities of up to 0.6 mA.cm^{-2} (Suzuki *et al.* 1971). On electrodes of ruthenium, fixed on polyhydroquinone/benzoquinone supported on a glassy carbon electrode, the potential for CO_2 reduction was as low as -0.5 V (vs. SCE). However when illuminated by visible light, an efficiency of 100 % could be obtained (Arakawa *et al.* 1992). On RuO_2 + TiO_2 coated on titanium foil, at -0.1 V (vs. Hg_2SO_4) in an acid solution, the reduction of methanol occurred with 24 % current efficiency, and at a current density of 0.52 mA.cm^{-2} (Bandi 1990).

In order to improve the selectivity and efficiency of alcohol production, alloy electrodes were also evaluated. On metals with high overpotential for hydrogen production, such as Hg, Cd, Ag and Cu, the current efficiency and product selectivity for carbon dioxide reduction are good, but the energy efficiency is low due to the high overpotentials. However, on metals with low overpotentials for hydrogen generation, such as Fe, Co and Ni, both the selectivity and the energy efficiency for carbon dioxide are poor. Improvements in the selectivity and the energy efficiency of CO_2 reduction can be achieved by introducing low hydrogen overpotential metals (such as group VIII metals) on the surface of high hydrogen overpotential metals (such as the group IB or IIB). These alloy electrodes enable catalytic reduction of surface-adsorbed CO_2 or reduced carbon intermediates by surface-adsorbed hydrogen atoms. On Cu-Ni alloy, for example, the formation of methanol almost occurred at the reversible potential (approximately -0.38 V vs. SHE). At a potential of -0.65 V (vs. SHE) a Faradaic efficiency of about 10 % and a partial current density of only 0.008 mA.cm^{-2} are reported (Watanabe *et al.* 1991).

Considerable decreases in the over voltage can also be achieved by using transition metal complexes as electron-transfer mediators (Fisher *et al.* 1980). Deposition of macro-cycles complexes on the electrodes was found to catalyze the reduction of carbon dioxide in aqueous or organic solvent. Nickel complexes, like Ni-cyclam[16], as well as a ruthenium complexes, are reported to be excellent catalysts for CO_2 electroreduction (Balazs *et al.* 1992, Beley *et al.* 1986, Fujihira *et al.* 1991).

As an alternative approach, electrochemical reduction of CO_2 is investigated by incorporating metal complexes into TiO_2 thin film electrodes.

---

[16] cyclam = 1,4,8,11-tetraazacyclotetradecane. In Appendix AA, structural formulas are given.

7.3. Materials and methods

a) Synthesis of complexes

Nickel-cyclam tetraacetic acid (Fig. 59) was synthesized in a yield of 35 % according to the procedure reported by Riesen (Riesen 1984). IR measurements (bands of COO^- or COO^-... Ni^{2+}: 1600 cm^{-1}; COOH: 1740 cm^{-1}, NH^+/OH: 2600 cm^{-1}) were used to identify the product. UV-Vis spectra gave signals, which at 345, 560 and 800 nm, were too weak to allow a meaningful characterization.

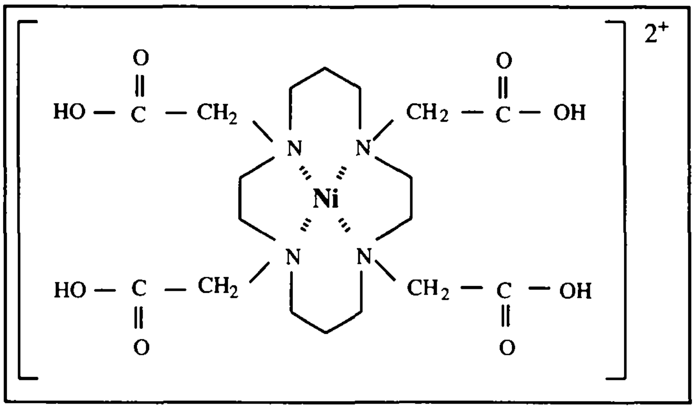

Fig. 59: Ni-cyclam complex structure
(Ni(II)-1,4,8,11-tetraazacyclotetradecane-1,4,8,11-tetraacetic acid)

Ruthenium complex (Fig. 60), prepared according to an established method, was kindly provided by M. K. Nazeeruddin (EPFL).

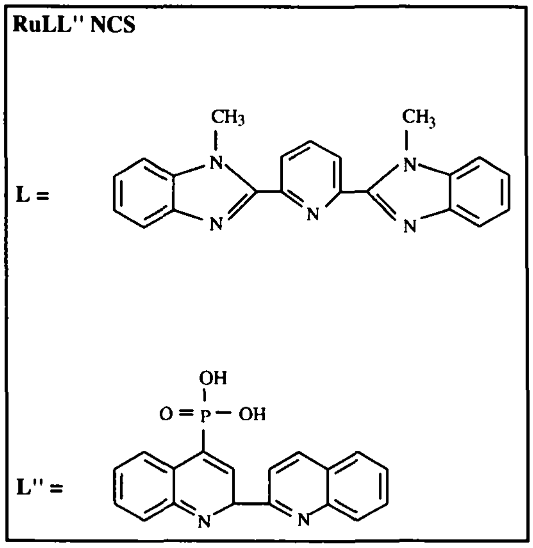

Fig. 60: Ru-ligand structures
(RuLL"NCS L = 2,6-bis (1'-methylbenzimidazol 2'-yl) pyridine
L" = 4-phosphonate 2,2'-biquinoline)

b) Electrode preparation

Nanocrystalline TiO_2 thin film electrodes were prepared as previously described (Nazeeruddin *et al.* 1993). Electrode impregnation involved placing the electrode (overnight) in a 10^{-5} M complex aqueous solution. Profilometry measurements showed that the TiO_2 film thickness was approximately 6 μm (Alpha-step 200 profilmeter, Tencor Instruments). The working area of the electrode was adjusted with a Teflon band leaving a free surface of 1 cm^2.

c) Electrochemical measurements

Electrochemical measurements used a conventional three-electrode cell design. The TiO_2 electrode (modified with a complex) formed the working electrode (1 cm^2), the counter electrode being glassy carbon and the reference electrode consisted of Ag/AgCl in contact with saturated KCl in water. All potentials are referenced to the Ag/AgCl/KCl (sat.) electrode without regard for the liquid junction potential. Current voltage curves (cyclic and differential pulsed voltametry) were measured using a scanning potentiostat (ECO Chemie Autolab).

As regards the cyclic voltametry, scans were performed at negative potential as low as -1.6 V vs. SCE. A sweep rate was chosen from 100 $mV.s^{-1}$ to 300 $mV.s^{-1}$. Before each experiment, a measurement was taken using a TiO_2 blank electrode. For differential pulsed voltametry, a solution containing the complex was prepared. Measurements were recorded as potentials varying from -1.5 to 1.5 V vs. SCE with a modulation amplification of 0.025 V. A measurement was previously taken in pure electrolyte as a blank.

To ensure saturation gases (carbon dioxide and argon) were vigorously bubbled through solutions for 15 min before the start of the experiments. During the experiments, gases were continuously flowing above the liquid surface. The products dissolved in the electrolyte were analyzed with a mass spectrometer (Balzers, Quadrupole QMA/QME-125). Spectra of pure compounds (CO_2, CO, CH_3OH, HCOOH, electrolyte, ...) were taken as references.

7.4. Results and discussion

7.4.1. Cyclic voltametry with the TiO_2/Ni-complex

Measurements taken with these electrodes show that the reduction in carbon dioxide is strongly dependent on the nature of the solvent. The most significant results are obtained with a tetrabutylammonium-perchlorate(TBAP) 0.1 M/DMF solution. In acetonitrile and trimethanolamine solutions smaller currents are observed. This is consistent with the fact that solvents that coordinate less well, such as DMF, present stronger catalytic effects because they do not interact with the nickel coordination sites (Hurrell *et al.* 1989).

When placed in an argon atmosphere, the Ni^{2+}/Ni^{+} complex couple seems to be irreversible. No particular potential wave is observed. However in the presence of CO_2, a strong rise in the current at -1.3 V indicates a catalytic reduction of CO_2 (Bill 1995a). Ni-cyclam deposited on a glassy carbon electrode allows the electrocatalytic reduction of CO_2 when the onset potential is still only -1.25 V vs. SCE (Akiba *et al.* 1992). Precise observation also shows that the first catalyst layer on the electrode reduces CO_2 more effectively than the subsequent layers.

7.4.2. Cyclic and differential pulsed voltametry with the TiO_2/Ru-complex

a) Differential pulsed voltametry of a Ru-complex solution on a GCE

Figure 61 shows both the background and the Ru-complex solution current density changes as a function of the applied potential. In the range 0 - 1 V, the current density changes are twice as large for the Ru-complex solution than for the pure electrolyte.

A local maximum of around +1.0 V is detected for the Ru complex solution, corresponding to the oxidation of the ruthenium (II) in ruthenium (III). Bolinger et al. obtained similar potential values for various Ru-complexes (Bolinger *et al.* 1985).

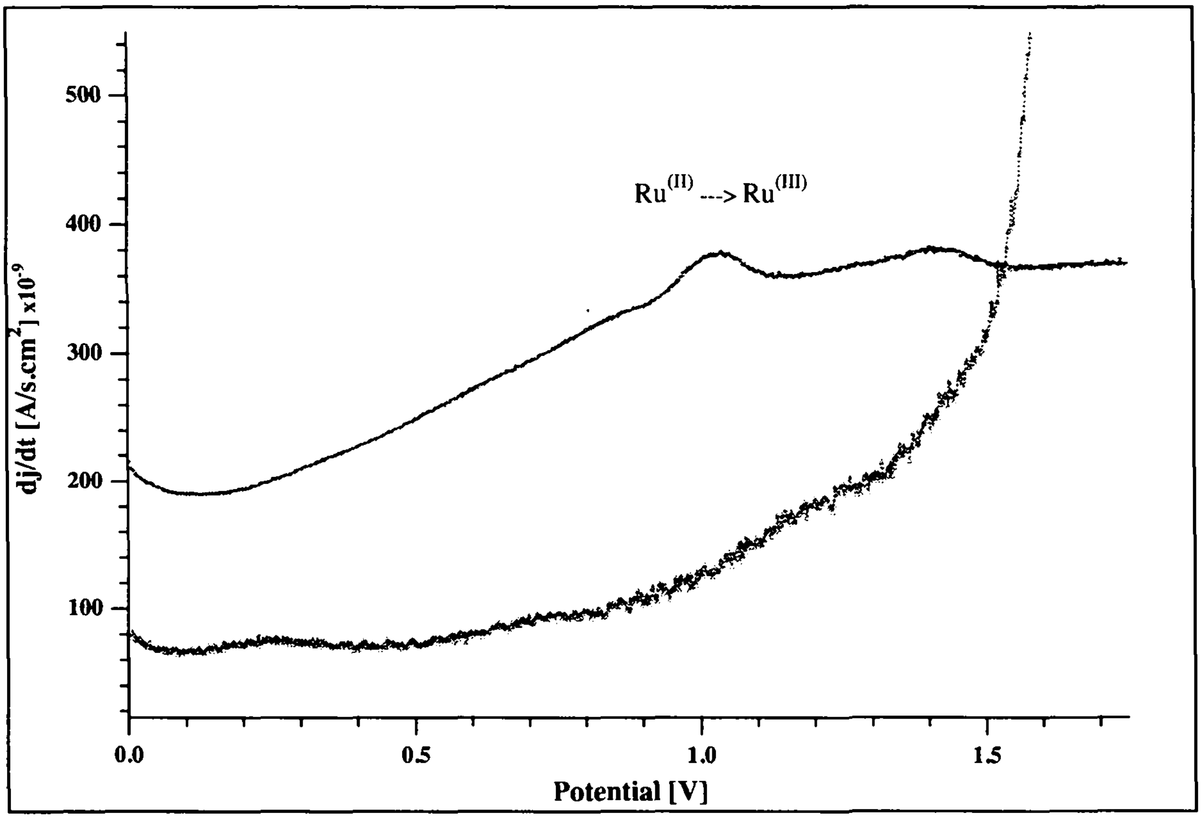

Fig. 61: upper curve: 1.8 10^{-4} M Ru-complex solution in a 0.1 M TBAP/DMF electrolyte
lower curve: 0.1 M TBAP/DMF solution
(modulation amplification: 0.025 V)

Figure 62 shows both the background and the Ru-complex solution current density time changes as a function of the applied potential. In the 0 - (-1.5) V range, this differential pulsed voltammogram again shows higher current density changes for the Ru complex solution than for the pure electrolyte solution. Ligands reduction is recorded at potentials of -1.3 V and -1 V.

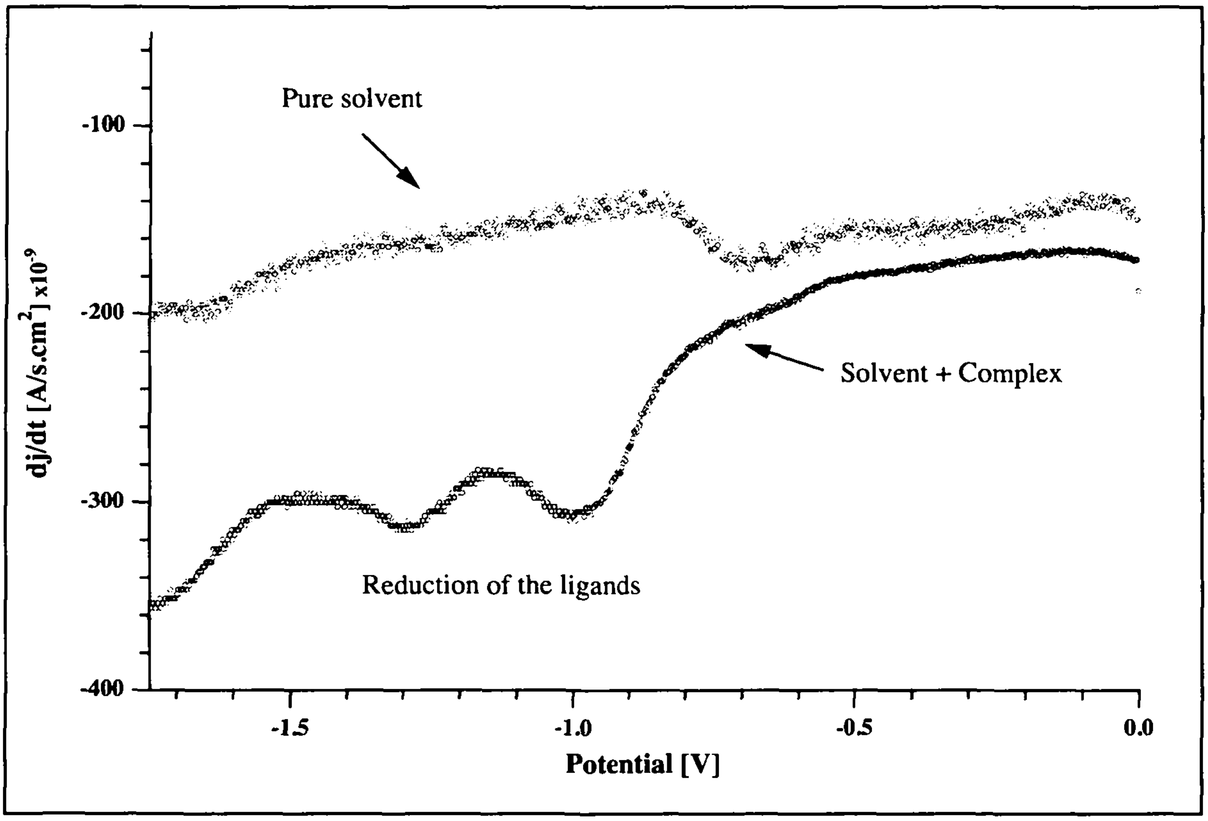

Fig. 62: upper curve: 1.8 10^{-4} M Ru-complex solution in a 0.1 M TBAP/DMF electrolyte
lower curve: 0.1 M TBAP/DMF solution
(modulation amplification: 0.025 V)

b) Cyclic voltametry the TiO_2/Ru complex thin film electrode

The variation of current densities as a function of the applied potential gives similar potential waves as the Ni-complex (Bill 1995b). Cathodic and anodic currents start to significantly increase below -1.0 V reaching a value of 5 μA at -1.5 V. Figure 63 shows both the background current density in Ar-purged electrolyte (broken curve) and the current density in CO_2-saturated electrolyte (solid curve) in cyclic voltammograms obtained at TiO_2/Ru-complex electrodes. In a CO_2 atmosphere, much higher currents (by a factor of 7) are observed. The cathodic current starts to significantly increase (relative to the Ar-purged electrode) at -1.2 V. The electroactivity for CO_2 reduction in aprotic solvent is respectable as current values around 0.2 mA are measured. On the back sweep, irreversible potential waves are observed (-1.1 V). These waves might be attributed to electron transfer in the complexes.

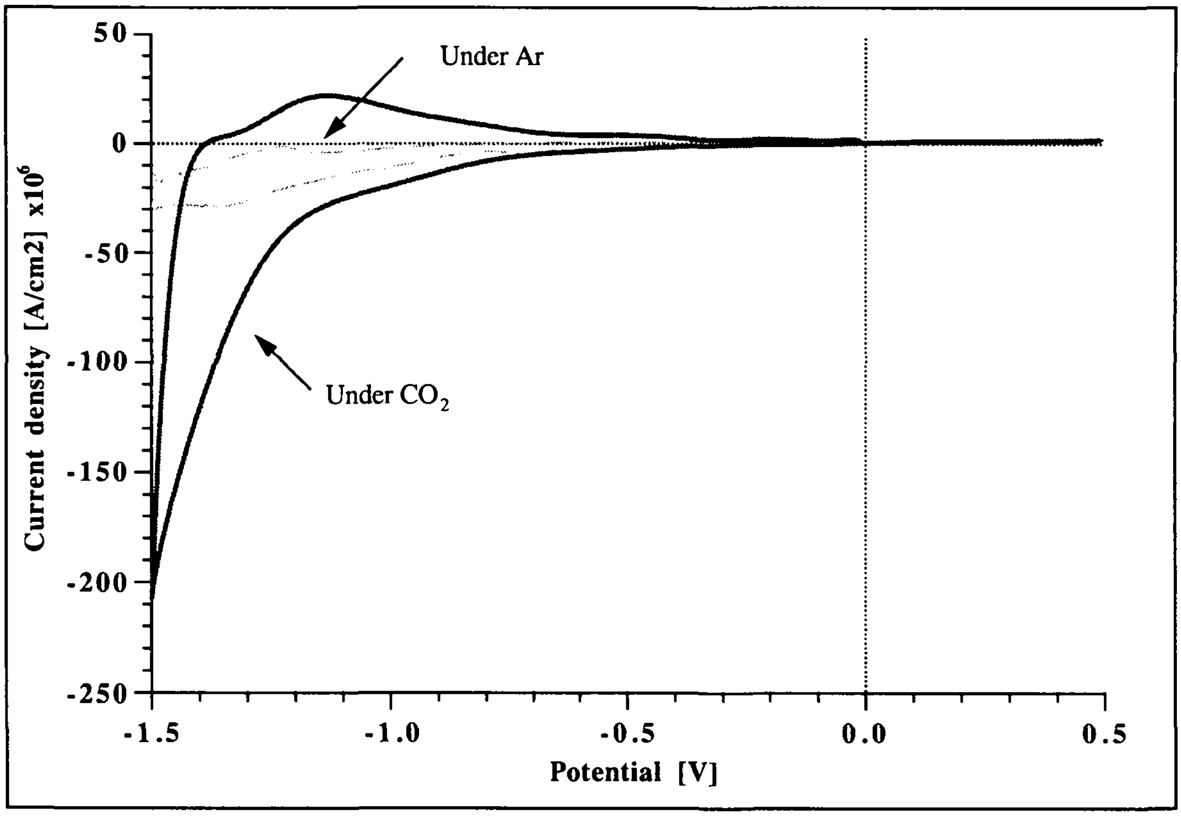

Fig. 63: Cyclic voltammograms of TiO_2/Ru-complex electrodes in a 0.1 M TBAP/DMF solution (Ar saturated and CO_2 saturated)

The curve shown in figure 64 gives the difference between the two curves in figure 63. The resulting curve is very similar to the one corresponding to CO_2 of the previous figure. Current changes (especially in the back sweep) are even better defined.

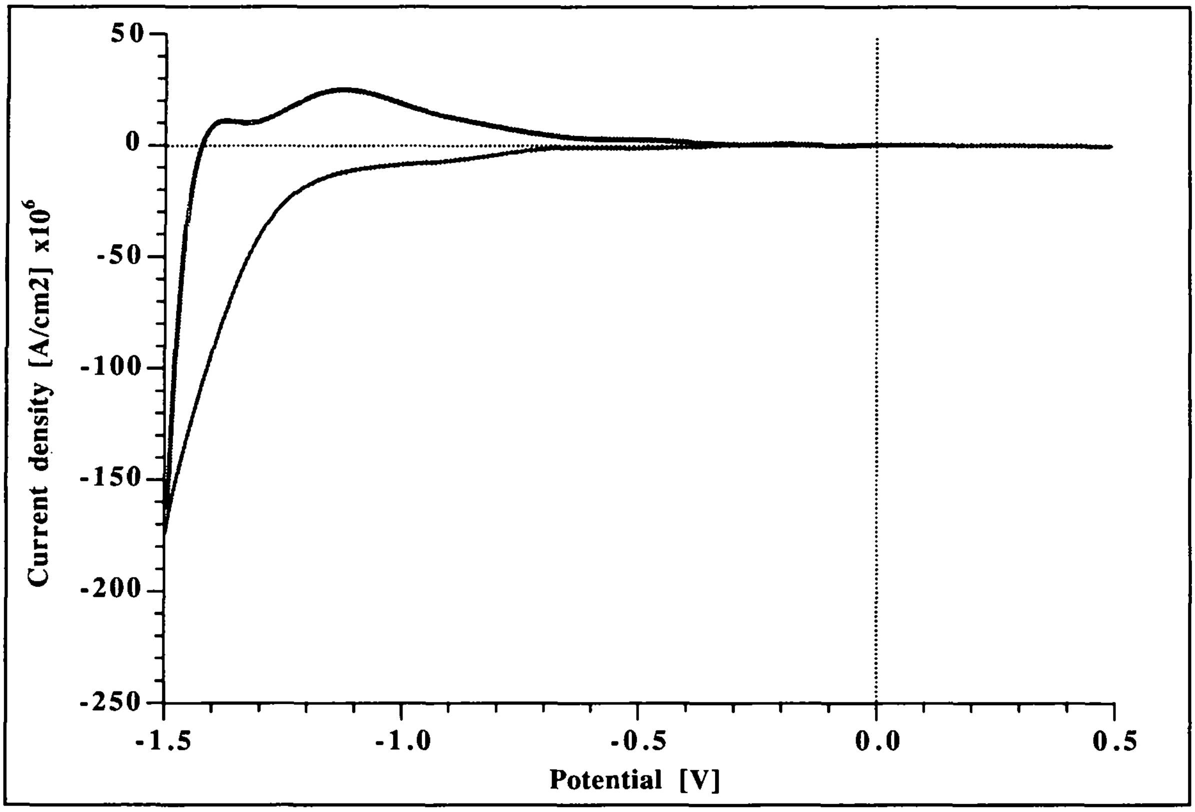

Fig. 64: Result of the difference between the two voltammograms (TiO$_2$/Ru-complex - TiO$_2$/blank) electrode in a 0.1 M TBAP/DMF solution (CO$_2$ saturated)

c) Products identification

Due to the absence of hydrogen ions and other proton donors in the selected electrolyte, the principal reaction products could be carbon monoxide and (or) oxalate ions.

$$CO_2 + 2H^+ + 2e^- \rightarrow CO + H_2O \qquad (36)$$

$$2CO_2 + 2e^- \rightarrow (COO^-)_2 \cdot \qquad (37)$$

In our case, the main product detected in the electrolyte was found to be oxalic acid and this is consistent with the results reported by Lamy et al. (Lamy *et al.* 1988).

7.5. Conclusions

Nickel and ruthenium complexes incorporated on TiO_2 thin film electrodes can be applied for the cathodic reduction of CO_2. Transition metal complexes, used as electron transfer mediators, considerable decrease the overvoltage, allowing respectable current densities to be achieved.

The main product in an aprotic electrolyte such as dimethylformamide are oxalic acid and, in traces, carbon monoxide.

8. Bibliography

8.1. Literature statistics

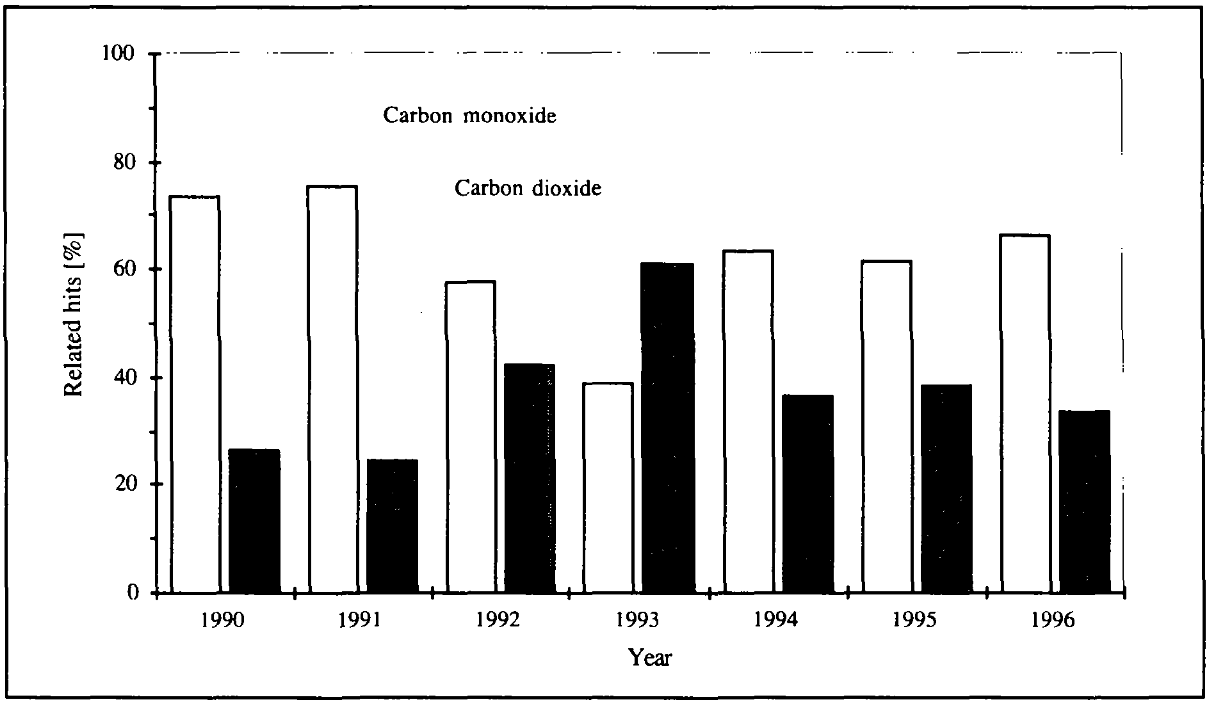

Fig. 65: Number of publications related to methanol synthesis in the past 7 years[17]

---

[17] Data obtained by searching various Dialog© databases using the following keywords and criteria:

- methanol synthesis from pure carbon monoxide:
(Carbon AND monoxide AND methanol AND catalyst?) NOT (carbon AND dioxide)
- methanol synthesis from pure carbon dioxide:
(Carbon AND dioxide AND methanol AND catalyst?) NOT (carbon AND monoxide)

The keyword could be anywhere in the article. ? was used to permit variation in the name (catalyst, catalysts, ...). Terms within the parentheses were executed first.

8.2. References

1. U. Akiba, Y. Nakamura, K. Suga, M. Fujihira, *Thin Solid Films* **210/211**, 381 (1992).
2. S. P. S. Andrew, Paper 12, Post Congress Symposium, 7th International Congress on Catalysis, Osaka (1980).
3. T. Andrews, P. G. Tait, *Trans. Roy. Soc. London* **150**, 113 (1860).
4. H. Arakawa, K. Sayama, Methanol Synthesis from CO_2 and H_2 over Supported Copper-Zinc Oxide Catalyst. Significant Influence of Support on Methanol Formation, G. L. e. al. (Ed.), New Frontiers in Catalysis, Budapest (Elsevier, 1992).
5. A. Baiker, M. A. Kohler, in *Catalysis, Kinetics and Reactor Engineering* N. P. Cheremisinoff (Ed.) (Gulf, 1989), vol. 3, pp. 3.
6. S. Bailey, G. F. Froment, J. W. Snoeck, K. C. Waugh, *Catalysis Lett.* **30**, 99 (1995).
7. J. E. Bailie, C. H. Rochester, G. J. Millar, *Catalysis Lett.* **31**, 333 (1995).
8. G. B. Balazs, F. C. Anson, *J. Electroanal. Chem.* **322**, 325 (1992).
9. A. Bandi, *J. Electrochem. Soc.* **137**, 2157 (1990).
10. R. Bardet, J. Thivolle-Cazat, Y. Tranbouze, *J. Chim. Phys. Phys.-Chim. Biol.* **78**, 135 (1981).
11. J. C. J. Bart, R. P. A. Sneeden, in *Alcohols from Synthesis Gas - A Status Report* C. Today (Ed.) (Elsevier Science Publisher B.V., Amsterdam, 1987), vol. 2, pp. 1.
12. H. Becker, *Wiss. Veröff. Siemens-Konz.* **1**, 76 (1920).
13. H. Becker, *Wiss. Veröff. Siemens-Konz.* **3**, 243 (1923).
14. M. Beley, J.-P. Collin, R. Ruppert, J.-P. Sauvage, *J. Am. Chem. Soc.* **108**, 7461 (1986).
15. A. Bill, "CO_2 Electroreduction by Ni(II) and Ru(II) complexes" *report 1* (1995a).
16. A. Bill, "CO_2 Electroreduction by Ni(II) and Ru(II) complexes" *report 2* (1995b).
17. A. Bill, B. Eliasson, E. Killer, U. Kogelschatz, W. A., *Energy Conversion and Management* **38**, S415 (1997).
18. L. Bisset, *Chem. Eng.* **84**, 155 (1977).
19. C. M. Bolinger, B. P. Sullivan, D. Conrad, W. J. Vining, *J. Chem. Soc. Chem. Commun.*, 1414 (1985).
20. G. C. Bond, *Heterogeneous Catalysis, Principles and Applications.* P. W. Atkins, J. S. E. Holker, A. K. Holliday (Ed.), Oxford Chemistry Series (Oxford University Press, Oxford, ed. Second, 1990).
21. M. Boudart, *La Cinétique des Réactions en Catalyse Hétérogène* (Masson, Paris, ed. First, 1982).
22. M. Boudart, *Ind. Eng. Chem. Fundam.* **25**, 656 (1986).
23. M. Bowker, R. A. Hadden, H. Houghton, J. N. K. Hyland, K. C. Waugh, *J. Catal.* **109**, 263 (1988).

24. M. Bowker, H. Houghton, K. C. Waugh, *J. Chem. Soc. Far. Trans.* **I77**, 3023 (1981).

25. E. Briner, B. Susz, *Helv. Chim. Acta* **13**, 678 (1930).

26. F. J. Bröcker, *DE Patent 2,846,614* (BASF, 1978).

27. S. P. Bugaev, *Plasma Chem. & Plasma Proc.* **16**, 669 (1996).

28. R. Burch, S. E. Golunski, M. S. Spencer, *Catalysis Lett.* **5**, 55 (1990).

29. D. Canfield, K. W. J. Frese, *J. Electrochem. Soc.* **130**, 1772 (1983).

30. J. J. Carberry, *Chemical and Catalytic Reaction Engineering* (MacGraw-Hill, New York, 1976).

31. T. Chafik, D. Bianchi, S. J. Teichner, *Top. Catal.* **2**, 103 (1995).

32. M. B. Chang, J. H. Balbach, M. J. Rood, M. J. Kushner, *J. Appl. Phys.* **69**, 4409 (1991).

33. M. B. Chang, M. J. Kushner, M. J. Rood, *Plasma Chem. Plasma Proc.* **12**, 565 (1992).

34. M. B. Chang, T. D. Tseng, *Journal of Environmental Engineering ASCE* **122**, 41 (1996).

35. M. W. Chase, *et al.*, J. o. P. a. C. R. Data (Ed.) (American Chemical Society and the American Institute of Physics for the National Bureau of Standards, 1985), vol. 14,.

36. V. M. Cherednichenko, Korpova, Physico-Chemical Institute, Moscow (1953).

37. G. C. Chinchen, *et al.*, *Am. Chem. Soc. Div. Fuel Chem.* **29**, 178 (1984).

38. G. C. Chinchen, P. J. Denny, J. R. Jennings, M. S. Spencer, K. C. Waugh, *Appl. Catal. A* **36**, 1 (1988).

39. G. C. Chinchen, P. J. Denny, D. G. Parker, M. S. Spencer, D. A. Whan, *Appl. Catal. A* **30**, 333 (1987).

40. G. C. Chinchen, K. C. Waugh, *J. Catal.* **97**, 280 (1986a).

41. G. C. Chinchen, K. C. Waugh, D. A. Whan, *Appl. Catal. A* **25**, 101 (1986b).

42. B. S. Clausen, *et al.*, *J. Catal.* **132**, 524 (1991a).

43. B. S. Clausen, H. Topsøe, *Catal. Today* **9**, 189 (1991b).

44. E. J. Clothiaux, J. A. Koropchak, R. R. Moore, *Plasma Chem. Plasma Proc.* **4**, 15 (1984).

45. G. Coudurier, F. Lefèbre, in *Catalyst Characterization* B. Imelik, J. C. Vedrine (Ed.) (Plenum Press Div Plenum Publishing Corp., New York, 1994) pp. 11.

46. A. Cybulski, *Catal. Re.-Sci. Eng.* **36**, 557 (1994).

47. F. M. Dautzenberg, Ten Guidlines for Catalyst Testing, S. A. Bradley, M. J. Gattuso, R. J. Bertolacini (Ed.), Characterization and Catalyst Development, Los Angeles, CA (American Chemical Society, 1988).

48. P. Davies, F. F. Snowdon, *US Patent 3,326,956* (ICI, 1967).

49. J.H. De Boer, *The Structure and Properties of Porous Materials*, Butterworth, london (1958)

50. J.-H. De Boer, B. G. Linsen, T. J. Osinga, *J. Catal.* **4**, 643 (1965a).

51. J.-H. De Boer, B. G. Linsen, T. Van der Plas, G. J. Zondervan, *J. Catal.* **4**, 649 (1965b).

52. B. Denise, R. P. A. Sneeden, *J. Mol. Catal.* **17**, 359 (1982).

53. P. R. Dennison, K. J. Packer, M. S. Spencer, *J. Chem. Soc. Far. Trans.* **85**, 3537 (1989).

54. J. C. Devins, *J. Electrochem. Soc.* **103**, 406 (1956).

55. I. Dybkjær, P. E. H. Nielsen, J. B. Hansen, , AiCh. E., 74th Ann. Meeting, New Orleans (1981).

56. B. Eliasson, CO_2 Chemistry: an Option for CO_2 Emission Control?, CO_2 Chemistry Workshop, Hemavan, Sweden (1993).

57. B. Eliasson, CO_2 Chemistry: An Option for CO_2 Emission Control?, C.-M. Pradier, J.-P. Pradier (Ed.), Carbon Dioxide Chemistry: Environmental Issues, Stockholm (The Royal Society of Chemistry, 1994).

58. B. Eliasson, W. Egli, U. Kogelschatz, *Pure & Appl. Chem.* **66**, 1275 (1994).

59. B. Eliasson, M. Hirth, U. Kogelschatz, *Journal of Physics D-Applied Physics* **20**, 1421 (1987).

60. B. Eliasson, U. Kogelschatz, *Appl. Phys. B* **46**, 299 (1988).

61. B. Eliasson, U. Kogelschatz, *IEEE Transactions on Plasma Science* **19**, 309 (1991a).

62. B. Eliasson, U. Kogelschatz, *IEEE Transactions on Plasma Science* **19**, 1063 (1991b).

63. B. Eliasson, U. Kogelschatz, B. Xue, L. M. Zhou, to be published, XIIIth International Symposium on Plasma Chemistry, Beijing (1997).

64. B. Eliasson, F. G. Simon, W. Egli, P. Brunner, *Swiss Phys. Soc.* (1991).

65. D. J. Evans, *Appl. Phys.* **74**, 5378 (1993).

66. E. Fiedler, G. Grossmann, B. Kersebohm, G. Weiss, C. Witte, in *Ullmann's Encyclopedia of Industrial Chemistry* (1990), vol. A 16, pp. 465.

67. Y. V. Filippov, V. A. Boblikova, V. I. Panteleev, "Electrosynthesis of Ozone" (Moscow State University, 1987).

68. B. Fisher, R. Eisenberg, *J. Am. Chem. Soc.* **102**, 7361 (1980).

69. K. W. Frese, in *Electrochemical and Electrocatalytic Reactions of Carbon Dioxide* B. P. Sullivan, K. Krist, H. E. Guard (Ed.) (Elsevier, Amsterdam, 1993) pp. Chap. 6.

70. K. W. Frese, D. Canfield, *J. Electrochem. Soc.* **131**, 2518 (1984).

71. C. Fröhlich, "In-situ FTIR Studien des CO_2 Hydrierung an Kupfer/Silber-Zirkondioxid Katalysatoren", ETHZ Thesis (1993).

72. S. Fuji, N. Takemura, *Advances in Chemistry Series* **21**, 334 (1959).

73. M. Fujihira, Y. Nakamura, Y. Hirata, U. Akiba, K. Suga, *Denki Kagaku* **59**, 532 (1991).

74. S. Fujita, M. Usui, H. Ito, N. Takezawa, *J. Catal.* **157**, 403 (1995).

75. S. Fujita, M. Usui, N. Takezawa, *J. Catal.* **134**, 220 (1992).

76. M. Fujiwara, H. Ando, M. Tanaka, Y. Souma, *Bull. Chem. Soc. Jpn.* **67**, 546 (1994).

77. J. Gallagher, Y. H. Kiold, *GB Patent 1,159,035* (ICI, 1965).

78. G. H. Graaf, P. J. J. M. Sijtsema, E. J. Stamhuis, G. E. H. Joosten, *Chem. Eng. Sci.* **41**, 2883 (1986).

79. G. H. Graaf, E. J. Stamhuis, A. A. C. M. Beenackers, *Chem. Eng. Sci.* **43**, 3185 (1988).

80. P. R. Griffiths, J. A. de Haseth, in *Fourier Transform Infrared Spectrometry* P. J. Elving, J. D. Winefordner, I. M. Kolthoff (Ed.) (John Wiley & Sons Inc., New York, 1986), vol. 83, pp. 195.

81. M. M. Halmann, *Chemical Fixation of Carbon Dioxide: Methods for Recycling CO_2 into Useful Products* (CRC PRESS Inc., Boca Raton, Florida, ed. Fisrt, 1993).

82. P. Hautefeuille, J. Chappuis, *Compt. Rend.* **92**, 80 (1881).

83. R. J. Hawkins, R. J. Kane, W. E. Slinkard, J. L. Trumbley, in *Encyclopedia of Chemical Processing and Design* J. J. Ketta, W. A. Cunningham (Ed.) (Marcel Dekker, New York, 1988) pp. 418.

84. J. G. Highfield, M. Prairie, A. Renken, *Catal. Today* **9**, 39 (1991).

85. J. U. Höltje, "Untersuchung der Makrokinetik der heterogen katalysierten Synthese aus Kohlendioxid und Wasserstoff zu Methanol", Forschungzentrum Jülich Thesis (1990).

86. H. M. Höppener, E. B. M. Doesburg, J. J. F. Scholten, *Appl. Catal. A* **25**, 109 (1986).

87. J. Horàk, J. Pasek, *Design of Industrial Chemical Reactors from Laboratory Data* (Heyden, 1978).

88. Y. Hori, Energy Utilization System and Electrochemical Reduction of Carbon Dioxide, M. Tomkiewicz, R. Haynes, H. Yoneyama, Y. Hori (Ed.), Environmental Aspects of Electrochemistry and Photoelectrochemistry (The Electrochemical Society, 1993).

89. H. C. Hurrell, A.-L. Mogstad, D. A. Usifer, K. T. Potts, H. D. Abruña, *Inorg. Chem.* **28**, 1080 (1989).

90. S. Ikeda, K. Ito, Artificial Photosynthetic Systems for CO_2 fixation, Int. Symposium on Chemical Fixation of Carbon Dioxide, Nagoya (1991).

91. S. D. Jackson, *J. Catal.* **115**, 247 (1989).

92. Y. B. Kagan, *et al.*, *Kinet. Katal.* **16** (1975).

93. S. Kanazawa, M. Kogoma, T. Moriwaki, S. Okazaki, *J. Phys. D: Appl. Phys.* **21**, 838 (1988).

94. F. R. Keene, in *Electrochemical and Electrocatalytic Reactions of Carbon Dioxide* B. P. Sullivan, K. Krist, H. E. Guard (Ed.) (Elsevier, Amsterdam, 1993) pp. Chap. 1.

95. A. Kiennemann, *et al.*, *Appl. Catal. A* **59**, 165 (1990).

96. S. Kinnaird, G. Webb, G. C. Chinchen, *J. Chem. Soc. Far. Trans.* **83**, 3399 (1987).

97. S. Kinnaird, G. Webb, G. C. Chinchen, *J. Chem. Soc. Far. Trans.* **84**, 2135 (1988).

98. Kirk et al., *Encyclopedia of Chemical Technology* (John Wiley & Sons Inc., New York, ed. 4th edition, 1991), vol. 1.

99. K. Klier, in *Advances in Catalysis* (Academic Press Inc., 1982), vol. 31, pp. 243.

100. K. Klier, V. Chatikvanij, R. G. Herman, G. W. Simmons, *J. Catal.* **74**, 343 (1982).

101. R. A. Koeppel, "Strukturelle und Katalytische Eigenschaften von Kupfer-Zirkondioxid Katalysatoren für die Synthese von Methanol aus Kohlendioxid und Wasserstoff", ETHZ Thesis (1991).

102. U. Kogelschatz, , XVIth Int. Conf. on Phenomena in Ionized Gases, Düsseldorf (1983).

103. U. Kogelschatz, *Pure & Appl. Chem.* **62**, 1167 (1990).

104. U. Kogelschatz, , XXth Int. Conf. on Phenomena in Ionized Gases, Pisa (1991).

105. U. Kogelschatz, , Xth Int. Conf. on Gas Discharges and their Applications, Swansea (1992).

106. U. Kogelschatz, J. Salge, Hochdruckplasmen: Barrieren- und Koronaentladungen Technik und Einsatzmöglichkeiten, D. H. F. f. Physik (Ed.), Greifswald (1996).

107. J. Kritzenberger, A. Wokaun, *J. Mol. Catal. A.* **118**, 235 (1997).

108. E. Lamy, L. Nadjo, M. Saveant, *J. Electroanal. Chem.* , 403 (1988).

109. F. Le Peltier, "Transformation du Gaz de Synthèse en Methanol en Présence de Catalyseurs Oxide Mixte à Base de Cuivre, Aluminium et de Zinc", Ecole Nationale Supérieure du Pétrole et des Moteurs/Université Pierre et Marie Curie Thesis (Paris VI) (1989).

110. F. Le Peltier, P. Chaumette, A. Kiennemann, J. Saussey, J. C. Lavalley, *J. Chim. Phys. Phys.-Chim. Biol.* **93**, 1376 (1996).

111. J. S. Lee, K. H. Lee, S. Y. Lee, Y. G. Kim, *J. Catal.* **144**, 414 (1993).

112. S. Lee, *Methanol Synthesis Technology* (CRC Press Inc., 1990).

113. O. Levenspiel, *Chemical Reaction Engineering* (John Wiley & Sons Inc., New York, ed. 2nd edition, 1962).

114. G. Liu, D. Willcox, M. Garland, H. H. Kung, *J. Catal.* **90**, 139 (1984).

115. R. W. Lunt, *Advances in Chemistry Series* **21**, 286 (1959).

116. F. Marschner, F. W. Moeller, *Appl. Ind. Cat.* **2**, 349 (1983).

117. M. Marwood, "Kinetic Studies of the Catalytic Carbon Dioxide Methanation under Transient Conditions-in-Situ Surface and Gas Phase Analysis", EPFL Thesis (1995).

118. F. Massines, C. Mayoux, R. Messaoudi, A. Rabehi, P. Ségur, Xth Int. Conf. on Gas Discharges and their Aplications, Swansea (1992).

119. Methanex, "Methanex Corporation Annual Report" (Methanex, Vancouver, Canada, 1995).

120. G. J. Millar, C. H. Rochester, S. Bailey, K. C. Waugh, *J. Chem. Soc. Faraday. Trans.* **88**, 2085 (1992a).

121. G. J. Millar, C. H. Rochester, C. Howe, K. C. Waugh, *J. Mol. Phys.* **76**, 833 (1991).

122. G. J. Millar, C. H. Rochester, K. C. Waugh, *Catalysis Lett.* **14**, 289 (1992b).

123. G. J. Millar, C. H. Rochester, K. C. Waugh, *J. Catal.* **155**, 52 (1995).

124. A. Mittasch, M. Pier, K. Winkler, *DE Patent 441,433* (BASF, 1923).

125. J. Nakamura, *et al.*, *Catalysis Lett.* **31**, 325 (1995).

126. G. Natta, R. H. Emmet (Ed.) (Reinhold Publ. Co., New York, 1955), vol. 3, pp. 349.

127. M. K. Nazeeruddin, *et al.*, *J. Am. Chem. Soc.* **115**, 6383 (1993).

128. I. Noda, *J. Am. Chem. Soc.* **111**, 8116 (1989).

129. I. Noda, *Appl. Spec.* **44**, 550 (1990).

130. I. Noda, A. E. Dowrey, C. Marcott, *Appl. Spec.* **47**, 1317 (1993).

131. P. Nowak, M. Lachowska, J. Skrzypek, *Chem. Eng. Sci.* **46**, 3324 (1991).

132. K. Okazaki, T. Nozaki, Y. Uemitsu, K. Hijikata, Direct Conversion from Methane to Methanol by a Pulsed Silent Discharge Plasma, XIIth International Symposium on Plasma Chemistry, Minneapolis (1995).

133. M.-P. Otto, *Bull. Soc. Franç. Electr.* **9**, 129 (1929).

134. G. E. Parris, K. Klier, *J. Catal.* **97**, 374 (1986).

135. P. B. Rasmussen, "Cu (100) as a Model Catalyst for the Methanol Synthesis", Technical University of Lyngby Thesis (1993).

136. P. B. Rasmussen, *et al.*, *Catalysis Lett.* **26**, 373 (1994a).

137. P. B. Rasmussen, M. Kazta, I. Chorkendorff, *Surface Sci.* **318**, 267 (1994b).

138. U. Reitz, "Barrierentladungen zur Plasmagestürzten Oberflächenbehandlung", TU Braunschweig (1992).

139. A. Renken, *Int. Chem. Eng.* **24**, 202 (1984).

140. A. Riesen, "Synthese und Struktur von Metallkomplexen mit 12-, 14- und 16- Gliedrigen Tetraazomakrozyklen -N, N', N'', N''' -TetraEssigsaueren", University of Basel Thesis (1984).

141. W. R. A. M. Robinson, "Structure and Activity of Copper-Containing Methanol Synthesis catalysts", University of Amsterdam Thesis (1989).

142. M. E. Royer, *C. R. Hebd. Sëances Acad. Sci.* **70**, 731 (1870).

143. A. Y. Rozovskii, *Kinet. Katal* **21**, 97 (1980).

144. A. Y. Rozovskii, *et al.*, *Kinet. Catal.* **15**, 1132 (1976).

145. R. Ryberg, *J. Chem. Phys.* **82**, 567 (1985).

146. V. G. Samoilovich, V. I. Gibalov, K. V. Kozlov, "Physical Chemistry of the Barrier Discharge" (Moscow State University, 1989).

147. I. Sardja, S. K. Dahli, *Appl. Phys. Lett.* **56**, 21 (1990).

148. L. Saussey, J. C. Lavalley, C. Bovet, *J. Chem. Soc. Far. Trans.* **78**, 1457 (1982).

149. C. Schild, "Oberflächenspektroskopische Untersuchungen an hochdispersen Metall/Zirkondioxid-Katalysatoren für die Hydrierung von Kohlendioxid", University of Bayreuth Thesis (1991).

150. M. Schneider, K. Kochloefl, J. Ladebeck, *EP Patent 0,125,689* (Süd Chemie, 1987).

151. G. R. Sheffer, T. S. King, *J. Catal.* **116**, 488 (1989a).

152. G. R. Sheffer, T. S. King, *J. Catal.* **115**, 376 (1989b).

153. R. S. Sheinson, N. S. Smyth, , VIIIth Int. Symp. on Plasma Chem., Tokyo (1987).

154. A. K. Shuaibov, V. S. Shevera, *Sov. Phys.-Tech. Phys.* **24**, 976 (1979).

155. W. Siemens, *Poggendorffs Ann. Phys. Chem.* **102**, 66 (1857).

156. G. Silvestri, S. Gambino, G. Filardo, Electrochemical Syntheses Involving Carbon Dioxide, C. I. Brändén, G. Schneider (Ed.), Carbon Dioxide Fixation and Reduction in Biological and Model Systems, Olso (Oxford University Press, 1991).

157. G. D. Sizgek, H. E. Curryhyde, M. S. Wainwright, *Appl. Catal. A* **115**, 15 (1994).

158. J. Skrzypek, M. Lachowska, M. Grzesik, J. Sloczynski, P. Nowak, *Chem. Eng. J. Biochem. Eng. J.* **58**, 101 (1995).

159. J. Skrzypek, J. Sloczynski, S. Ledakowicz, *Methanol Synthesis - Science and Engineering* (Polish Scientific Publishers, Warszawa, 1994), vol. 58.

160. J. Sloczynski, R. Grabowski, J. Janas, J. Skrzypek, *Chem. Eng. Sci.* **46**, 2599 (1991).

161. A. Smith, in *Greenhouse Issues* (1996) pp. 1.

162. M. S. Spencer, *Surface Sci.* **339**, L897 (1995).

163. D. G. Storch, M. J. Kushner, *J. Appl. Phys.* **73**, 51 (1993).

164. E. Supp, *How to Produce Methanol from Coal* (Springer Verlag, Berlin, 1990).

165. E. M. Suzuki, W. R. Gresham, *Journal of Forensic Sciences* **31**, 931 (1986).

166. M. Suzuki, J. M. Smith, *J. Catal.* **21**, 336 (1971).

167. M. Tagawa, M. Ohsugi, *J. Catal.* **107**, 161 (1987).

168. Y. Takenaka, M. Kuzumoto, K. Yasui, S. Yagi, M. Tagashira, *IEEE J. Quantum Electron.* **27**, 2482 (1991).

169. T. E. Teeter, P. Van Rysselberghe, Reduction of Carbon Dioxide on Mercury Cathodes, 6th Meeting International Commitee of Electrochemical Thermodynamics and Kinetics, Poitiers (Butterworths, 1954).

170. J. M. Thomas, W. J. Thomas, *Introduction to the Principles of Heterogeneous Catalysis* (Acad. Press. Inc., 1967).

171. H. Topsøe, "Methanol Synthesis Catalyst MK-101" (Haldor Topsøe A/S, 1987).

172. G. A. Vedage, R. Pitchai, R. G. Hermann, K. Klier, *Am. Chem. Soc. Div. Fuel Chem.* **29**, 196 (1984).

173. G. A. Volkova, N. N. Kirillova, E. N. Pavlovskaya, A. V. Yakovleva, *J. Appl. Spectrosc.* **41**, 1194 (1984).

174. L. E. Wade, R. B. Gengelbach, J. L. Trumbley, W. L. Hallbauer, in *Kirk Othmer Encyclopedia of Chemical Technology* (John Wiley & Sons Inc., New York, 1981), vol. 15, pp. 398.

175. E. Warburg, *Ann. Physik* **13**, 464 (1904).

176. E. Warburg, *Z. tech. Phys.* **6**, 625 (1925).

177. E. Warburg, G. Leithaüser, *Ann. Physik* **28**, 313 (1909).

178. M. Watanabe, M. Shibata, A. Kato, M. Azuma, T. Sakata, *J. Electrochem. Soc.* **138**, 3382 (1991).

179. J. Weigel, "Surface Species in Carbon Monoxide and Carbon Dioxide Hydrogenation Reactions over Zirconia Supported Catalysts for the Synthesis of Methanol - A DRIFT Spectroscopical Study", ETHZ Thesis (1996).

180. J. Weigel, C. Frohlich, A. Baiker, A. Wokaun, *Appl. Catal. A* **140**, 29 (1996).

181. D. Welti, *Infrared Vapour Spectra* (Heyden & Son Ltd., London, 1970).

182. A. Wokaun, J. Weigel, M. Kilo, A. Baiker, *Fresenius J. Anal. Chem.* **349**, 71 (1994).

183. G. Wrobel, L. Jalowiecki, J. P. Bonnelle, F. Bali, A. Bettahar, *New J. Chem.* **11**, 10 (1987).

184. S. Yagi, N. Tabata, , IEEE/OSA Conf. on Lasers and Electro-Opt., Washington DC (1981).

185. K. H. Yang, O. A. Hougen, *Chem. Eng. Prog.* **46**, 146 (1950).

186. K. Yasui, M. Kuzumoto, *IEEE J. Quantum Electron.* **25**, 836 (1989).

187. S. A. Yeboah, S.-H. Wang, P. R. Griffiths, *Appl. Spec.* **38**, 259 (1984).

Appendix

A.1. Chemical equilibrium constants

Assuming ideal gas behavior, the equilibrium constant (at a given temperature T in Kelvin) can be defined as a function of the partial pressure (p_i) or as a function of the mole fractions (y_i) and the total pressure (P). The equations for each reaction (38 to 40) are:

$$K_1(T) = \frac{p_{CH_3OH}}{p_{H_2}^2 \cdot p_{CO}} = \frac{1}{P^2} \cdot \frac{y_{CH_3OH}}{y_{H_2}^2 \cdot y_{CO}} \tag{38}$$

$$K_2(T) = \frac{p_{H_2O} \cdot p_{CH_3OH}}{p_{H_2}^3 \cdot p_{CO_2}} = \frac{1}{P^2} \cdot \frac{y_{H_2O} \cdot y_{CH_3OH}}{y_{H_2}^3 \cdot y_{CO_2}} \tag{39}$$

$$K_3(T) = \frac{p_{H_2} \cdot p_{CO_2}}{p_{CO} \cdot p_{H_2O}} = \frac{y_{H_2} \cdot y_{CO_2}}{y_{CO} \cdot y_{H_2O}} \tag{40}$$

Corrections for non-ideal gas behavior (at a pressure greater than 30 bar) result in significantly closer agreement between experimental and calculated data. The use of the appropriate fugacity coefficients is extensively discussed by Skrzypek et al. (Skrzypek *et al.* 1994).

A number of numerical formulations exist for calculating the temperature dependence of the equilibrium constant. Graaf et al. (Graaf *et al.* 1986) using a fixed bed reactor determined the equilibrium constants for the methanol synthesis from CO, $K_1(T)$, and for the water-gas shift reaction, $K_3(T)$, as a function of temperature:

$$K_1(T) = 10^{\left(\frac{5139}{T} - 12.621\right)} \quad [\text{bar}^{-2}] \tag{41}$$

$$K_3(T) = 10^{\left(\frac{2073}{T} - 2.029\right)} \quad [\text{bar}^{-2}] \tag{42}$$

There are various established relationships for $K_1(T)$ in the literature which do not always agree. For example, Cherednichenko (Cherednichenko 1953) (eq 43) proposes the following formulation:

$$K_1(T) = 9.740 \cdot 10^{-5} \cdot \exp(21.225 + \frac{9143.6}{T} - 7.492 \cdot \ln T + 4.076 \cdot 10^{-3} - 7.161 \cdot 10^{-8} \cdot T^2) \; [\text{kPa}^{-2}] \tag{43}$$

On the other hand, $K_3(T)$ is much better established. In 1977 Bisset (Bisset 1977) presented a very accurate relationship (eq 44):

$$K_3(T) = \exp(-13.148 + \frac{5639.5}{T} - \frac{49170}{T^2} + 1.077 \cdot \ln T + 5.44 \cdot 10^{-4} \cdot T - 1.125 \cdot 10^{-7} \cdot T^2) \ [\mathrm{kPa}^{-2}] \quad (44)$$

The last two equations were used to calculate the equilibrium concentration of CO_2, H_2, CO, CH_3OH and H_2O at various pressures and feed gas compositions. Two conditions apply to these two equations, when the system is in equilibrium, namely that the sum of the mole fractions equals one and that the total pressure remains constant.

The equilibrium conversion of CO_2 to methanol as a function of temperature is shown in figure 66. Data is expressed for feed mole ratios of 1, 3, 5, 10 at a pressure of 20 bar. For a feed ratio of 3, the equilibrium was also determined at a pressure of 30 bar.

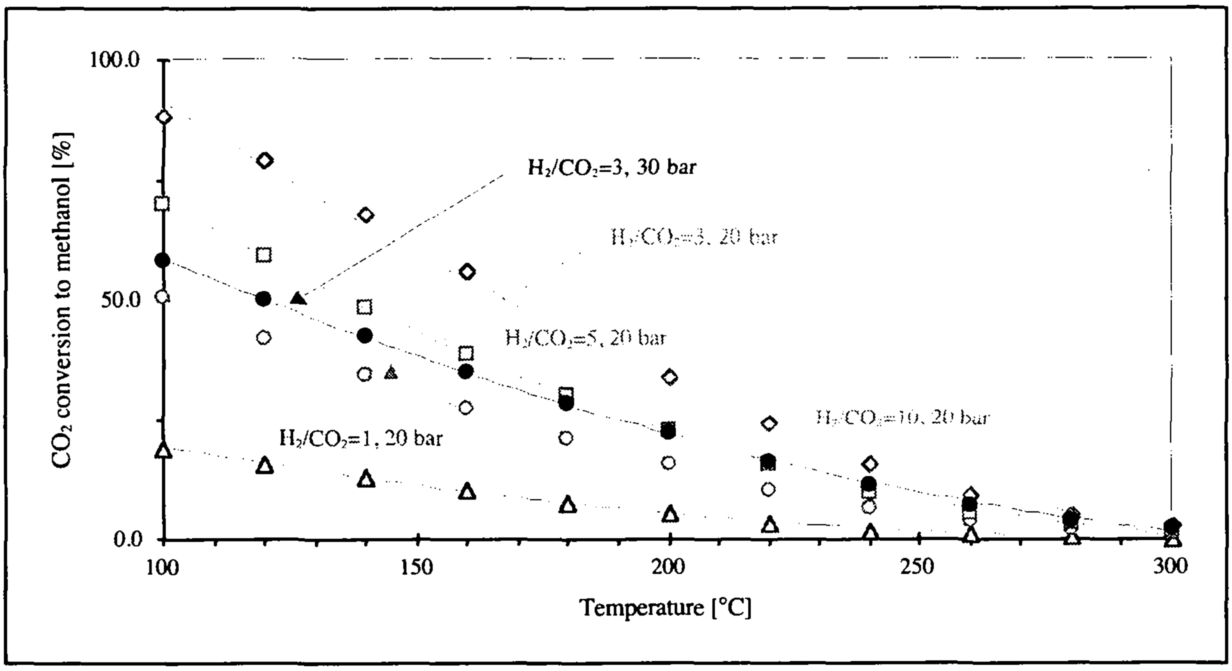

Fig. 66: Equilibrium conversion of CO_2 to methanol as a function of temperature, feed mole ratio and pressure

The equilibrium conversion of CO_2 to CO as a function of temperature is shown in figure 67. It was calculated given the same conditions as in figure 66.

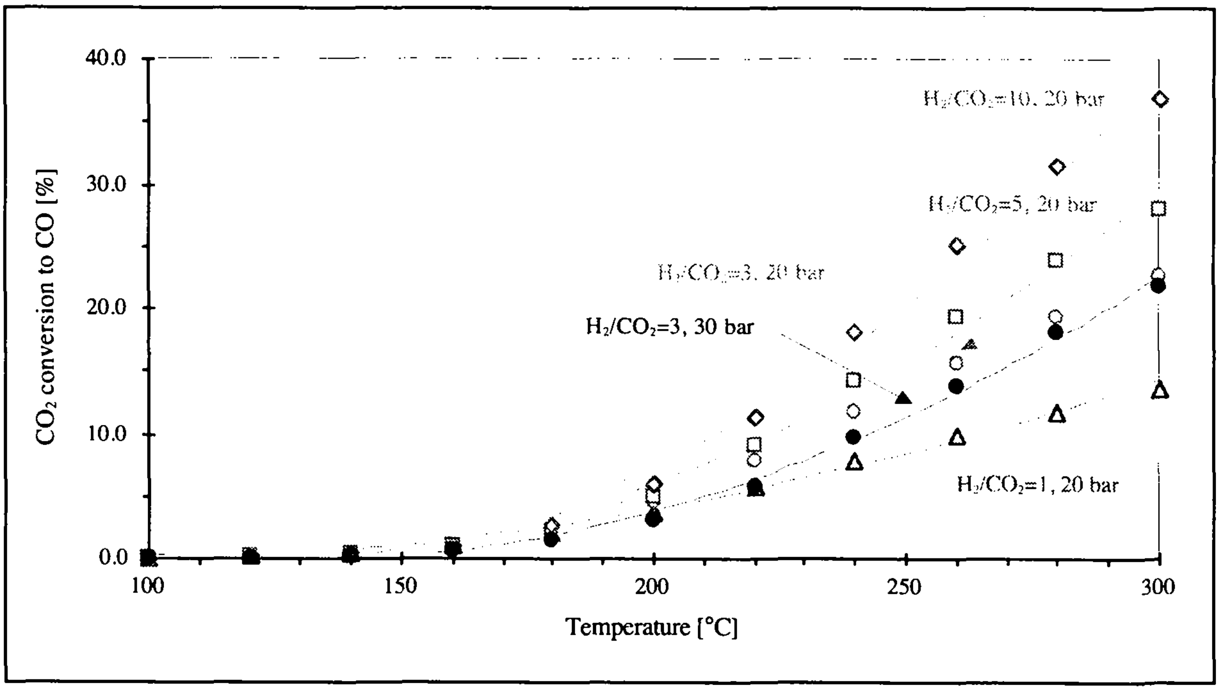

Fig. 67: Equilibrium conversion of CO_2 to CO as a function of temperature, feed mole ratio and pressure

A.2. Catalysis parameters

Several parameters have been calculated to characterize catalyst performance. Their formulas are listed below:

Feed mole ratio (r)

The mixture composition of the inlet gases is expressed in terms of mole ratio.

$$r = \frac{\dot{n}_{H_2}}{\dot{n}_{CO_2}} \qquad [-] \qquad (45)$$

$\dot{n}_{H_2}$: inlet molar flow of hydrogen $[mol.h^{-1}]$

$\dot{n}_{CO_2}$: inlet molar flow of carbon dioxide $[mol.h^{-1}]$

Mole fraction

The amount of specie i in a mixture is expressed in terms of mole fraction.

$$x_i = \frac{\dot{n}_i}{\sum_{i=1}^{n} \dot{n}_i} \qquad [-] \qquad (46)$$

$\dot{n}_i$: molar flow rate of specie i $[mol.h^{-1}]$

$\sum_{i=1}^{n} \dot{n}_i$: sum of all molar flow rates of all i species $[mol.h^{-1}]$

Gas hourly space velocity (GHSV) or space velocity (S_v)

This parameter is calculated by dividing the fluid volumetric flow rate by the volume of the catalyst. It is the same as the inverse of the transit time.
For all the measurements it is expressed given standard conditions.

$$S_V = \frac{Q_{total}}{V_{cat}} \qquad [h^{-1}] \qquad (47)$$

Q_{total} : total volumetric flow rate in the reactor $[Nml.h^{-1}]$

V_{cat} : catalyst volume $[Nml]$

CO_2 conversion

A measure of the fraction of CO_2 which has been used up during the reaction. It depends on the working conditions (T, P,...).

$$X_{CO_2}(t) = \frac{\dot{n}_{CO_2}(in) - \dot{n}_{CO_2}(t)}{\dot{n}_{CO_2}(in)} \qquad [-] \qquad (48)$$

$\dot{n}_{CO_2}(in)$:	inlet molar flow rate of CO_2	[mol.h^{-1}]
$\dot{n}_{CO_2}(t)$:	outlet molar flow rate of CO_2 at time t	[mol.h^{-1}]

Methanol yield or CO_2 conversion to methanol

A measure of the fraction of the inlet CO_2 which has been converted to methanol.

$$X_{\underset{\text{from } CO_2}{CH_3OH}}(t) = \frac{\dot{n}_{CH_3OH}(t)}{\dot{n}_{CO_2}(in)} \qquad [-] \qquad (49)$$

$\dot{n}_{CO_2}(in)$:	inlet molar flow rate of CO_2	[mol.h^{-1}]
$\dot{n}_{CH_3OH}(t)$:	outlet molar flow rate of CH_3OH at time t	[mol.h^{-1}]

CO yield or CO_2 conversion to CO

In this case, the amount of CO that has been produced from CO_2 is calculated:

$$X_{\underset{\text{from } CO_2}{CO}}(t) = \frac{\dot{n}_{CO}(t)}{\dot{n}_{CO_2}(in)} \qquad [-] \qquad (50)$$

$\dot{n}_{CO_2}(in)$:	inlet molar flow rate of CO_2	[mol.h^{-1}]
$\dot{n}_{CO}(t)$:	outlet molar flow rate of CO at time t	[mol.h^{-1}]

Selectivity of species i

The selectivity of the specie i (CH_3OH, CO and CH_4) is defined as the yield of specie i divided by the total amount of CO_2 converted.

$$S_i(t) = \frac{1}{\dot{n}_{CO_2}(in)} \cdot \frac{\dot{n}_i(t)}{X_{CO_2}(t)} \qquad [-] \qquad (51)$$

$\dot{n}_{CO_2}(in)$:	inlet molar flow rate of CO_2	$[mol.h^{-1}]$
$\dot{n}_i(t)$:	outlet molar flow rate of specie i	$[mol.h^{-1}]$
$X_{CO_2}(t)$:	CO_2 conversion at time t	[-]

A.3. Reactors in detail and their parameters

A.3.1. The tubular reactor

A schematic view of the tubular reactor is shown in figure 68.

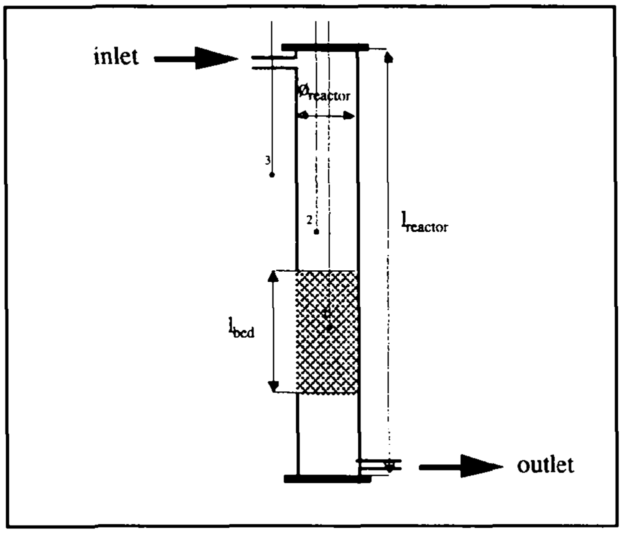
inlet
$\varnothing_{reactor}$
3
2
$l_{reactor}$
l_{bed}
outlet

Fig. 68: Close-up of the laboratory reactor
(1,2,3: thermocouples)

Diameter of the tubular reactor:	$\varnothing_{reactor} = 1.5 \cdot 10^{-2}$ m
Length of the tubular reactor:	$l_{reactor} = 1.5 \cdot 10^{-1}$ m
Length of the catalytic bed:	$l_{bed} = 4.5 \cdot 10^{-2}$ m (typical value for the testing of catalyst (chapter 3))

A.3.2. The DRIFTS reactor

A schematic view of the DRIFTS reactor is given in figure 69.

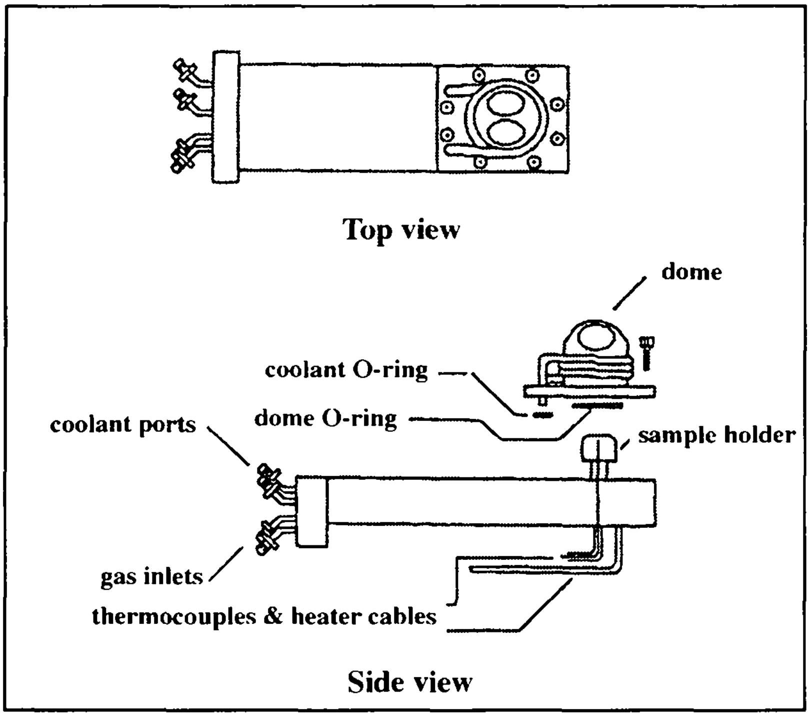
Top view
dome
coolant O-ring
coolant ports
dome O-ring
sample holder
gas inlets
thermocouples & heater cables
Side view

Fig. 69: Close-up of the DRIFTS reactor

A.3.3. The modulation reactor

A schematic view of the modulation reactor is given in figure 70.

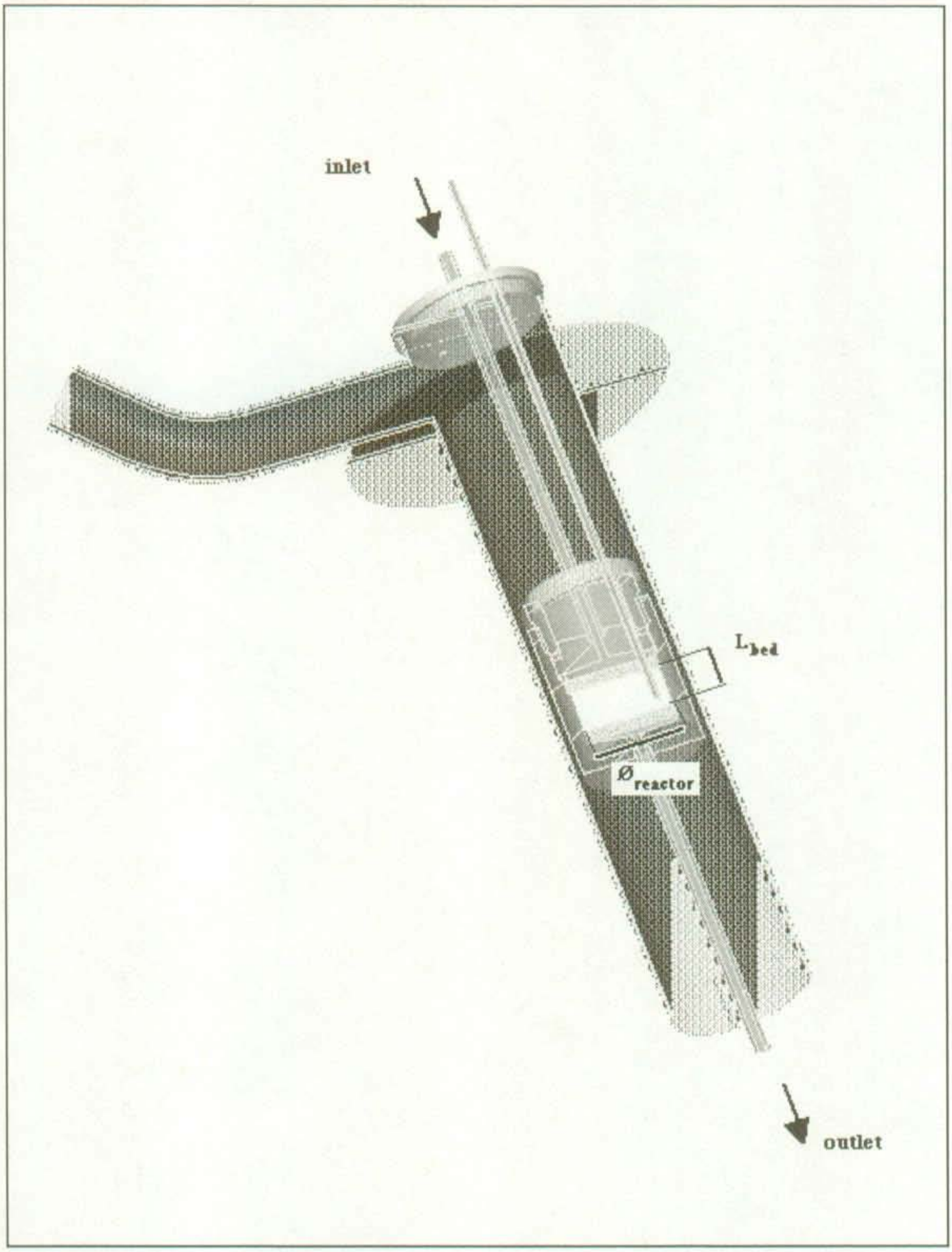
inlet
L_{bed}
$Ø_{reactor}$
outlet

Fig. 70: Close-up of the modulation reactor

Diameter of the tubular reactor: $\varnothing_{reactor} = 1.5 \cdot 10^{-2}$ m

Length of the tubular reactor: $l_{reactor}$ = variable
(typical values in chapter 5)

Length of the catalytic bed: l_{bed} = variable
(typical values in chapter 5)

A.4. Calibration of the GC

(Example for the HRGC 5300 Carlo Erba instrument)

The GC was calibrated with several gas mixtures and with methanol/water solutions in the appropriate range. As the calibration was carried out at room temperature and the measurements taken at 135 °C, all the partial pressures had to be corrected for the temperature difference.

Five different gas mixtures were used (Sauerstoffwerk, Lenzburg, CH). Their composition is given in table 18.

Table 18: Composition of gases used for the calibrations

	Gas composition				
	H_2 [% mol]	CO [% mol]	CO_2 [% mol]	CH_4 [% mol]	CH_3OH [% mol]
Gas bottle 1	74.54	24.77	0.49	0.20	-
Gas bottle 2	49.65	0.25	50.00	0.10	-
Gas bottle 3	82.6	1.00	16.00	0.40	-
Gas bottle 4	-	10.03	80	9.97	-
Gas bottle 5	-	-	99.5	-	0.5

Figures 71 to 75 show the calibration curves obtained with the gases given in table 18.

The multi level calibration curves show the relationship between the area of the peak registered by the GC (in millivolt.seconds) and the partial pressure (in mbar) of the gases.

FID calibrations:

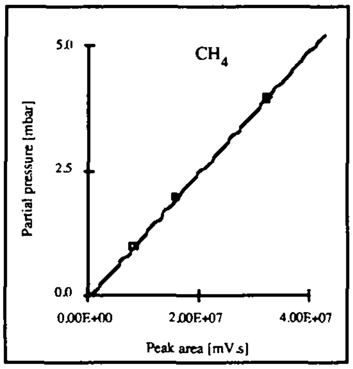

Fig. 71: CH_4 calibration curve

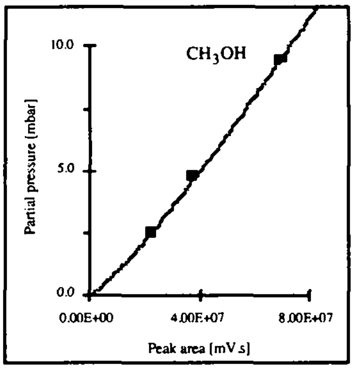

Fig. 72: CH_3OH calibration curve

TCD calibrations:

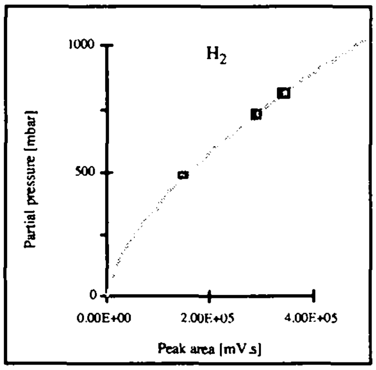

Fig. 73: H_2 calibration curve

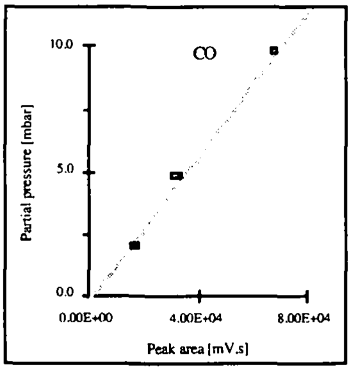

Fig. 74: CO calibration curve

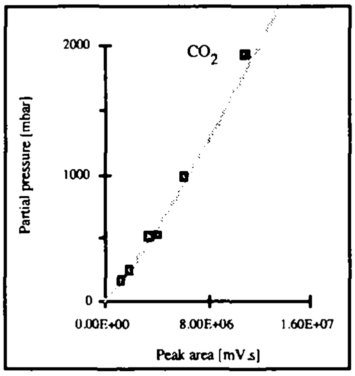

Fig. 75: CO_2 calibration curve

Similar calibration procedures were followed for the other gas chromatographs.

A.5. Simulation of the periodic experiments

Three models (listed below) were tested to find which reaction pathway could be the most probable. A continuous plug-flow was assumed for the mass balance and the following initial conditions were used:

The CO_2 flow rate is given by: $(CO_2)_{in} = (CO_2)_0 + A_{CO_2} \cdot \cos(\omega_{CO_2} \cdot t)$ (52)

where $A_{CO_2} = 25$ ml.min^{-1} and $(CO_2)_0 = 50$ ml.min^{-1}

The H2 flow rate is: $(H_2)_0 = 580$ ml.min^{-1}

The residence time (τ) is set to 0.06 s (Vcat≈2 ml, $\dot{V}$=33.33 ml.s^{-1})

The different rate constant are varied between 1 and 1000

Solving the differential equations was carried out using the OCTAVE 1.1.1. program from J. W. Euton.

A.5.1. Case of parallel reactions

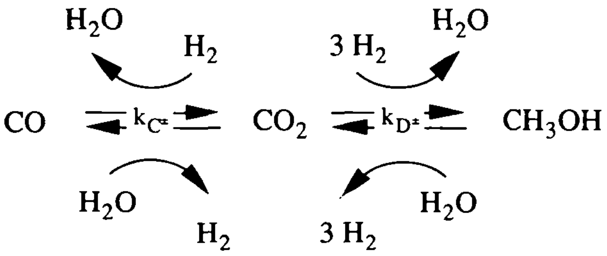

Fig. 76: parallel reaction scheme

Mass balance for a continuous reactor:

$$\frac{d\,CO_2}{d(t/\tau)} = (CO_2)_{in} + k_{C^+} \cdot \tau \cdot CO \cdot H_2O - k_{C} \cdot \tau \cdot CO_2 \cdot H_2 + k_{D^-} \cdot \tau \cdot CH_3OH \cdot H_2O - k_{D^+} \cdot \tau \cdot CO_2 \cdot [H_2]^3 - CO_2 \quad (53)$$

$$\frac{d\,CO}{d(t/\tau)} = k_{C^-} \cdot \tau \cdot CO_2 \cdot H_2 - k_{C^+} \cdot \tau \cdot CO \cdot H_2O - CO \quad (54)$$

$$\frac{d\,CH_3OH}{d(t/\tau)} = k_{D+}\cdot\tau\cdot CO_2\cdot\left[H_2\right]^3 - k_{D-}\cdot\tau\cdot CH_3OH\cdot H_2O - CH_3OH \tag{55}$$

$$\frac{d\,H_2O}{d(t/\tau)} = k_{C+}\cdot\tau\cdot CO_2\cdot H_2 - k_{C-}\cdot\tau\cdot CO\cdot H_2O + k_{D+}\cdot\tau\cdot CO_2\cdot\left[H_2\right]^3 - k_{D-}\cdot\tau\cdot CH_3OH\cdot H_2O - H_2O \tag{56}$$

$$\begin{aligned}\frac{d\,H_2}{d(t/\tau)} = {} & \left(H_2\right)_{in} + k_{C-}\cdot\tau\cdot CO\cdot H_2O - k_{C+}\cdot\tau\cdot CO_2\cdot H_2 + 3\cdot k_{D-}\cdot\tau\cdot CH_3OH\cdot H_2O \\ & - 3\cdot k_{D+}\cdot\tau\cdot CO_2\cdot\left[H_2\right]^3 - H_2\end{aligned} \tag{57}$$

A.5.2. Case of consecutive reactions

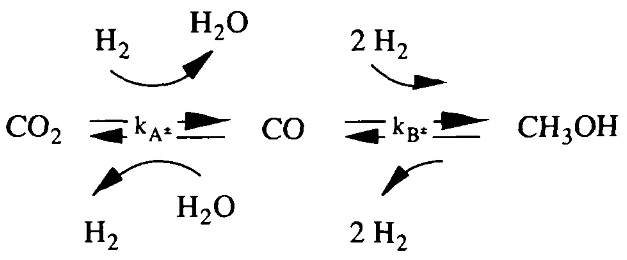

Fig. 77: consecutive reaction scheme

Mass balance for a continuous reactor:

$$\frac{d\,CO_2}{d(t/\tau)} = \left(CO_2\right)_{in} + k_{A-}\cdot\tau\cdot CO\cdot H_2O - k_{A+}\cdot\tau\cdot CO_2\cdot H_2 - CO_2 \tag{58}$$

$$\frac{d\,CO}{d(t/\tau)} = k_{A+}\cdot\tau\cdot CO_2\cdot H_2 - k_{A-}\cdot\tau\cdot CO\cdot H_2O + k_{B-}\cdot\tau\cdot CH_3OH - k_{B+}\cdot\tau\cdot CO\cdot\left(H_2\right)^2 - CO \tag{59}$$

$$\frac{d\,CH_3OH}{d(t/\tau)} = k_{B+}\cdot\tau\cdot CO\cdot\left(H_2\right)^2 - k_{B-}\cdot\tau\cdot CH_3OH - CH_3OH \tag{60}$$

$$\frac{d\,H_2O}{d(t/\tau)} = k_{A+}\cdot\tau\cdot CO_2\cdot H_2 - k_{A-}\cdot\tau\cdot CO\cdot H_2O - H_2O \tag{61}$$

$$\frac{d\,H_2}{d(t/\tau)} = \left(H_2\right)_{in} + k_{A-}\cdot\tau\cdot CO\cdot H_2O - k_{A+}\cdot\tau\cdot CO_2\cdot H_2 + 2\cdot k_{B-}\cdot\tau\cdot CH_3OH - 2\cdot k_{A+}\cdot\tau\cdot CO\cdot\left(H_2\right)^2 - H_2 \tag{62}$$

A.5.3. Case of consecutive and parallel reactions

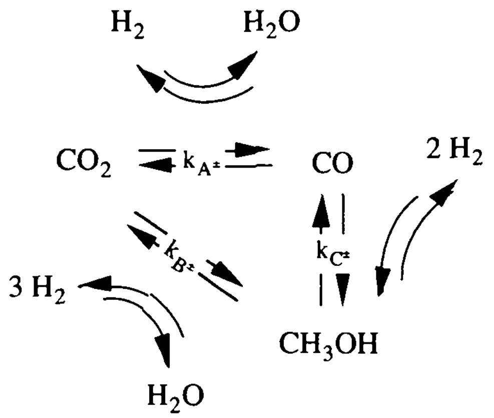

Fig. 78: consecutive and parallel reaction scheme

Mass balance for a continuous reactor:

$$\frac{d\,CO_2}{d(t/\tau)} = (CO_2)_{in} + k_{A-}\cdot\tau\cdot CO\cdot H_2O - k_{A+}\cdot CO_2\cdot H_2 + k_{B-}\cdot CH_3OH\cdot H_2O - k_{B+}\cdot CO_2\cdot[H_2]^3 - CO_2 \qquad (63)$$

$$\frac{d\,CO}{dt} = k_{A+}\cdot CO_2\cdot H_2 - k_{A-}\cdot CO\cdot H_2O + k_{C-}\cdot CH_3OH - k_{C+}\cdot CO\cdot(H_2)^2 - CO \qquad (64)$$

$$\frac{d\,CH_3OH}{dt} = k_{B+}\cdot CO_2\cdot[H_2]^3 - k_{B-}\cdot CH_3OH\cdot H_2O + k_{C+}\cdot CO\cdot[H_2]^2 - k_{C-}\cdot CH_3OH - CH_3OH \qquad (65)$$

$$\frac{d\,H_2O}{dt} = k_{A+}\cdot CO_2\cdot H_2 - k_{A-}\cdot CO\cdot H_2O + k_{B+}\cdot CO_2\cdot[H_2]^3 - k_{B-}\cdot CH_3OH\cdot H_2O - H_2O \qquad (66)$$

$$\frac{d\,H_2}{dt} = k_{A-}\cdot CO\cdot H_2O - k_{A+}\cdot CO_2\cdot H_2 + 3\cdot k_{B-}\cdot CH_3OH\cdot H_2O - 3\cdot k_{B+}\cdot CO_2\cdot[H_2]^3$$
$$+\ 2\cdot k_{C-}\cdot CH_3OH - 2\cdot k_{C+}\cdot CO\cdot[H_2]^2 - H_2 \qquad (67)$$

CURRENT RÉSUMÉ

Surname	BILL
First names	Alain, Christophe
Date of birth	5th September 1968
Place of birth	Caracas, Venezuela
Status	Married
Nationality	Swiss (Münchenbuchsee / BE)

Education	1986	Baccalauréat français type C
	1986-1987	Cours de mathématiques spéciales EPFL
	1987-1992	Diplôme d'ingénieur chimiste EPFL (The practical diploma work has been done in biotechnology, Prof. Dr. U. von Stockar)

Probationary periods	1988 (8 weeks)	Ciba-Geigy Ltd, Basel, Analytic service, Dr. J. Gutmannsbauer
	1990-1992	Student-assistant from professors Dr. E. Plattner, Dr. P. Lerch et Dr. P. Javet for "Chimie Générale pour Ingénieurs EPFL"
	1993 (6 months)	Ciba-Geigy Ltd, Basel, Protein chemistry, Research position, Dr. H. Grossenbacher

List of Publications

A. BILL, B. ELIASSON, E. KILLER, U. KOGELSCHATZ

"Greenhouse gas chemistry"

Energy Convers. Mgmt, Vol. 38, pp S415-S422, 1997
(Proc. 3rd International Conference on Carbon Dioxide Removal (ICCDR-3), Cambridge, USA, September 1996)

A. BILL, B. ELIASSON, F. GEIGER, J. HIGHFIELD, E. UENALA

"The role of simple alcohols in renewable hydrogen energy cycles"

Proc. 11th International Symposium of Alcohol Fuels (ISAF XI), Sun City, South Africa, April 1996

List of Publications (continued)

A. BILL, B. ELIASSON, E. KILLER, U. KOGELSCHATZ
"Direct oxidation of methane to methanol in a silent discharge"
and
"Methanol synthesis from pure CO_2"
Swiss Physical Society (Spring Meeting), Fribourg, Switzerland, March 1996

A. BILL
"Calorimetric control of ethanol production by immobilized yeast"
diploma work, EPFL, February 1993

Posters

A. BILL, B. ELIASSON, U. KOGELSCHATZ, L.-M. ZHOU
"Comparison of CO_2 hydrogenation in a catalytic reactor and in a dielectric-barrier discharge"
4th International Conference on Carbon Dioxide Utilization (ICCDU-4), Kyoto, Japan, September 1997

A. BILL, B. ELIASSON, E. KILLER, U. KOGELSCHATZ
"Hydrogenation of carbon dioxide in a packed-bed reactor"
11th World Hydrogen Energy Conference, Stuttgart, Germany, June 1996

A. BILL, B. ELIASSON, J. HIGHFIELD, E. KILLER
"Synthesis and steam-reforming of simple alcohols: an option for a CO_2 neutral energy cycle"
3rd International Conference on Carbon Dioxide Utilization (ICCDU-3), Norman (Ok), USA, May 1995

Patents

A. BILL, B. ELIASSON, E. KILLER, U. KOGELSCHATZ
"Verfahren und Vorrichtung zum Umwandeln eines Treibhausgases"
Nr. 6196 21 653.2, 30.05.1996

A. BILL, B. ELIASSON, E. KILLER, U. KOGELSCHATZ
"Direkte Umwandlung von Methan mit Luft zu Methanol"
Nr. 196 05 547.4, 15.02.1996

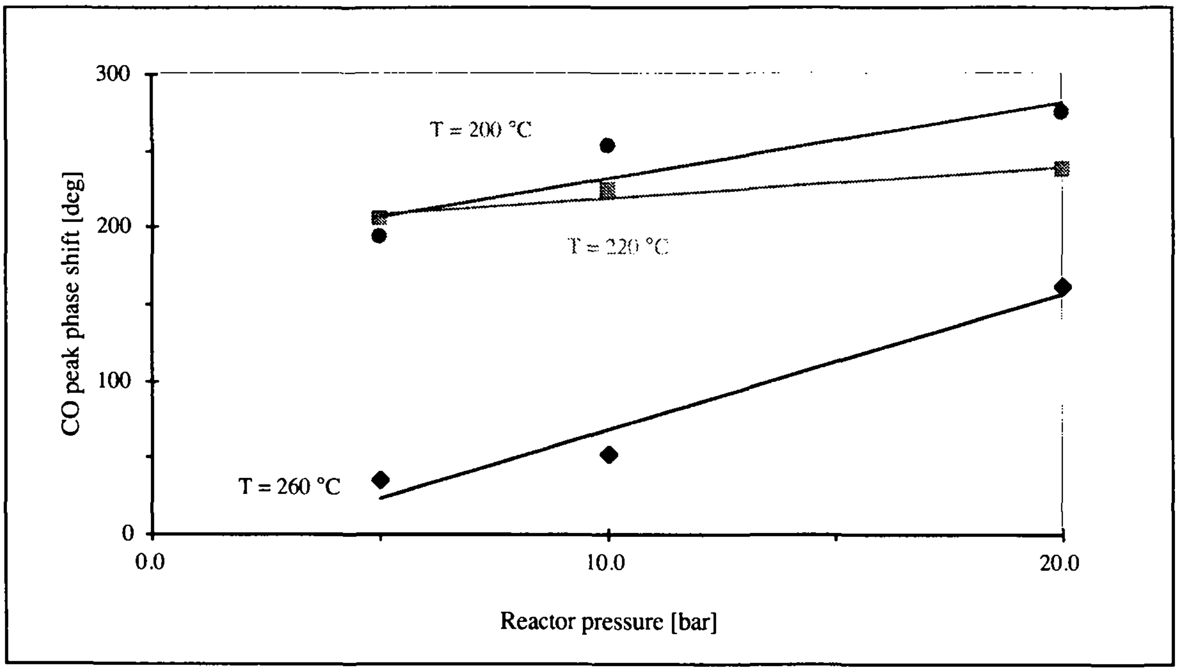

Fig. XY: CO phase shift ϕ *(relative to the* CO_2 *signal) for different pressures and temperatures* ($\omega = 1.67 \cdot 10^{-2}$ *Hz*, $Q_{H_2} = 390 \pm 100$ *Nml.min*$^{-1}$, $Q_{CO_2} = 50$ *Nml.min*$^{-1}$, $Q_{tot} = 2$ *Nl.min*$^{-1}$, *(compensation with* N_2*))*